A Wide Brownian Land: Drought Adaptation and Niche Diversification in an Australian Conifer

Meredith Cosgrove

December 2017

A thesis submitted for the degree of Doctor of Philosophy of The Australian National University

I love a sunburnt country,
A land of sweeping plains,
Of ragged mountain ranges,
Of droughts and flooding rains.
I love her far horizons,
I love her jewel-sea,
Her beauty and her terror
The wide brown land for me!

My Country, Dorothea Mackellar (1904)

DECLARATION

The research presented in this thesis is my own original work except where due reference is given. I am the principal contributor to all the chapters in this thesis. No part of this thesis has been submitted for any previous degree.

Meredith Cosgrove
December 2017

THESIS PLAN

This thesis is presented in three research chapters and an appendix featuring a plant field guide that I wrote and published in February 2014. Figures appear at the end of each chapter. All photographs and images are my own. Chapters 1-3 are intended for submission, as such the pronoun 'we' is used to represent co-authors in material intended for publication. Below I outline the contribution of my co-authors.

Mike Crisp (MDC) identified the opportunity to use the Heady *Callitris* woody trait dataset to study trait evolution in *Callitris*. MDC provided the phylogenetic trees for the Callitroideae used in all chapters.

Chapter 1:

Callitroid thickening is correlated with extreme drought resistance in Australian conifers

I was responsible for design, coding in R, statistical analyses, and writing. Lyn Cook (LC) suggested the novel convergence test. MDC and LC provided editorial comments. This chapter was in first draft on 17 February 2017 when Larter et al. (2017) was published in April with almost identical results. This resulted in a redraft with the addition of new analyses and change of focus to highlight findings missing from the Larter et al (2017) study. Some analyses may therefore appear identical or similar to the Larter et al (2017) study, but were the result of independent research as our research group was unaware of that study.

Chapter 2:

Not a radiation: *Callitris* climatic niche evolution and diversification

I was responsible for design, coding in R, statistical analyses, and writing.

Chapter 3:

Signal loss: Assessing the impact of extinctions on trait evolution models via simulations

I was responsible for design, coding in R, statistical analyses, and writing.

Appendix:

Photographic Guide to Native Plants of the Australian Capital Territory

During my PhD I also published a field guide to native plants of the Australian Capital Territory. I was solely responsible for the concept, layout, photographs, text, plots and data collection.

ACKNOWLEDGMENTS

Thank you to my supervisors, Mike Crisp and Lyn Cook

Thanks to lab associates, friends and family:

Bokyung Choi

Bee Gunn

Paul Lin

Thomas Semple

Celeste Linde

Cosgroves-Burns-Lueths

OVERVIEW

Plants cover most of earth's landmasses. Their ability to adapt to changing climates through evolutionary time has formed the distinctive biomes we see today. In plants, maintaining water supply from the roots to the leaves is critical because leaves are the sites of photosynthesis, where the sugars necessary for growth are produced. The failure of a plant's hydraulic system can ultimately lead to death, so drought imposes a high selection pressure on plant traits. Species adapted to dry and arid climates have evolved traits that maintain the water supply critical to life. If species cannot survive changing climatic conditions they risk extinction, and drought therefore also poses a serious threat to species diversity. Plant lineages that have evolved drought-tolerance often have higher diversification rates because they can 'radiate' into new arid niches that most other species cannot exist in.

Callitris is an ecologically diverse, cupressoid conifer genus native to Australia and New Caledonia. Drought-adapted *Callitris* species are the world's most drought-tolerant trees. No other trees can operate under such water-tensions without suffering significant injury or mortality. Additionally, drought-adapted *Callitris* species do not experience a hydraulic conductance-saftey trade-off. The traits related to an absence of the hydraulic trade-off has not been identified. *Callitris* therefore presents an ideal study group to investigate trait-related radiations into droughted environments. *Callitris* species possess 'callitroid thickenings' in their water-conducting tracheids, but drought-adapted *Callitris* have a much higher frequency of thickenings than *Callitris* from wet habitats, suggesting that callitroid thickenings are a trait critical to drought-tolerance.

This thesis investigates the evolution of drought-tolerance in *Callitris* from a macroevolutionary perspective. I used data from R.D. Heady's (1997) SEM study of callitroid thickening and a new phylogeny of the southern hemisphere component of the Cupressaceae, the Callitroideae, to investigate the evolution of climatic niches and drought-tolerance traits in *Callitris*. The trait evolution studies emphasised a weakness in phylogenetic comparative methods (PCMs), leading to a simulation-based study that investigated the effect of extinctions on tree reconstruction and subsequently on PCMs.

The first chapter in this thesis investigates the evolution of hydraulic drought-tolerance traits in *Callitris* by comparing the evolution of key hydraulic traits. I expected the frequency of callitroid thickenings (FCT) to be evolving under selection because of its strong ecological signal. Instead I found that FCT fitted a Brownian Motion (BM) model, suggesting evolution via drift. However, I also found that FCT was convergent with arid habitats, revealing that FCT appears to be under selection. The seemingly contradictory pattern of a trait under selection fitting a model of evolutionary drift suggests that FCT may be critical to drought-adaptation and speciation. FCT might enable high conductance and high safety by reinforcing pit borders, rather than by reducing pit apertures.

Chapter two investigates climatic niche evolution in the Callitroideae to ask whether the *Callitris* has evolved into a drier niche than its closest relatives and if the evolution of arid niches has led to higher diversification in *Callitris*. I found that *Callitris* has a drier, hotter and flatter niche than the rest of the Callitroideae (RoC). Sister-pair comparisons showed that drought-adapted *Callitris* had divergent niches as a result of geographic fragmentation. Despite extraordinary drought-tolerance *Callitris* had a lower diversification rate than the RoC, suggesting high selection and recent extinctions. Range fragmentation appears to have been the result of intensifying aridification, leading to local adaptation and geographic speciation.

Finally, chapter three investigates the effect of tree reconstructions on PCMs. I simulated phylogenies under four random extinction scenarios and traits under BM and Ornstein–Uhlenbeck (OU) models. Using extant only taxa from the simulations, I reconstructed phylogenies in BEAST. I found that the 'slowdown' in lineages-through-time plots was only observed in the reconstructed trees, suggesting it is an artefact of phylogenetic reconstruction methods. Reconstructed trees produced higher phylogenetic signal, erroneous ancestral trait reconstructions and incorrect inferences of the evolutionary model. In particular, traits simulated under a BM model were inferred as evolving under Early Burst models and traits simulated under an OU model were inferred as fitting a BM model. These results show that PCMs are heavily influenced by tree shape, which can lead to the erroneous interpretation of evolutionary histories. They also explain how traits under selection and associated with geographic speciation could fit a BM model.

CONTENTS

Chapter 1

Callitroid thickenings confer extraordinary drought-tolerance in *Callitris*

Callitris glaucophylla in Mutawintji National Park, New South Wales

Callitroid thickenings confer extraordinary drought-tolerance in *Callitris*

ABSTRACT

Hydraulics-related wood traits are critical to plant survival because they supply water to the leaves, where photosynthesis creates the sugars necessary for life. Hydraulic failure is either costly or deadly, and therefore species must adapt to aridifying climates or become extinct. *Callitris*, a conifer genus native to Australia and New Caledonia, contains the world's most drought-adapted trees. Drought-adapted *Callitris* species operate at far higher levels of water stress than mesic *Callitris* and yet do not suffer any reduction in water conductance. Conduit diameter and interconduit pit diameter are wood traits known to affect conductance and cavitation resistance, but no hydraulic safety-efficiency trade-off has been found in drought-tolerant *Callitris* species. All *Callitris* possess bar-like 'callitroid' thickenings at interconduit pits, a trait that is more frequent in drought-adapted species, but the function of these thickenings remains unknown. Here, we use a new, highly resolved phylogeny of Southern Hemisphere callitroids to investigate whether callitroid thickenings are an adaptation to drought. Evolutionary models inferred that the frequency of callitroid thickening (FCT) evolved according to a Brownian Motion (BM) model. BM simulations of FCT showed that FCT is highly convergent with arid habitat, and unlikely to have evolved via drift. The BM model probably represents a process of ecological speciation in *Callitris*, as aridity caused localised extinction and selected for high FCT, drought-tolerant species in dry climatic niches. Pit apertures and tracheids with callitroid thickenings show no phylogenetic signal and are not associated with aridity, suggesting that callitroid thickenings may prevent cavitation by stabilising pit borders under extremely negative xylem pressure, allowing conductance to remain high in drought-tolerant species. This is the first study to show that callitroid thickenings are key in drought-tolerance evolution in the most arid adapted tree in the world.

INTRODUCTION

Water limitation and high evaporation rates are serious threats to plant survival. Traits that facilitate water movement are therefore under high selection pressure and influence species' ranges and diversification (Brodribb and Hill 1999; Brodribb et al. 2010; Crisp and Cook 2013; Cavender-Bares et al. 2016; Wilson 2016; Larter et al. 2017). In conifers, adaptation to drought in warm climates is uncommon. Only two extant conifer lineages (cypresses and pines) have diversified into warm, dry climates. Of these, the southern hemisphere cypress genus *Callitris* contains the most drought-tolerant trees in the world (Bouche et al. 2014; Larter et al. 2015; Larter et al. 2017). Surprisingly, despite keen interest in drought-tolerance of plants, the traits that confer its extreme tolerance remain elusive.

Wood traits play a key role in the evolution of drought-tolerance in plants, especially the water-transporting xylem. The conduit size of xylem is critical to the efficient movement of water: conduits with larger diameters are more efficient because an increase in diameter is accompanied by an exponential (n^4) increase in water conductance (following the Hagen-Poisuielle equation) (Tyree et al. 1994). In drought-tolerant plants, larger conduits should therefore be favoured by selection. However, larger conduits are prone to hydraulic failure under water stress because as water supply diminishes, the tension in the water column increases (i.e. pressure become more negative). Water in the xylem can transition into a gas (water vapour) as pressure become more negative, a process known as cavitation. Cavitation creates air bubbles within the conduit and can lead to the total failure of water conductance if air and water vapour fill a conduit, creating an embolism. If embolisms accumulate across conduits, it leads to a reduction in water supply and photosynthesis, and can cause plant mortality.

Cavitation vulnerability can be measured by P_{50}, the negative pressure required to cause a 50% loss of xylem sap conductance. At these pressures, embolisms leading to hydraulic failure escalate, causing local tissue and ultimately, whole plant death (Choat et al. 2012). P_{50} and conductance are measured on stem sections and are therefore measures of xylem performance. While conduit width is important because of its benefit to water conductance, other characteristics such as conduit length, pit structure, pit

number, pit size and pit aperture contribute to cavitation resistance ('safety') and hydraulic efficiency (Hacke et al. 2004).

Hydraulic Safety–Efficiency Trade-off

The Safety-Efficiency Trade-off hypothesis (Tyree and Ewers 1991; Tyree and Zimmermann 2002) predicts that there should be a trade-off between conductance and the risk of embolism (P_{50}). Larger conduits have higher conductance ('efficiency') but should be more vulnerable to embolisms, and narrow conduits should be 'safe' from embolisms but have lower conductance.

Water Transport in Conifers

In conifers, water is transported through tracheids, single-celled conduits that collectively form the wood of the plant. Tracheids have two purposes: they provide support to the canopy of the plant and they conduct water. Water moves between tracheids through perforations in the tracheid walls known as inter-tracheid or bordered pits. Pits are bounded by a raised disc, the pit border, and an aperture with a 'torus-margo' valve, through which water passes (see Valli et al. 2002 for a schematic diagram). The torus is a centrally located, impermeable disc connected to the pit margins by a ring of margo strands. When the torus is in a neutral position, water passes between the margo strands. When a water-filled tracheid has more negative pressure than a neighbouring (embolised) tracheid, the pressure difference pulls the torus against the inner rim of the bordered pit creating a seal. Under extreme pressures, the walls of water-filled tracheids can warp inwards, and even collapse, referred to as implosion. Tracheids with thicker walls are less susceptible to implosion (Hacke et al. 2001).

Cavitation commonly occurs when negative pressures cause the torus to slip in the bordered pit, leading to air bubbles 'seeding' into the tracheid, causing embolisms that prevent water flow (Delzon et al. 2010). Pits are therefore critical to water management because they partition embolised tracheids and prevent escalating cavitation rates (Choat et al. 2008; Cochard et al. 2009; Delzon et al. 2010; Pittermann et al. 2010).

Smaller pit aperture diameters are associated with species from dry habitats because they are more fail-safe (Bouche et al. 2014), but they impede water movement (Schulte et al. 2015). The ideal combination of narrow, cavitation resistant pits and wide, efficient tracheids is not feasible because pits are a chief source of hydraulic resistance,

rendering wide tracheids redundant (Sperry et al. 2006; Pittermann et al. 2010). To maintain efficient flow in wide tracheids would require more pits, potentially weakening the tracheid walls and thereby increasing the risk of implosion (Hacke et al. 2004; Sperry et al. 2006; Choat et al. 2012).

Evidence for a Safety–Efficiency Trade-off in Conifers

Given the large efficiency gains that can be made by a small increase in conduit width, it would be expected that an efficiency-safety trade-off would be frequently detected in plants. At a broad scale, there is evidence for a safety-efficiency trade-off in gymnosperms compared to angiosperms. Gymnosperms have lower conductance and are more cavitation resistant than angiosperms, because tracheids are smaller than large angiosperm vessels, which are specialised for water movement (Maherali et al. 2004; Choat et al. 2012; Gleason et al. 2016). Whether this is a direct or indirect trade-off remains unclear because narrow tracheids built to cope with load-bearing wood may coincidentally confer cavitation resistance (Hacke et al. 2001; Bouche et al. 2014). However, under freezing or dry conditions, the angiosperm advantage disappears: conifers are as efficient or more efficient than angiosperms when cavitations are more likely to occur. The conifer advantage seems to rest in the unique structure of the torus-margo pit, which has far higher conductance than angiosperm pits (Hacke et al. 2004; Pittermann et al. 2005).

Evidence of a Hydraulic Trade-off within Conifers

In conifers, tracheid width and pit size scale with tree height and environment. Tracheids and pits decrease in size with distance away from the roots (Domec et al. 2008; Lazzarin et al. 2016), in freezing environments (Pittermann and Sperry 2003), and with increasing aridity (Pittermann et al. 2010). Pits have been found to contribute up to 70% conductance resistance (Domec et al. 2006; Pittermann et al. 2006), indicating that, vulnerability to cavitation probably occurs at the pit level, rather than the tracheid level. Because hydraulic failure is frequently a result of pit failure, tracheid widths have often been found to be uncoupled from cavitation risk,(Pittermann et al. 2006; Delzon et al. 2010).

Pits with a larger torus overlap have greater cavitation resistance (Delzon et al., 2010), and many conifer species in dry environments have high torus overlap and thicker tracheid walls (Bouche 2014). Larger torus overlap is achieved by reducing pit

apertures, which leads to a larger area for the torus to seal against, but also an increase in pit resistance (Delzon et al. 2010; Pittermann et al. 2010). Given this, it would be expected that a trade-off of higher resistance to cavitation with lower conductance would most likely be a consequence of pit anatomy (Choat et al. 2008; Pittermann et al. 2010; Schulte et al. 2015). However, in *Callitris*, the world's most cavitation-resistant trees, there is no apparent trade-off between P_{50} and conductance (Larter et al., 2017). Larter et al. (2017) found that drought-adapted species had narrower tracheids and were more cavitation resistant than mesic species, but did not have higher pit resistance. Additionally, the lack of a trade-off was not related to tracheid dimensions, wood density, pit density or pit structure.

The Heady Hypothesis for Callitris

Heady (1997) investigated wood anatomical traits in *Callitris* using SEM (Heady 1997). SEM allowed the first accurate observations of callitroid thickenings, a trait common to *Callitris*, but apparently rare in other conifers. Callitroid thickenings are pairs of distinctive, bar-like structures that bracket bordered pits (Fig. 1) with an unknown function.

Heady (1997) observed different forms of callitroid thickenings and frequency of callitroid thickenings (FCT) in species growing in different habitats. Species in dry habitats tended to have high FCT and a high proportion of Type 2 form thickenings, whereas species in wet habitats had low FCT and Type 1 form thickenings (Fig. 1). Furthermore, the presence of thickenings was related to tracheid width (Heady, 1997). Tracheids with callitroid thickenings were narrower than those without thickenings, such that species with low FCT also tended to have larger tracheids, on average, than species with high FCT. Within wood samples, there was a range of wide and narrow tracheids, and pits with thickenings. Within a tree, the frequency of callitroid thickening did not differ with height from the roots or with distance from the pith to the bark. Heady suggested that callitroid thickening could operate as a structural support in tracheids, preventing implosion under extremely negative pressure, particularly at pits where tracheid-wall failure typically begins.

The extreme drought-tolerance of *Callitris* remains puzzling. Drought-adapted *Callitris* are able to operate at much lower negative pressures than other conifers, and yet there is no evidence that they suffer a loss of conductance compared to wet and mesic *Callitris*

species. Using Heady's data, we investigate whether callitroid thickening: 1) explains the lack of a hydraulic trade-off in *Callitris*;
2) could be an evolutionary adaptation to drought; and 3) is a trait convergent with adaptation to aridity.

METHODS

Study Species

Callitris is a small, ecologically diverse conifer genus of 24 species, endemic to Australia (21 species) and New Caledonia (3 species). Here we follow the species-level taxonomy of (Hill 1998). *Callitris* is found in habitats that include tropical and subtropical rainforest, temperate woodland and heath, subtropical savannah, and arid shrubland.

Callitris Phylogeny

The modelling of niche and trait evolution requires a phylogenetic framework and timescale. A relaxed molecular clock phylogeny, including all species of *Callitris* recognised by Hill (1998), was estimated using Bayesian inference in BEAST ver. 1.8.0 (Drummond et al. 2012) (Supplementary Fig. 1). The data comprised DNA sequences obtained using the standard Sanger method from the chloroplast and three nuclear loci (Crisp et al. in prep.). In addition to the maximum clade credibility (MCC) tree, a set of 100 trees was evenly sampled, to avoid autocorrelation, from across the post-burnin posterior of the BEAST analysis for downstream analyses of trait and niche evolution.

Tree Pruning

After estimating the time-calibrated phylogeny, we pruned the trees to include only those species for which trait data were available. In cases where our phylogeny showed east-west divergences within species, we followed Heady's collection sites and used only the lineage from the region in which he collected his sample, e.g., *C. glaucophylla* has three geographic lineages (Sakaguchi et al. 2013) but we used only the eastern lineage, excluding the western and central Australian lineages. Following Heady's collection locations (and Hill's taxonomy), we treated *C. preissii* as a taxon confined to the Western Australian coast near Perth, and *C. columellaris* as confined to the northern

New South Wales and southern Queensland coast. *Callitris verrucosa* records from Western Australia were treated as *C. tuberculata*, and *C. verrucosa* as an eastern Australian species (Hill 1998). *Callitris macleayana* has two disjunct populations along the eastern coast of Australia, and the northern lineage was excluded.

Woody Trait Data

Woody trait data for 19 species (17 Australian, two New Caledonian) were taken from Heady's (1997) SEM study of the wood anatomy of *Callitris* (Heady 1997). Heady collected 5 mm diameter wood cores from wild, adult trees growing within their native range and made observations on 34,800 pits from a total of 171 wood samples (4–22 individuals per species, mean = 8). Unfortunately Heady did not sample *Actinostrobus* (3 spp.) or *Neocallitropsis* (1 sp.), which molecular and morphological data indicate are within *Callitris* (Piggin and Bruhl 2010) (Pye et al. 2003; Mao et al. 2012). There is also no trait data available for closely related outgroups.

Variability in wood traits could be a plastic response to environment, rather than an evolutionary adaptation. Heady (1997) tested the plasticity of *Callitris* woody traits in a three-year common garden experiment, using high and low water treatments on *Callitris* grown from seed. He found no significant differences in FCT, but tracheids were broader in high-water treatment plants, indicating that tracheid width alone does not determine FCT. Environment-related differences in wood traits were also found in field-based studies of *C. columellaris s.l.* (Bowman et al. 2011; Prior et al. 2012), but these differences might be due to the presence of cryptic species in this taxon (phylogeny presented here).

We investigated six woody traits putatively related to drought-resistance: diameter of bordered pits (BPD), diameter of pit aperture (PAD), the frequency of callitroid thickening (FCT), tracheid width with callitroid thickening (TW+*t*), and tracheid width without callitroid thickening (TW–*t*). Heady's FCT data are logit regression model predictions based on counts of pits with or without thickenings from wood samples, and are not the original data (Heady 1997). Our FCT scores were extracted from his graphs.

Because Heady noted that tracheids without thickenings are consistently wider than tracheids with thickenings, we included maximum (PADmax) and minimum (PADmin)

pit aperture, to investigate whether pits scaled with tracheid widths. If this were the case then pits in TW+*t* should be significantly correlated with minimum pit aperture.

We added maximum plant height (MaxH) to Heady's data because water relations are known to limit plant growth and drought-adaptation may be achieved by a reduction in stature (Domec et al. 2008). Plant heights were taken from (Hill 1998) and The Gymnosperm Database (Earle 2017). All trait data used in subsequent analyses were log-transformed mean values.

Climatic Niche Data

Locality Data

Publically available locality data for vouchered specimens of *Callitris* species were downloaded from Australia's Virtual Herbarium (AVH) <http://avh.chah.org.au>, the Database Virot botanical herbarium of IRD Nouméa (NOU) <http://herbier-noumea.plantnet-project.org> and the Global Biodiversity Information Facility (GBIF) <http://www.gbif.org>. Records were cleaned prior to analyses by removing records for cultivated plants and erroneous records, e.g., those plotting in the ocean. We also removed duplicate records so that there were no multiples at any one site. We selected the most recent collections where possible because these are less likely to have erroneous coordinates. These data were edited according to the same taxonomic criteria as the phylogeny (described below).

Environmental Data

We downloaded the base nineteen global Bioclim v1.4 climate layers for the period 1950-2000 (Hijmans et al. 2005) as 30 arc-second rasters, equivalent to approximately one kilometre at the equator (30 seconds = 0.93 x 0.93 km = 0.86 km^2 at the equator). These temperature and precipitation layers account for the major influences of temperature and precipitation on climatic niche. We additionally downloaded the Aridity Index (AI) raster from the Global Aridity and PET Database <http://www.cgiar-csi.org/data/global-aridity-and-pet-database>. The Aridity Index is calculated as Mean Annual Precipitation (MAP)/Mean Annual Potential Evapo-Transpiration (MAE), and is a measure of moisture availability, not including soil moisture. When MAP and MAE are equal, AI = 1. Because the denominator is MAE, when precipitation is low and evaporation is high, AI is low.

We follow the generalised climate classification scheme for Global-Aridity, which classifies habitat according to AI: Humid > 0.65; Dry sub-humid = 0.65–0.5; Semi-Arid = 0.5–0.2; Arid = 0.2–0.03 (UNEP 1997). Australia has no Hyper Arid environments (AI <0.03). Water availability is critical to plant survival, and AI is a more realistic measure than precipitation because it accounts for water lost from the environment via evaporation.

The 20 global layers were clipped in QGIS (QGIS 2016) to include only Australia (map limits = 108, 155 E, -44, -10 S) or New Caledonia (map limits = 163.55 168.20 E,-22.75 -19.54 S). Because Australia spans approximately 30 degrees of latitude, Bioclim layers were transformed from WGS84 (EPSG:4326) to Australian Albers GDA94 (EPSG:3577), an equal-areas projection that satisfies MaxEnt modelling assumptions (Elith et al. 2011). As New Caledonia lies approximately 1400 km off the eastern coast of Australia and is outside the GDA94 bounds, New Caledonian layers were transformed to the equal area Lambert New Caledonia (EPSG:3163) projection. We extracted point climatic values for all species occurrences from the 20 layers in QGIS.

Analyses

Species Climatic Niche

We used univariate and multivariate methods to estimate environmental niches in *Callitris*. A single variable might be a significant driver of niche evolution, but complex climatic niches might be better described by multivariate space. In the univariate approach, we used environmental niche models (ENMs) to predict species' climatic niches and then created predicted niche occupancy (PNO) profiles for each climate variable (Phillips et al. 2006; Evans et al. 2009). In the multivariate approach, we used point data extracted from the Bioclim layers and estimated niche differentiation using Outlying Mean Index (OMI), a form of two-table ordination (Dolédec et al. 2000).

MaxEnt Models and Predicted Niche Occupancy

To construct ENMs for all *Callitris* species we used MaxEnt (Phillips et al. 2006). Because Bioclim variables are correlated, we excluded highly correlated variables (Spearman's rho ≥ 0.8). This left 12 variables: Bio 1, Bio 3, Bio 5, Bio 6, Bio 7, Bio 8, Bio 9, Bio 15, Bio 17, Bio 18, Bio 19, and AI. We ran 10 MaxEnt replicates per species using random seeds, a regularisation multiplier of one, and sampled from a maximum 10,000 background points across the Australian or New Caledonian landmass. Seventy-

five percent of the data were used to train the model, and 25% used as test data. The area under the curve (AUC) values of the receiver operating characteristic (ROC) curve was assessed for all species modelled to indicate whether the MaxEnt model could accurately predict test occurrences. An AUC of 0.5 indicates that the model prediction is no better than expected by chance and 1.00 indicates a perfect recovery of novel occurrences used to test the model. (Phillips et al. 2006).

We combined the Australian and New Caledonian average MaxEnt probabilities and produced a profile of each species' PNO for each variable using the R package phyloclim (Heibl and Calenge 2013). PNOs are created by integrating the MaxEnt probability of a species occurring in a pixel with the values from a climatic layer for the same pixel (see Evans et al. 2009 for details). The climatic means weighted by the cumulative probability of the MaxEnt model (weighted means) were extracted from the PNOs and log transformed prior to use in analyses.

Outlying Mean Index

Outlying Mean Index (OMI) is a form of two-table ordination that allows for the use of multivariate environmental data and corrects for uneven sampling (Dolédec et al. 2000). The first principal coordinate analysis (PCA) creates ordinate space for all species based on climatic point data. The centroid of this ordination represents the mean environmental conditions for all species. A second PCA, orthogonal to the first, defines the niche of each species, with the mean for each species lying at a marginal distance from the mean environmental conditions for all species. We used climatic point data for the same 12 Bioclim layers as used in MaxEnt models. A total 3910 observations were used in the analysis, ranging from eight (*C. neocaledonica*) to 798 (*C. glaucophylla*) per species (median = 86, mean = 205, sd = 224).

Phylogenetic Signal

Phylogenetic signal can be seen as a way of measuring how clustered or dispersed traits are, relative to the expected value determined by the tree and a Brownian Motion (BM) model. The BM model predicts that traits will co-vary according to their degree of relatedness, the timing of species divergences, and the cumulative variances of a non-directional, random walk. When the phylogeny and a BM model accurately predict the values found at the tips of the tree, the phylogenetic 'signal' is strong. We estimated phylogenetic signal using both Pagel's Lambda (λ) (Pagel 1999, 2002) and Blomberg's

K (*K*) (Blomberg et al. 2003). All phylogenetic signal analyses were run in the R (R-Core-Team 2017) package phytools (Revell 2012).

Pagel's Lambda

Pagel's Lambda (Pagel 1999, 2002) employs a scaling branch-modification method. Branch lengths are altered by multiplying the off-diagonal elements of a variance-covariance matrix that describes the tree by a value of λ. Since the diagonals are the summed branch lengths, multiplying the off-diagonals alters the lengths of the internal branches in the tree. If the trait has evolved according to a BM model (λ = 1), the internal branches are not altered, as the distances between relatives account for trait values observed at the tips. If λ = 0, branch lengths have been altered to the point where they are all equal, creating a star phylogeny, in which case relatedness has had no effect on trait evolution. If λ > 1, tip values are more alike than the phylogeny predicts under BM, indicating that some kind of constraint is limiting or canalising trait evolution.

Blomberg's Kappa

Blomberg's *K* is a standardised ratio, comparing the mean square error of the tip data fitted to the tree compared to the mean square error of tip data simulated along the same tree according to a BM expectation (Blomberg et al. 2003; Kamilar and Cooper 2013). As with lambda, when $K = 1$, traits are evolving according to BM. $K < 1$ indicates that traits are less similar than would be expected under a BM model. We estimated significance for λ and *K* for the MCC tree using 1000 random permutations of the tip data. The null hypothesis is that there is no phylogenetic signal in the data. Support for phylogenetic signal is interpreted when the values differ significantly between the observed and randomly permuted tip values.

Phylogenetic Uncertainty

Variation among trees from a BEAST analysis can be large. As trait modelling relies on the topology and branch lengths of a tree, we incorporated phylogenetic uncertainty by analysing 100 trees sampled from the posterior.

Macroevolutionary Modelling

Analyses of phylogenetic signal identify whether trait data fit a BM pattern or not, but it cannot identify an evolutionary process (Revell et al. 2008). To investigate evolutionary processes we ran maximum likelihood analyses using seven models: lambda, kappa,

delta, BM, Early Burst (EB), single-optimum Ornstein-Uhlenbeck (OU), and White Noise (WN) (details in Supplementary material). Trait data were log-transformed to allow for comparisons between traits (Harmon et al. 2010). We ran analyses for an optimal (MCC) tree, and for a set of 100 posterior trees from the BEAST analysis. Model selection was performed using second-order Akaike information criterion corrected for small sample sizes ($AICc_w$) weights (Burnham and Anderson 2002). Analyses were run in the R package geiger (Pennell et al. 2014).

Phylogenetic Generalised Least Squares (PGLS)

We used phylogenetic generalised least squares (PGLS) regression to investigate whether the evolution of traits was correlated (Grafen 1989; Martins and Hansen 1997; Pagel 1997). We chose PGLS because it estimates the phylogenetic signal of the regression model using the residual error of the response variable (Revell 2010; Symonds and Blomberg 2014). In the absence of a phylogenetic effect on correlated trait evolution the PGLS model collapses to an ordinary least squares (phylogenetically uncorrected) model.

We used the branch-transformation method with Pagel's lambda (λ) to correct for phylogenetic signal in the traits being correlated. Lambda is insensitive to the number of taxa in the phylogeny, and unlike Blomberg's K, does not directly imply rate variation (Freckleton et al. 2002; Münkemüller et al. 2012). Lambda was estimated with maximum likelihood (ML). We regressed woody traits against each other to see if they showed correlated evolution, and against niche position (OMI) and climatic niche traits to see if woody traits were associated with climatic niche. We used the PNO weighted means and OMI axes to describe the climatic niche as the independent variables. If a single climatic trait results in better PGLS fit than the OMI axis, it suggests that the additional information in the axis is not critical to trait evolution. All PGLS analyses were performed using the `pgls` function in the R package caper (Orme 2013).

Convergent Evolution in FCT

Water availability is critical to plant survival. Because of this, traits that confer drought tolerance are expected to be under strong selection in aridifying environments. When trait values are more alike in species with similar climatic niches than in those that are most closely related phylogenetically, it indicates convergence in trait evolution. However, trait clustering could also be a chance result of drift.

Polygon Morphospace Method

One approach used to evaluate convergence is to simulate traits under a null model and compare how often observed and simulated data share the same trait space (Stayton 2015). Under selection, traits should converge on an optimal solution, and convergent traits should be more clustered in trait space than traits evolving under a BM model. To test whether FCT is a convergent trait shaped by increasing aridity, we simulated FCT under a BM model and plotted FCT against AI. A polygon was plotted around the resulting points to assess the position and area of each polygon within trait space.

If FCT has evolved under selection by increasing aridification, and is convergent in drought-adapted species, we expect that the trait space of drought-tolerant species 1) will be more clustered in the observed data than in data simulated by the null BM models and 2) will occupy a distinct position within trait space. If FCT is not convergent under increasing aridification, then the trait space of the observed data should be similar to the trait space of simulations generated under a BM model. Furthermore, polygons should not differ in area (i.e. how aggregated or dispersed species traits are in trait space) or in position on the Y-axis (i.e. how often high FCT values result from a BM model). Additionally, if FCT has not evolved as a drought-tolerance trait, then there should be no association between FCT and AI.

FCT Trait Simulation

The phylogenetic root value (*z0*) and variance (σ^2) of FCT were estimated for the MCC tree and 100 evenly sampled posterior trees based on the observed values of FCT for 19 *Callitris* species. Ancestral character estimation was done using the `ace` function in the R package ape (Paradis et al. 2004).

Using the estimated root value and variance, the evolution of FCT was simulated under a bounded BM model for each tree. Callitroid thickening in the Heady data is expressed as a frequency, so bounds were included to limit the simulated range of FCT from 0.001 to 100%, matching the observed range. This produced 100 simulations for each of the 101 trees (total = 10100 simulated datasets). Simulations were run in the R package phytools using the `fastBM` function (Revell et al. 2012). All data were simulated as log transformed values for subsequent use.

Convex Hull Polygons

To create morphospace plots for the simulated data, we plotted simulated FCT values against observed AI values. A polygon for the observed values of FCT and AI, and a polygon for each of the 100 BM simulations of FCT per tree (10100 polygons in total) were plotted in morphospace. Polygons were plotted around species found in semiarid to arid habitats (AI < 0.5) because this was the region of interest for adaption to aridity. Polygons were plotted to describe the broadest possible polygon boundary, and points plotting inside polygon boundary were ignored. AI remained the same for each species because no assumption was made that FCT and AI were correlated. Polygon shape was therefore a result of differing values of FCT, not AI. Convex hulls were used in preference to concave hulls because the choice of concavity (alpha) is sensitive to the distances between points, and results in an arbitrary hull boundary depending on the spacing of points and degree of concavity. Convex hulls were created using the `Polygon` function in the R package sp (Pebesma and Bivand 2005).

For each simulation the area, maximum and mean position on the FCT-axis of the polygon was calculated. We also investigated the Y-axis position of the smallest polygon from every simulation to see if high FCT values were tightly clustered in trait space, suggesting convergence. Polygons from the simulations were compared to that of the actual data to assess whether a polygon with such a small area and high mean FCT could be the result of a 'null' BM model. Significance was evaluated using one-sided Monte-Carlo permutation tests. Tests were run in R, using the `randtest` function from the package ade4 (Dray and Dufour 2007).

RESULTS

Species Climatic Niche

MaxEnt Models and PNOs

The area under the curve (AUC) values of the receiver operating characteristic (ROC) curve ranged from 0.91-1.00 for all species modelled, indicating that the MaxEnt model could recover test occurrences accurately. For some species the predicted climatic niche was broader than the current geographic range (Supplementary Fig. 2). Species occurring in south-western or south-eastern Australia were predicted to also occur on the opposite side of the continent at lower probabilities. In particular, species occurring

in the Flinders Ranges in South Australia were predicted to have suitable habitat in south-western Australia, and vice versa.

The PNO weighted means confirmed that *Callitris* has a broad climatic niche (Supplementary Table 1). Predicted MAT ranged from 12.2 ºC (*C. oblonga*) to 25.8 ºC (*C. intratropica*). PDryQ ranged from 18 mm (*C. intratropica*) to 281 mm (*C. neocaledonica*) and PWarmQ varied from 54 mm (*C. canescens*) to 716 mm (*C. neocaledonica*). *C. neocaledonica* has the wettest niche (PDryQ = 281 mm, PWarmQ = 716 mm, AI = 1.59), with the least variation in temperature (13.8 ºC). *C. tuberculata* has the most arid niche (AI = 0.2; the boundary between semi-arid and arid), with the highest annual temperature range (28.8 ºC). *C. oblonga* occupies the coolest niche with the most even rainfall. The niche of *C. intratropica* is unique within *Callitris*. It has the most seasonal rainfall and the highest temperatures, receiving all of its rainfall during the summer monsoon of northern Australia.

Outlying Mean Index

The first three PCA axes accounted for 85% of the total variability in climate across all species. Axis 1 (34%) was primarily associated with temperature and precipitation seasonality; Axis 2 (31%) with precipitation and annual temperature range; and Axis 3 (20%) with seasonal variability in temperature and rainfall (Supplementary Table 1). The second PCA of species' niches within environmental space accounted for 95% of the variability in species' climatic niche (Axis1 = 42%, Axis 2 = 35%, Axis 3 = 18%). Correlations with environmental variables were similar to those in the first PCA. *C. neocaledonica* and *C. intratropica* had the most outlying niches compared to the mean climatic space for all species. Species niche point data shows a hard boundary at the lower right corner that seems to be linked to aridity (Fig. 2).

Phylogenetic Signal

Woody Traits

Woody traits varied considerably in phylogenetic signal. Lambda ranged from 0 to 0.98 and Blomberg's K from 0.34 to 1 (Table 1). FCT (λ = 0.98, K = 1.00) and TW–t (λ = 0.98, K = 0.75) showed significant phylogenetic signal, indicating a high level of inheritance according to a BM model. TW+t and MaxH showed significant signal according to Blomberg's K, but not Pagel's Lambda (TW+t, λ = 0.69, K= 0.57, MaxH, λ = 0.90, K = 0.63). There was no phylogenetic signal detected in PAD according to

Pagel's Lambda, and Blomberg's K was relatively low and non-significant ($\lambda = 0$, $K = 0.34$).

Climatic Niche Traits

For climatic traits, lambda ranged from 0 to 1.07 and Blomberg's K from 0.22 to 0.74 (Table 1). Four traits showed significant phylogenetic signal: ATR, PWarmQ, OMI and OMI Axis 2 ($\lambda = 0.72–1.07$, $K = 0.65–0.75$). Iso, MeanTWetQ, MeanTDryQ, PS, PColdQ, OMI Axis1 and OMI Axis 3 had very low phylogenetic signal ($\lambda = 0$, $K = 0.22–0.51$).

Phylogenetic Uncertainty

Mean lambda across 100 evenly sampled posterior trees was marginally lower than for the MCC tree for all traits. However, the spread of lambda was sometimes large, skewed or bimodal across 100 trees (Supplementary Fig. 3). While in general the phylogenetic signal of the MCC tree was close to the mode of the posterior trees, there was one notable exception: 58% of lambdas calculated for TW+*t* lay between 0 and 0.1, compared to 0.69 for the MCC tree. Mean K for 100 trees was slightly lower than for the MCC tree for all traits and the standard deviation ranged between 0.041 and 0.101 (Supplementary Fig. 4). Because Blomberg's K is a standardised measure, distributions were less skewed than lambda. K for the MCC tree lay near the mode for all traits across all 100 trees.

Macroevolutionary Modelling

FCT, TW-*t*, OMI, PwarmQ and OMI Axis 2 fitted a BM model (Table 2). Model support was low for climatic niche variables for the MCC tree and posterior, but was strong for FCT and TW-*t* across the posterior trees (AICc weights, Supplementary Fig. 5). TW+*t*, BDP and PAD all fitted a white noise (WN) model confirming that that phylogeny had no influence on evolution of these traits. Model support for pit data was high for both the MCC and posterior trees. All other climatic niche variables fitted a WN model except ATR, which fitted a lambda model ($\lambda = 0.71$), and AI and MAT, which fitted a pure speciational model ($\varkappa = 0$). MAT is used to calculate AI and so is highly correlated with AI. Full results are presented in Supplementary Table 2.

Phylogenetic Generalised Least Squares

Species Niche Position (OMI)

Species niche position had a near perfect positive correlation with PWarmQ (Bio18, r^2 = 0.998). OMI was negatively correlated with FCT (r^2 = 0.47) and positively correlated with TW-*t* (r^2 = 0.44). Significant results of PGLS analyses are presented in Table 3. Full results are presented in Supplementary Table 3.

Frequency of Callitroid Thickening

FCT was negatively correlated with OMI Axis 2 (r^2 = 0.70), and therefore also with AI (r^2 = 0.65), and positively correlated with ATR (Bio7, r^2 = 0.57). Thickenings were weakly associated with pits with narrow apertures (r^2 = 0.27). FCT had no correlation with tracheid widths.

Tracheid Width

Tracheid widths were positively correlated with MeanTWetQ (Bio8, r^2 = 0.41), and PWarmQ (Bio18, TW+*t*, r^2 = 0.31; TW–*t*, r^2 = 0.38), whether they had thickenings or not. TW+*t* alone was positively correlated with MAT (Bio1, r^2 = 0.36). Tracheid widths were correlated with one another (r^2 = 0.67), and both were correlated with maximum tree height, although the correlation between MaxH and TW-*t* was weaker than with TW+*t* (TW+*t*, r^2 = 0.68; TW-*t*, r^2 = 0.47). Tracheid widths and bordered pits were positively correlated (TW+*t*, r^2 = 0.50; TW-*t*, r^2 = 0.21). TW-t and PAD were correlated (r^2 = 0.40), but TW+*t* showed a non-significant trend with PAD (r^2 = 0.17, P = 0.084). Tracheid widths were not correlated with FCT.

Bordered Pits

BPD was most strongly positively correlated with PDryQ (Bio17, r^2 = 0.44) and OMI Axis 2 (r^2 = 0.42). PAD was positively correlated with OMI Axis 2 (r^2 = 0.46) and with PWarmQ (r^2 = 0.35), and had a weak correlation with PDryQ (r^2 = 0.28).

DBP and PAD were significantly positively correlated (r^2 = 0.69). Neither was correlated with TW+*t*, but both were positively correlated with TW-*t* (BPD, r^2 = 0.50; PAD, r^2 = 0.40). As TW-*t* have wider diameters, using a mean PAD value may not account for allometric scaling of PAD in narrower TW+*t*. However, the overall result remained non-significant whether using mean, maximum (PADmax) or minimum (PADmin), although TW+*t* showed the strongest relationship with PADmin (r^2 = 0.18),

indicating that pits do scale with tracheid width. PAD and BPD were negatively correlated with FCT, but the relationship with PAD was stronger (BPD, $r^2 = 0.23$; PAD, $r^2 = 0.38$).

Maximum Height

MaxH was positively correlated with AI ($r^2 = 0.33$) and with MAT (Bio1, $r^2 = 0.30$). It was positively correlated with both TW+*t* ($r^2 = 0.68$), and TW–*t* ($r^2 = 0.47$), but not with BPD or FCT.

Several broad patterns emerged from PGLS analyses of niche, woody and climatic traits. Species position in niche space was determined by aridity and hydraulic traits, chiefly FCT and TW-*t*. Species height in arid environments was lower than those in wet and mesic environments. Tracheids were widest in warm, wet niches, and narrowest in cold, wet niches. TW-*t* became narrower as PWarmQ diminished and aridity increased, whereas TW+*t* narrowed with MeanTWetQ and MAT, but not increasing aridity. There was no relationship between tracheid widths (TW-*t* and TW+*t*) and FCT. In drought-adapted species, FCT increased as pit apertures decreased. Pit apertures scaled with TW-*t*, becoming smaller with increasing aridity, but there was no significant relationship between PAD and TW+*t*.

Polygon Morphospace

The simulations resulted in 100 polygons for the MCC tree and 100 posterior trees (10100 polygons in total). Polygon shape and location in morphospace was the result of FCT simulated under a BM model along a chosen tree. Polygons were plotted for semi-arid to arid species (AI < 0.5) because this was the area of interest for adaption to aridity (Fig. 3). AI remained the same for each species in all simulations, and only differing values of FCT simulated under a BM model altered polygon shape.

Polygon Area

The observed polygon area was smaller than the majority of the 10100 polygon areas simulated across all trees, and was significantly different from the distribution of simulated polygon areas ($P = 0.001$, Fig. 4A). However, the area of the observed polygon was not significantly different to the smallest polygon of each of the 100 posterior tree simulations ($P = 0.088$, Fig. 4D), although it was smaller than any polygons simulated on the MCC tree.

Polygon Position on Y-Axis

The highest single point of a polygon on the Y-axis was significantly higher for the observed polygon than the 10100 simulations ($P = 0.030$, Fig. 4B), as was the mean of points defining a polygon ($P = 0.000$, Fig. 4C). Even when considering the smallest polygons within simulations, the position of the observed polygon was unlikely to be produced under a BM model. It differed in maximum point on the Y-axis ($P = 0.029$, Fig. 4E) and in mean of points making up polygons ($P = 0.010$, Fig. 4F).

DISCUSSION

R.D. Heady Heady (1997)1997) suggested that callitroid thickenings could act as a reinforcement to tracheid walls, preventing tracheid implosion under water stress. Since the pressure required to cause implosion is much more negative than that to cause cavitation (Hacke et al. 2004; Bouche et al. 2014), it seems unlikely that callitroid thickenings limits implosion. If thickenings prevent implosion, we would expect them to be found either in wide, implosion-vulnerable tracheids, where they would allow high conductance without wall collapse, or in narrow tracheids where they could act as a super-reinforcement at very negative pressures. Tracheid width in *Callitris* does not appear to be related to implosion or cavitation risk. This is because wood samples within an individual have both tracheids with and without thickenings, and we found no relationship between the width of tracheids and FCT, whether tracheids had callitroid thickenings or not. Drought-adapted species tended to be smaller in stature, but there was no association between species plant height and FCT, indicating that FCT probably does not prevent tracheid implosion. If it did, taller species from moist environments should have higher FCT.

Callitris species in more arid niches had higher FCT. According to OMI analyses, FCT and TW-*t* explained the position of species niches in environmental ordination space. Tracheid widths in species experiencing low summer rainfall were narrower than those in wet climates, but only tracheids without thickenings became smaller in arid environments. Tracheids with thickenings in arid environments did not become narrower. Therefore, there appears to be a trade-off between the frequency of callitroid thickenings and wider, more efficient unthickened tracheids.

Pit apertures were smaller in drought-adapted species, and became smaller as TW-*t* narrowed, but there was no relationship between pit aperture and TW+*t*. Pit apertures in drought-adapted *Callitris* are not always smaller than in their mesic relatives, and while the smallest pit apertures had the highest FCT, some species with quite large apertures also had high FCT. It therefore seems that not only tracheid widths, but also pit apertures are uncoupled from cavitation resistance in *Callitris*. In particular, in tracheids with callitroid thickenings, pit apertures are not smaller in narrow tracheids. This allows drought-adapted species to maintain high conductance relative to their mesic relatives.

Lack of hydraulic trade-off

These data indicate that the lack of hydraulic trade-off in drought-tolerant *Callitris* might be explained by the presence of callitroid thickenings. Failure of the torus-margo valve is a common cause of cavitation (Choat et al. 2008; Cochard et al. 2009; Delzon et al. 2010; Bouche et al. 2014). Conifers have evolved a tight valve seal by decreasing the pit aperture relative to the pit border margin, which results in reduced conductance, a pattern not detected in *Callitris* (Larter et al. 2017). Callitroid thickenings could prevent deformation of the pit border under extreme water stress, creating a stable surface for the torus to seal against, without sacrificing hydraulically efficient pit apertures. Drought-tolerant Cupressaceae species with lower P_{50} have thickened pit borders (Pittermann et al. 2010), suggesting that weak pit borders may contribute to torus slippage under extreme water stress. Callitroid thickenings could also be reinforcing tracheids to prevent implosion, but as embolised tracheids in *Callitris* do not seem to be repaired (Brodribb and Cochard 2009), it seems far more likely that thickenings assist in preventing the propagation of embolisms throughout the xylem. The frequency of callitroid thickening is convergent in drought-adapted species. Not only do drought-adapted species have higher FCT, they also have more reinforced forms of thickenings (Heady (2000), which is a major indication that thickenings are critical to survival in droughted habitats. Callitroid thickenings might secure cavitation resistance by stabilising pit borders under extremely negative pressures, explaining the lack of a trade-off between conductance and tracheid width or pit diameter.

If FCT secures survival in semi-arid environments, it should be under high selection, yet it showed very high phylogenetic signal and fitted a BM model. This seems surprising, since a common interpretation of traits fitting a BM model is that they are

under drift, not selection. This interpretation stems from two questionable assumptions: that the genes used to construct the phylogeny are evolving under neutral genetic drift (Kimura 1968; Ohta 1992), and that the random walk of the BM model does not have a directional trend toward a selection optimum (Hansen and Martins 1996). If traits are under high selection pressure they should converge in trait space. Our simulations of FCT generated under a BM model showed that FCT clustered in a significantly smaller and more remote area of trait space than the BM simulated data, giving strong evidence that FCT is convergent with aridity. It is highly unlikely that FCT could have evolved by chance under a BM model. In fact, all traits associated with aridity (Table 2), except AI and MAT, had high phylogenetic signal and fitted a BM model. AI fitted a pure speciational model ($\kappa = 0$), indicating that trait evolution is a result of speciation.

The strong BM signal in FCT and TW+*t*, and the speciational model of AI may instead be evidence of ecological speciation in *Callitris*. The aridification of the Australian continent caused genetic bottlenecks in *Callitris* (Sakaguchi et al. 2013), and cryptic species in *C. canescens* and *C. glaucophylla* suggests that population fragmentation has led to speciation (Crisp et al. in prep). If this is so, FCT has been a trait critical to drought adaptation and inseparable from the process of speciation itself. If geographically based environmental conditions have exerted a critical selection pressure, then a high phylogenetic signal might be expected to be the outcome, especially if adaptation has been gradual.

In drought-adapted species cavitation risk is not related to tracheid diameter. Larter et al. (2017) found tracheid diameters in *Callitris* were highly labile. This study also found that tracheids without thickenings fitted a BM model. Tracheid widths with thickenings fitted a white noise model, indicating that evolutionary relationships among species do not shape their evolution. Larter *et al*. (2017) found no evidence of reduced pit conductance in drought-adapted species with high cavitation resistance, and we also found that small pit apertures were not associated with dry environments.

Callitroid thickening is not exclusive to drought-adapted species. It is also found in wet and mesic-dwelling species, but at lower frequencies and in different forms (Heady and Evans 2000). As with FCT, TW-*t* fitted a BM model, and the proportion of TW-*t* varied with climate and tree position. In warm, wet climates, where cavitation risk is low, most tracheids are wide and do not have thickenings. As cavitation becomes more likely

because of drought, the frequency of tracheids with thickenings relative to those without increases, but TW+*t* do not become narrower. This suggests that callitroid thickenings prevent cavitation by reinforcing pits, leaving tracheid and pit dimensions free to optimise conductance. Thus other hydraulic traits might be labile and free to evolve to optimise conductance because callitroid thickening has secured cavitation resistance. In other words, trait lability is not necessarily a sign that traits are under strong selection, nor BM a sign that they are not under strong selection.

Callitroid thickenings are not unique to *Callitris*. Other drought-tolerant cupressoid conifers with high cavitation resistance also have callitroid thickenings, including *Cupressus sempervirens, Juniperus procera* and *Tetraclinis articulata* (Heady 1997; Bouche et al. 2014), implicating callitroid thickening in drought-adaptation. Further studies are needed to investigate how widespread callitroid thickenings are within Cupressaceae and in non-cupressoid conifers with very high cavitation resistance. X-ray tomography (microCT and nanoCT) scanning and 3D imaging offer new opportunities to model hydraulic dynamics in realistic representations of wood structure (Vaziri et al. 2015; Choat et al. 2016; Nolf et al. 2017). Combining hydraulic and genomic methods should lead to a clearer picture of the role of callitroid thickenings in drought-adaptation and in ecological speciation.

Table 1. Phylogenetic signal estimated with Pagel's Lambda and Blomberg's K for the maximum clade credibility (MCC) tree and 100 evenly sampled posterior trees. Significance for the MCC tree was estimated with 1000 permutations of the tip values.

			Pagel's Lambda				**Blomberg's K**			
			MCC Tree		100 posterior trees		MCC Tree		100 posterior trees	
	Trait	Code	λ	*P* value	Mean λ	SD	*K*	*P* value	Mean *K*	SD
Wood Traits	Bordered Pit Diameter	BPD	0.334	0.495	0.332	0.058	0.376	0.397	0.363	0.063
	Pit Aperture Diameter	PAD	0.000	1.000	0.000	0.000	0.341	0.550	0.322	0.049
	Frequency Callitroid Thickening	FCT	0.983	**0.005**	0.949	0.077	1.003	**0.002**	0.953	0.093
	Tracheid Width with Callitroid Thickening	TW+*t*	0.691	1.000	0.301	0.376	0.571	0.051	0.536	0.054
	Tracheid Width without Callitroid Thickening	TW-*t*	0.980	**0.035**	0.936	0.089	0.746	**0.007**	0.725	0.072
	Maximum Height	MaxH	0.901	0.139	0.900	0.085	0.628	**0.037**	0.605	0.084
Climate Traits	Mean Annual Temperature	Bio1	0.548	0.386	0.483	0.105	0.505	0.163	0.462	0.078
	Isothermality	Bio3	0.000	1.000	0.000	0.000	0.274	0.772	0.257	0.056
	Maximum Temperature of Warmest Month	Bio5	0.566	0.232	0.562	0.071	0.488	0.159	0.474	0.072
	Minimum Temperature of Coldest Month	Bio6	0.670	0.112	0.614	0.067	0.565	0.077	0.505	0.081
	Annual Temperature Range	Bio7	0.715	**0.021**	0.688	0.036	0.654	0.053	0.599	0.101
	Mean Temperature of Wettest Quarter	Bio8	0.000	1.000	0.000	0.000	0.398	0.337	0.375	0.049
	Mean Temperature of Driest Quarter	Bio9	0.000	1.000	0.262	0.258	0.489	0.140	0.477	0.056
	Precipitation Seasonality	Bio15	0.000	1.000	0.000	0.000	0.233	0.895	0.214	0.042
	Precipitation of Driest Quarter	Bio17	0.444	0.187	0.452	0.047	0.422	0.255	0.425	0.096
	Precipitation of Warmest Quarter	Bio18	1.102	**0.015**	0.747	0.259	0.664	**0.015**	0.605	0.083
	Precipitation of Coldest Quarter	Bio19	0.000	1.000	0.000	0.000	0.224	0.885	0.217	0.046
	Aridity Index	AI	0.566	0.163	0.528	0.046	0.508	0.084	0.463	0.084
	Outlying Mean Index	OMI	1.072	0.167	0.728	0.294	0.647	**0.016**	0.593	0.080
	OMI Axis1	Axis1	0.000	1.000	0.000	0.000	0.325	0.641	0.304	0.065
	OMI Axis2	Axis2	0.788	**0.023**	0.744	0.050	0.747	**0.010**	0.680	0.092
	OMI Axis3	Axis3	0.000	1.000	0.000	0.000	0.230	0.954	0.224	0.041

Table 2. Best fitting macroevolutionary models according to AICc weights for wood traits (upper panel) and climatic niche traits (lower panel). Parameter = model parameters used to fit model; σ^2 = sigma squared, the variance of the random walk; z0 = estimated root value (log scale); lnL = lognormal likelihood; k = number of parameters in mode; AICc = small sample size corrected Akiake Information Criterion; delta AICc = difference of a given AICc from the best-fitting (lowest AICc) model; rel.LL = relative log-likelihood.

Trait	Model	Parameter	σ^2	z0	lnL	k	AICc	Δ AICc	rel.LL	AICc weight
Frequency Callitroid Thickening	**BM**	–	0.01	-0.79	-13.11	2	30.97	0.00	1.00	0.40
Tracheid Width with Callitroid Thickening	White	–	0.01	1.19	14.50	2	-24.26	0.00	1.00	0.27
Tracheid Width without Callitroid Thickening	**BM**	–	0.00	1.37	14.39	2	-24.04	0.00	1.00	0.38
Pit Aperture Diameter	White	–	0.01	0.54	21.88	2	-39.02	0.00	1.00	0.65
Bordered Pit Diameter	White	–	0.00	1.19	24.50	2	-44.26	0.00	1.00	0.60
Maximum Height	**BM**	_	0.00	1.09	-3.26	2	11.28	0.00	1.00	0.27
Mean Annual Temperature	Kappa	$\varkappa$ = 0.00	0.00	1.23	26.21	3	-44.82	0.00	1.00	0.31
Isothermality	White	–	0.00	-0.30	49.21	2	-93.66	0.00	1.00	0.66
Maximum Temperature of Warmest Month	White	–	0.00	1.47	34.16	2	-63.58	0.00	1.00	0.31
Minimum Temperature of Coldest Month	Kappa	$\varkappa$ = 0.00	0.02	0.76	4.63	3	-1.65	0.00	1.00	0.45
Annual Temperature Range	Lambda	λ = 0.71	0.00	1.33	22.38	3	-37.16	0.00	1.00	0.29
Mean Temperature of Wettest Quarter	White	–	0.02	1.24	11.83	2	-18.90	0.00	1.00	0.60
Mean Temperature of Driest Quarter	White	–	0.01	1.23	16.04	2	-27.34	0.00	1.00	0.42
Precipitation Seasonality	White	–	0.02	1.59	8.41	2	-12.06	0.00	1.00	0.67
Precipitation of Driest Quarter	White	–	0.09	1.97	-3.75	2	12.26	0.00	1.00	0.44
Precipitation of Warmest Quarter	**BM**	–	0.01	2.34	-7.91	2	20.57	0.00	1.00	0.27
Precipitation of Coldest Quarter	White	–	0.06	2.21	-0.37	2	5.49	0.00	1.00	0.67
Aridity Index	Kappa	$\varkappa$ = 0.00	0.02	-0.31	1.28	3	5.03	0.00	1.00	0.32
Outlying Mean Index	**BM**	–	0.00	0.36	22.94	2	-41.13	0.00	1.00	0.25
OMI Axis1	White	–	3.43	-0.38	-38.68	2	82.10	0.00	1.00	0.56
OMI Axis2	**BM**	–	0.27	1.98	-42.90	2	90.55	0.00	1.00	0.24
OMI Axis3	White	–	1.39	0.28	-30.07	2	64.88	0.00	1.00	0.67

Table 3. Significant Phylogenetic GLS results. Regressions between wood traits are shown in grey rows, and regressions of wood traits and climatic traits are in white rows. The first term in each model is the response variable. Results are ranked by AICc weights.

PGLS Model	Intercept	Slope	Lambda	Sigma	R_squared	P value	LogLk	AICc	Δ AICc	rel.LL	AICc weights
FCT ~ PAD	0.879	-3.014	0.742	0.083	0.267	0.023	-10.579	25.907	11.756	0.003	0.003
FCT ~ Axis2	-0.320	-0.196	0.000	0.053	0.699	0.000	-5.602	15.955	0.000	1.000	0.778
FCT ~ AI	-1.029	-1.928	0.000	0.058	0.648	0.000	-7.082	18.914	2.959	0.228	0.177
FCT ~ PNO7	-7.630	5.224	0.001	0.063	0.572	0.000	-8.932	22.614	6.659	0.036	0.028
BPD ~ PAD	0.795	0.724	0.000	0.006	0.692	0.000	35.677	-66.604	0.000	1.000	0.989
BPD ~ TW+*t*	0.685	0.370	0.000	0.008	0.500	0.001	31.090	-57.429	9.175	0.010	0.010
BPD ~ PNO17	0.878	0.155	0.533	0.009	0.436	0.002	30.012	-55.274	0.000	1.000	0.459
BPD ~ Axis2	1.164	0.017	0.000	0.008	0.423	0.003	29.729	-54.708	0.567	0.753	0.346
PAD ~ BPD	-0.593	0.955	0.000	0.007	0.692	0.000	33.057	-61.363	0.000	1.000	0.995
PAD ~ TW-*t*	0.025	0.379	0.000	0.010	0.399	0.004	26.723	-48.696	12.668	0.002	0.002
PAD ~ Axis2	0.513	0.021	0.000	0.009	0.461	0.001	27.754	-50.758	0.000	1.000	0.535
PAD ~ AI	0.586	0.199	0.000	0.010	0.416	0.003	26.995	-49.241	1.518	0.468	0.251
TW+*t* ~ MaxH	0.858	0.309	0.000	0.011	0.675	0.000	25.180	-45.609	0.000	1.000	0.625
TW+*t* ~ TW-*t*	0.075	0.825	1.000	0.016	0.667	0.000	24.665	-44.580	1.029	0.598	0.374
TW+*t* ~ PNO8	0.575	0.505	0.755	0.017	0.406	0.003	19.264	-33.779	0.000	1.000	0.455
TW+*t* ~ PNO1	-0.061	1.010	0.000	0.015	0.359	0.007	18.735	-32.721	1.058	0.589	0.268
TW-*t* ~ TW+*t*	0.396	0.809	1.000	0.015	0.667	0.000	24.846	-44.943	0.000	1.000	0.985
TW-*t* ~ MaxH	1.072	0.276	0.782	0.017	0.469	0.001	20.191	-35.632	9.311	0.010	0.009
TW-*t* ~ PNO18	0.932	0.188	0.874	0.019	0.376	0.005	18.797	-32.844	0.000	1.000	0.437
TW-*t* ~ PNO8	0.683	0.552	0.496	0.016	0.412	0.003	18.648	-32.546	0.298	0.861	0.376
MaxH ~ TW+*t*	-1.521	2.182	0.000	0.028	0.675	0.000	6.622	-8.494	0.000	1.000	0.974
MaxH ~ TW-*t*	-1.247	1.700	0.766	0.041	0.470	0.001	2.941	-1.131	7.363	0.025	0.025
MaxH ~ AI	1.195	0.604	1.000	0.056	0.325	0.011	0.468	3.814	0.000	1.000	0.360
MaxH ~ PNO1	-1.969	2.458	0.000	0.041	0.302	0.015	-0.639	6.029	2.215	0.330	0.119
OMI ~ PNO18	-0.098	0.197	0.861	0.001	0.998	0.000	79.701	-154.653	0.000	1.000	1.000
OMI ~ AI	0.412	0.262	0.000	0.006	0.737	0.000	34.809	-64.867	89.785	0.000	0.000
OMI ~ FCT	0.300	-0.087	0.000	0.009	0.466	0.001	28.085	-51.419	0.000	1.000	0.484
OMI ~ TW-*t*	-0.183	0.393	0.001	0.009	0.440	0.002	27.632	-50.513	0.906	0.636	0.308

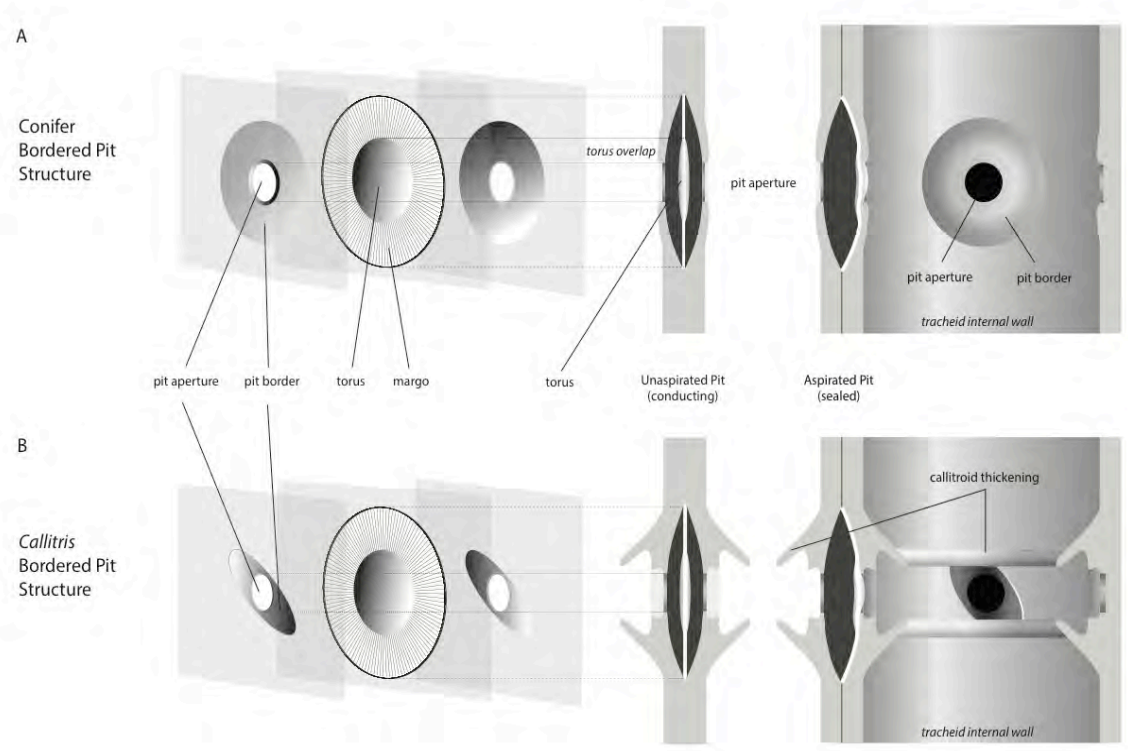

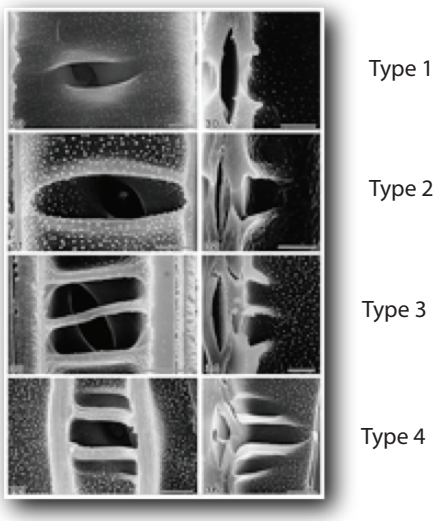

Figure 2. Schematic illustration of conifer tracheids and bordered pits. (A) Depicts a typical conifer pit with the pit structure expanded to show the pit aperture and torus-margo valve (left), and the pit border within a tracheid wall with the pit in an unaspirated an aspirated state (right).; (B) A *Callitris* bordered pit with elliptical cupressoid pits and Type 2 callitroid thickening; (C) SEM photographs of callitroid thickenings and their forms (Type 1–4) taken from Heady's (1997) study.

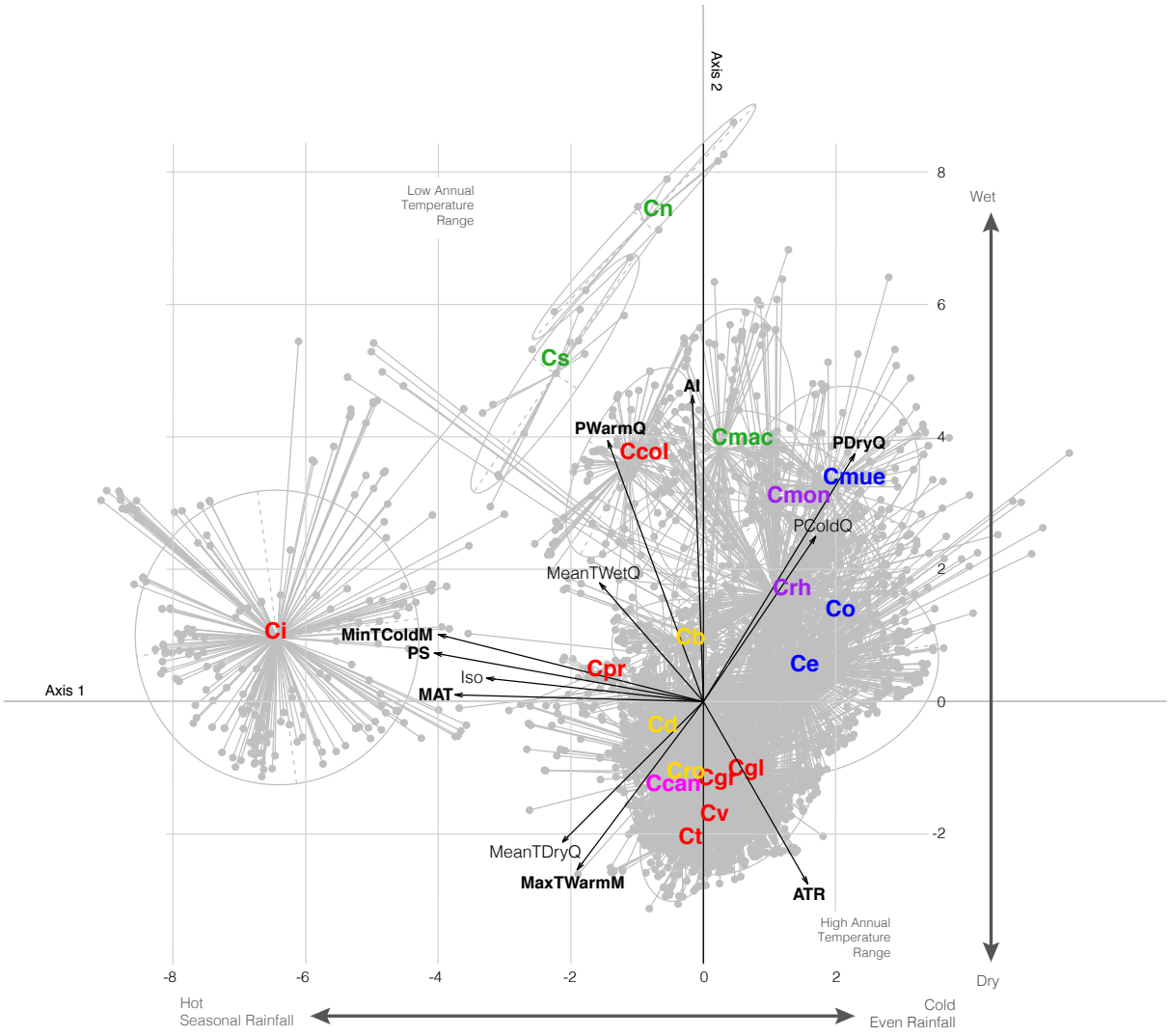

Figure 2. Outlying Mean Index (OMI) analysis showing the two main axes of climatic space and species locations within it. Species niche positions are represented by species name abbreviations, and coloured by subclade. Niches are shown as ellipses and occurrence data as points linked to the niche centroid by lines (all in grey). Black arrows show the correlations of climate variables and main axes. Arrows emerge from the mean of climatic space for all species. Axis 1 is correlated with temperature and rainfall seasonality. Axis 2 is correlated with aridity. *C. intratropica*, *C. neocaledonica* and *C. sulcata* have clearly outlying niches.

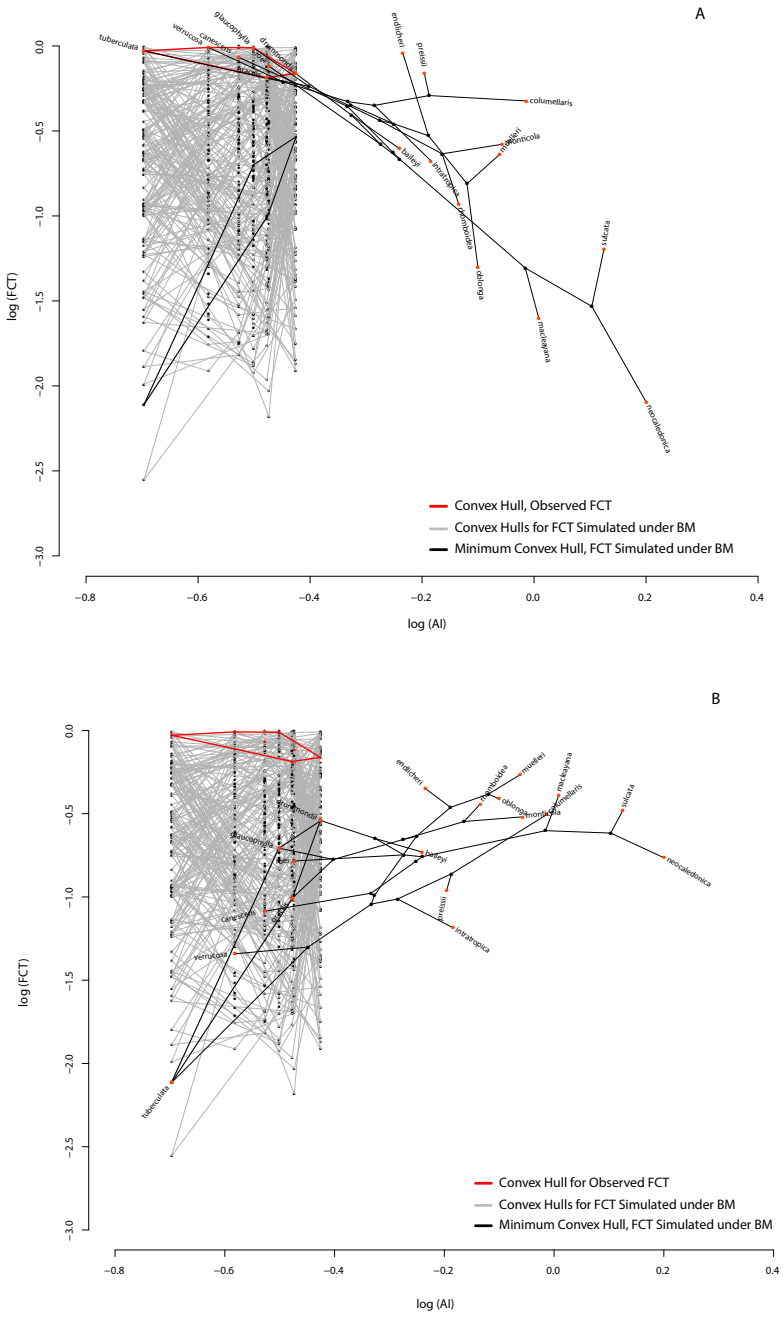

Figure 3. Examples of morphospace polygons based on FCT data simulated under a BM model on the MCC tree. The observed data for semi-arid species is shown as a red polygon, with 100 polygons based on simulations of FCT in grey, and the smallest polygon from the 100 simulations in black. A phylomorphospace plot of the MCC tree is plotted for two morphospace polygons: A) for the observed data, and B) a the simulated polygon. A phylomorphospace plot warps a phylogenetic tree to fit the trait values at the tips. Note that species positions only change on the y-axis. Species positions on the x-axis do not change because AI was not simulated, and remains the same as the observed values.

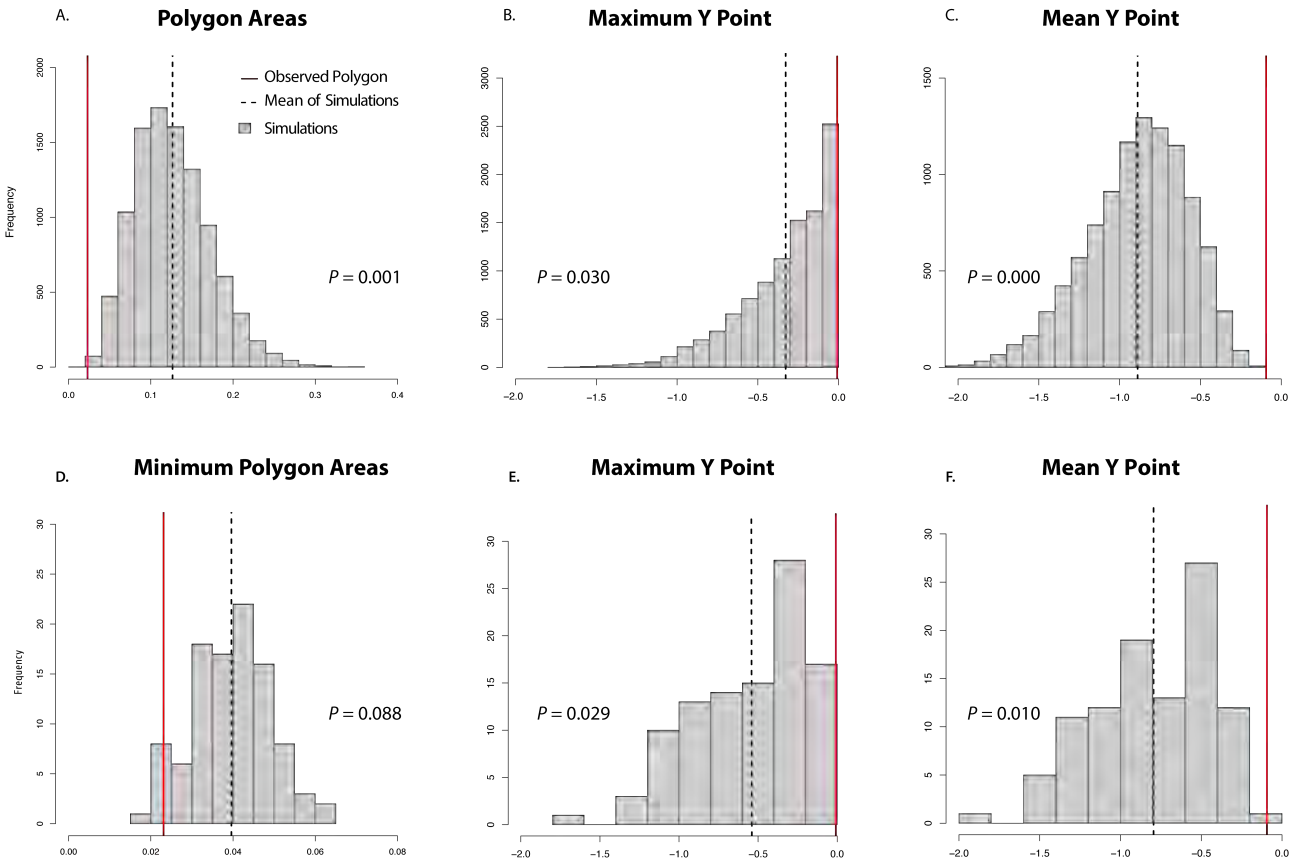

Figure 4. Significance tests comparing observed morphospace polygons to those with FCT modelled under BM. Significance was estimated with permutation tests. A) Area of observed and simulated polygons; B) Highest point on the Y-axis in any polygon; C) Mean of points defining a polygon on the Y-axis; D) Area of observed polygon and the smallest polygon from each simulation set; E) Highest point on the Y-axis of the observed and smallest polygons; F) Mean Y position of the observed and smallest polygons. Simulated polygons are shown as grey bars, the observed data as a red line and the mean of the simulations as a dashed black line. The observed polygon was significantly smaller or higher on the Y-axis in all except D.

SUPPLEMENTARY MATERIAL

Trait macroevolution models

We used eight macroevolutionary models to investigate woody trait and niche evolution in the southern hemisphere conifer, *Callitris*. All analyses were run in the R package geiger (version 2.0.3), using the function fitContinuous (Pennell et al. 2014).

Details of Evolutionary Models

Pagel's lambda (λ), kappa (κ) and delta (δ) are all models based on tree transformations (Pagel 1999). Lambda is a measure of phylogenetic signal according to a Brownian Motion (BM) expectation. When $\lambda=0$ the tree is a single polytomy and there is no influence of phylogeny on trait evolution. When $\lambda=1$, trait evolution is equivalent to a BM model. Values $\lambda > 1$ indicate that traits are more similar than expected among related taxa. Kappa is a punctuational/gradualist model; when $\kappa=0$, branch lengths are all equal and speciation alone accounts for trait evolution. $\kappa > 1$ indicates graduational trait evolution over time, as the influence of elongating branch lengths accounts for more trait change than speciation does. Delta is a rate model in which node depths are raised to the power of δ. When $\delta=0$, there has been no change in the rate over time. When $\delta > 1$ the rate of trait evolution increases exponentially toward the present. The Brownian motion (BM) model is a stochastic drift model, where the trait mean amongst lineages remains zero ($\alpha=0$), but trait variance ($\sigma 2$) increases over time (Felsenstein 1973). The early burst (EB), or adaptive radiation model, uses a rate change parameter (*r*) to model a decelerating rate of trait evolution toward the tips of the tree (Harmon et al. 2010). Trend is a model in which the random walk has a linear trend toward greater or smaller rates over time. The OU model constrains a random walk to a central tendency (θ) with a strength of attraction ($\alpha \neq 0$) to the central tendency (Butler and King 2004). High values of α indicate a stronger attraction to the optimal value θ. OU models can be interpreted as a model of stabilizing or directional selection. We used a single optimum OU model.

Supplementary Table 1. PNO weighted means extracted from MaxEnt models for each species. Weighted means and summary statistics of climatic niche variables from PNO analyses derived from MaxEnt predictions. The weighted mean is the climatic mean weighted by the cumulative probability of the MaxEnt model. MAT = Mean Annual Temperature; MaxTWarmM = Maximum Temperature of Warmest Month; MinTColdM = Minimum Temperature of Coldest Month; ATR = Annual Temperature Range; MeanTWetQ = Mean Temperature of Warmest Quarter; MeanTDryQ = Mean Temperature of Driest Quarter; PS = Precipitation Seasonality; PDryQ = Precipitation of Driest Quarter; PWarmQ = Precipitation of Warmest Quarter; PColdQ = Precipitation of Coldest Quarter.

***Callitris* species**	**MAT (ºC)**	**Isothermality (%)**	**MaxTWarmM (ºC)**	**MinTColdM (ºC)**	**ATR (ºC)**	**MeanTWetQ (ºC)**	**MeanTDryQ (ºC)**	**PS (%)**	**PDryQ (mm)**	**PWarmQ (mm)**	**PColdQ (mm)**	**Aridity Index (MAP/MAE)**
baileyi	17.81	50.99	29.88	3.87	26.01	23.01	12.77	39.90	117.64	324.74	128.82	0.57
canescens	16.97	50.15	30.93	5.70	25.23	12.10	21.06	45.37	48.51	54.79	162.20	0.30
columellaris	19.64	50.44	29.04	8.20	20.84	23.42	15.93	42.67	161.00	473.58	211.77	0.97
drummondii	16.25	53.40	28.62	6.21	22.41	12.12	20.56	39.22	63.07	69.39	177.61	0.38
endlicheri	16.34	48.57	29.89	2.90	26.99	19.52	13.64	31.24	128.38	255.71	156.21	0.58
glaucophylla	17.76	48.15	32.36	3.96	28.40	19.60	16.07	28.88	79.18	137.15	101.61	0.32
gracilis	15.95	49.86	29.94	4.62	25.31	12.26	20.29	31.48	66.54	73.75	143.57	0.33
intratropica	25.80	57.56	35.00	14.55	20.45	27.74	22.35	107.02	18.52	431.97	25.57	0.65
macleayana	16.86	50.10	27.15	5.06	22.09	21.13	12.45	38.28	169.75	455.00	217.82	1.02
monticola	15.96	49.85	27.18	3.47	23.72	20.89	10.98	38.47	153.46	425.17	178.19	0.88
muelleri	15.10	48.27	26.76	2.90	23.86	19.99	10.21	29.84	168.28	342.41	205.94	0.87
neocaledonica	20.71	52.07	27.52	13.69	13.82	23.69	19.67	35.19	281.46	716.19	330.59	1.59
oblonga	12.21	50.50	23.10	3.14	19.95	9.62	16.31	21.69	137.62	140.07	229.04	0.79
preissii	18.69	50.46	30.01	9.58	20.43	15.22	22.67	83.35	40.92	65.21	390.29	0.64
rhomboidea	15.00	49.78	26.76	4.33	22.43	14.69	15.80	33.77	126.25	221.97	216.43	0.73
roei	16.35	51.28	29.91	5.71	24.21	11.93	20.82	44.01	55.93	61.89	175.57	0.34
sulcata	21.32	53.07	28.13	14.17	13.96	24.27	19.97	37.90	237.18	641.87	277.34	1.33
tuberculata	18.72	48.06	33.84	5.04	28.80	17.64	18.61	35.95	43.18	65.92	95.14	0.20
verrucosa	16.61	49.54	31.17	4.47	26.70	13.44	20.17	26.33	63.60	69.21	111.26	0.26
Minimum	12.21	48.00	23.10	2.90	13.82	9.62	10.21	21.69	18.52	54.79	25.57	0.20
Median	16.86	50.00	29.88	5.04	23.72	19.52	18.61	37.90	117.64	221.97	177.61	0.64
Mean	17.58	50.63	29.33	6.40	22.93	18.01	17.39	41.61	113.71	264.53	186.05	0.67
Maximum	25.80	58.00	35.00	14.55	28.80	27.74	22.67	107.02	281.46	716.19	390.29	1.59
Standard Deviation	2.90	2.29	2.75	3.84	20.22	4.14	5.25	3.92	70.59	210.87	84.75	0.38

Supplementary Table 2. Full results from macroevolutionary modelling. Parameter = model parameters used to fit model; $\sigma^{2-sigma}$ squared, the variance of the random walk; z0 = estimated root value (log scale); lnL = log normal likelihood; k = number of parameters in mode; AICc = small sample size corrected Akiake Information Criterion; delta AICc = difference of a given AICc from the best-fitting (lowest AICc) model; rel.LL = relative log-likelihood.

Trait	Model	Parameter		σ^2	z0	lnL	k	AICc	Δ AICc	rel.LL	AICc weight
MAT	**Kappa**	κ =	0.00	0.00	1.23	26.21	3	-44.82	0.00	1.00	0.31
Bio1	White		–	0.00	1.24	24.42	2	-44.08	0.74	0.69	0.22
	OU	α =	0.07	0.00	1.23	25.47	3	-43.33	1.49	0.47	0.15
	Delta	δ =	3.00	0.00	1.23	25.19	3	-42.77	2.05	0.36	0.11
	Lambda	λ =	0.55	0.00	1.24	24.79	3	-41.98	2.84	0.24	0.08
	Trend	slope =	100.00	0.00	1.24	24.55	3	-41.50	3.32	0.19	0.06
	BM		–	0.00	1.24	23.12	2	-41.48	3.34	0.19	0.06
	EB	a =	0.00	0.00	1.24	23.12	3	-38.63	6.19	0.05	0.01
Iso	**White**		–	0.00	-0.30	49.21	2	-93.66	0.00	1.00	0.66
Bio3	OU	α =	0.44	0.00	-0.30	49.21	3	-90.82	2.84	0.24	0.16
	Lambda	λ =	0.00	0.00	-0.30	49.21	3	-90.81	2.85	0.24	0.16
	Kappa	κ =	0.00	0.00	-0.30	46.80	3	-86.01	7.66	0.02	0.01
	Delta	δ =	3.00	0.00	-0.29	45.51	3	-83.43	10.23	0.01	0.00
	Trend	slope =	100.00	0.00	-0.29	44.14	3	-80.69	12.97	0.00	0.00
	BM		–	0.00	-0.29	41.94	2	-79.12	14.54	0.00	0.00
	EB	a =	0.00	0.00	-0.29	41.94	3	-76.27	17.39	0.00	0.00
MaxTWarmM	**White**		–	0.00	1.47	34.16	2	-63.58	0.00	1.00	0.31
Bio5	OU	α =	0.08	0.00	1.46	35.13	3	-62.67	0.91	0.63	0.20
	Lambda	λ =	0.57	0.00	1.46	34.88	3	-62.16	1.42	0.49	0.15
	Kappa	κ =	0.00	0.00	1.47	34.70	3	-61.80	1.78	0.41	0.13
	Delta	δ =	3.00	0.00	1.46	34.54	3	-61.49	2.09	0.35	0.11
	Trend	slope =	100.00	0.00	1.46	33.69	3	-59.79	3.79	0.15	0.05
	BM		–	0.00	1.46	32.02	2	-59.28	4.29	0.12	0.04
	EB	a =	0.00	0.00	1.46	32.02	3	-56.43	7.14	0.03	0.01
MinTColdM	**Kappa**	κ =	0.00	0.02	0.76	4.63	3	-1.65	0.00	1.00	0.45
Bio6	White		–	0.05	0.75	1.80	2	1.15	2.81	0.25	0.11
	Lambda	λ =	0.67	0.00	0.77	3.06	3	1.47	3.13	0.21	0.09
	OU	α =	0.05	0.00	0.74	3.05	3	1.51	3.16	0.21	0.09
	Delta	δ =	3.00	0.00	0.74	2.94	3	1.72	3.38	0.18	0.08
	BM		–	0.00	0.77	1.50	2	1.75	3.40	0.18	0.08
	Trend	slope =	100.00	0.00	0.75	2.60	3	2.39	4.05	0.13	0.06
	EB	a =	0.00	0.00	0.77	1.50	3	4.60	6.25	0.04	0.02
ATR	**Lambda**	λ =	0.71	0.00	1.33	22.38	3	-37.16	0.00	1.00	0.29
Bio7	BM		–	0.00	1.33	20.34	2	-35.93	1.23	0.54	0.16
	Kappa	κ =	0.34	0.00	1.35	21.63	3	-35.67	1.50	0.47	0.14
	OU	α =	0.04	0.00	1.34	21.47	3	-35.34	1.83	0.40	0.12
	Delta	δ =	3.00	0.00	1.34	21.28	3	-34.97	2.20	0.33	0.10
	Trend	slope =	100.00	0.00	1.34	21.14	3	-34.68	2.48	0.29	0.08
	White		–	0.01	1.35	19.70	2	-34.66	2.51	0.29	0.08
	EB	a =	0.00	0.00	1.33	20.34	3	-33.08	4.08	0.13	0.04
MeanTWetQ	**White**		–	0.02	1.24	11.83	2	-18.90	0.00	1.00	0.60
Bio8	OU	α =	0.17	0.01	1.23	11.96	3	-16.31	2.59	0.27	0.16
	Lambda	λ =	0.00	0.00	1.24	11.83	3	-16.05	2.85	0.24	0.14
	Delta	δ =	3.00	0.00	1.23	10.66	3	-13.72	5.18	0.08	0.04
	Trend	slope =	100.00	0.00	1.24	9.82	3	-12.05	6.86	0.03	0.02
	BM		–	0.00	1.24	8.28	2	-11.81	7.10	0.03	0.02
	Kappa	κ =	0.51	0.00	1.22	8.79	3	-9.97	8.93	0.01	0.01
	EB	a =	0.00	0.00	1.24	8.28	3	-8.96	9.95	0.01	0.00

Supplementary Table 2 continued

Trait	Model	Parameter		σ^2	z0	lnL	k	AICc	Δ AICc	rel.LL	AICc weight
MeanTDryQ	**White**		–	0.01	1.23	16.04	2	-27.34	0.00	1.00	0.42
Bio9	OU	α =	0.08	0.00	1.22	16.49	3	-25.39	1.95	0.38	0.16
	Delta	δ =	3.00	0.00	1.22	16.24	3	-24.87	2.47	0.29	0.12
	Lambda	λ =	0.00	0.00	1.23	16.04	3	-24.49	2.85	0.24	0.10
	BM		–	0.00	1.22	14.37	2	-23.99	3.35	0.19	0.08
	Trend	slope =	100.00	0.00	1.22	15.67	3	-23.75	3.59	0.17	0.07
	Kappa	ϰ =	0.73	0.00	1.22	14.52	3	-21.43	5.91	0.05	0.02
	EB	a =	0.00	0.00	1.22	14.37	3	-21.14	6.20	0.05	0.02
PS	**White**		–	0.02	1.59	8.41	2	-12.06	0.00	1.00	0.67
Bio15	OU	α =	0.53	0.03	1.59	8.41	3	-9.21	2.85	0.24	0.16
	Lambda	λ =	0.00	0.00	1.59	8.41	3	-9.21	2.85	0.24	0.16
	Kappa	ϰ =	0.00	0.01	1.61	5.61	3	-3.62	8.44	0.01	0.01
	Delta	δ =	3.00	0.00	1.58	3.72	3	0.17	12.23	0.00	0.00
	Trend	slope =	100.00	0.00	1.58	2.15	3	3.29	15.36	0.00	0.00
	BM		–	0.00	1.58	-0.22	2	5.19	17.26	0.00	0.00
	EB	a =	0.00	0.00	1.58	-0.22	3	8.04	20.11	0.00	0.00
PDryQ	**White**		–	0.09	1.97	-3.75	2	12.26	0.00	1.00	0.44
Bio17	Lambda	λ =	0.44	0.00	2.03	-2.88	3	13.37	1.11	0.57	0.25
	OU	α =	0.11	0.02	2.00	-3.41	3	14.42	2.16	0.34	0.15
	Kappa	ϰ =	0.00	0.04	1.91	-3.88	3	15.35	3.09	0.21	0.09
	Delta	δ =	3.00	0.00	2.03	-4.77	3	17.14	4.88	0.09	0.04
	Trend	slope =	100.00	0.00	2.04	-5.75	3	19.11	6.85	0.03	0.01
	BM		–	0.01	2.05	-7.54	2	19.83	7.57	0.02	0.01
	EB	a =	0.00	0.01	2.05	-7.54	3	22.68	10.42	0.01	0.00
PWarmQ	**BM**		–	0.01	2.34	-7.91	2	20.57	0.00	1.00	0.27
Bio18	Delta	δ =	3.00	0.00	2.31	-7.09	3	21.79	1.22	0.54	0.15
	OU	α =	0.04	0.01	2.31	-7.19	3	21.99	1.41	0.49	0.13
	Trend	slope =	100.00	0.00	2.32	-7.24	3	22.08	1.51	0.47	0.13
	Kappa	ϰ =	0.48	0.02	2.26	-7.41	3	22.42	1.85	0.40	0.11
	White		–	0.15	2.27	-8.93	2	22.60	2.03	0.36	0.10
	Lambda	λ =	1.00	0.01	2.34	-7.91	3	23.42	2.85	0.24	0.06
	EB	a =	0.00	0.01	2.34	-7.91	3	23.42	2.85	0.24	0.06
PColdQ	**White**		–	0.06	2.21	-0.37	2	5.49	0.00	1.00	0.67
Bio19	OU	α =	150.00	18.26	2.21	-0.37	3	8.34	2.85	0.24	0.16
	Lambda	λ =	0.00	0.00	2.21	-0.37	3	8.34	2.85	0.24	0.16
	Kappa	ϰ =	0.00	0.04	2.25	-4.27	3	16.14	10.65	0.00	0.00
	Delta	δ =	3.00	0.00	2.26	-5.89	3	19.37	13.88	0.00	0.00
	Trend	slope =	100.00	0.00	2.27	-7.55	3	22.71	17.22	0.00	0.00
	BM		–	0.01	2.28	-10.05	2	24.84	19.35	0.00	0.00
	EB	a =	0.00	0.01	2.28	-10.05	3	27.69	22.20	0.00	0.00
AI	**Kappa**	ϰ =	**0.00**	0.02	-0.31	1.28	3	5.03	0.00	1.00	0.32
Aridity Index	White		–	0.06	-0.24	-0.42	2	5.59	0.56	0.76	0.25
	Lambda	λ =	0.57	0.00	-0.19	0.55	3	6.50	1.46	0.48	0.16
	OU	α =	0.08	0.01	-0.21	0.24	3	7.11	2.08	0.35	0.11
	Delta	δ =	3.00	0.00	-0.20	-0.27	3	8.14	3.11	0.21	0.07
	BM		–	0.00	-0.18	-2.17	2	0.00	4.06	0.13	0.04
	Trend	slope =	100.00	0.00	-0.19	-0.87	3	9.33	4.30	0.12	0.04
	EB	a =	0.00	0.00	-0.18	-2.17	3	11.95	6.91	0.03	0.01

Supplementary Table 2 continued

Trait	Model	Parameter		σ^2	z0	lnL	k	AICc	Δ AICc	rel.LL	AICc weight
OMI	**BM**		–	0.00	0.36	22.94	2	-41.13	0.00	1.00	0.25
Species'	Delta	δ =	3.00	0.00	0.36	23.84	3	-40.08	1.05	0.59	0.15
Position in	OU	α =	0.04	0.00	0.36	23.73	3	-39.87	1.26	0.53	0.14
OMI Niche	Trend	slope =	100.00	0.00	0.36	23.66	3	-39.71	1.42	0.49	0.13
Space	White		–	0.01	0.35	22.13	2	-39.51	1.62	0.44	0.11
	Kappa	κ =	0.47	0.00	0.35	23.43	3	-39.27	1.86	0.39	0.10
	Lambda	λ =	1.00	0.00	0.36	22.94	3	-38.28	2.85	0.24	0.06
	EB	a =	0.00	0.00	0.36	22.94	3	-38.28	2.85	0.24	0.06
OMI Axis 1	**White**		–	3.43	-0.38	-38.68	2	82.10	0.00	1.00	0.56
	OU	α =	0.20	1.39	-0.29	-38.57	3	84.75	2.65	0.27	0.15
	Kappa	κ =	0.00	1.43	-0.41	-38.67	3	84.94	2.83	0.24	0.14
	Lambda	λ =	0.00	0.08	-0.38	-38.68	3	84.95	2.85	0.24	0.13
	Delta	δ =	3.00	0.13	-0.16	-40.85	3	89.30	7.20	0.03	0.02
	Trend	slope =	100.00	0.00	-0.23	-42.09	3	91.77	9.67	0.01	0.00
	BM		–	0.30	-0.28	-44.17	2	93.09	10.99	0.00	0.00
	EB	a =	0.00	0.30	-0.28	-44.17	3	95.94	13.84	0.00	0.00
OMI Axis 2	**BM**		–	0.27	1.98	-42.90	2	90.55	0.00	1.00	0.24
	Kappa	κ =	0.09	1.65	0.94	-41.71	3	91.03	0.47	0.79	0.19
	Lambda	λ =	0.79	0.17	1.95	-42.00	3	91.60	1.05	0.59	0.14
	OU	α =	0.03	0.43	1.82	-42.26	3	92.12	1.57	0.46	0.11
	Delta	δ =	2.42	0.16	1.78	-42.36	3	92.33	1.77	0.41	0.10
	Trend	slope =	100.00	0.00	1.85	-42.39	3	92.38	1.82	0.40	0.10
	EB	a =	0.00	0.27	1.98	-42.90	3	93.40	2.85	0.24	0.06
	White		–	6.38	1.25	-44.57	2	93.88	3.33	0.19	0.05
OMI Axis 3	**White**		–	1.39	0.28	-30.07	2	64.88	0.00	1.00	0.67
	OU	α =	149.91	415.80	0.28	-30.07	3	67.73	2.85	0.24	0.16
	Lambda	λ =	0.00	0.03	0.28	-30.07	3	67.73	2.85	0.24	0.16
	Delta	δ =	3.00	0.07	0.33	-35.07	3	77.74	12.86	0.00	0.00
	Trend	slope =	100.00	0.00	0.32	-36.56	3	80.72	15.84	0.00	0.00
	Kappa	κ =	0.07	1.01	0.56	-36.75	3	81.10	16.22	0.00	0.00
	BM		–	0.17	0.32	-38.84	2	82.42	17.54	0.00	0.00
	EB	a =	0.00	0.17	0.32	-38.84	3	85.27	20.39	0.00	0.00
FCT	**BM**		–	0.01	-0.79	-13.11	2	30.97	0.00	1.00	0.40
Frequency of	OU	α =	0.00	0.01	-0.79	-13.08	3	33.77	2.80	0.25	0.10
Callitroid	Trend	slope =	0.01	0.01	-0.79	-13.09	3	33.77	2.80	0.25	0.10
Thickening	Delta	δ =	1.15	0.01	-0.79	-13.09	3	33.79	2.82	0.24	0.10
	Lambda	λ =	0.98	0.01	-0.79	-13.11	3	33.81	2.84	0.24	0.10
	Kappa	κ =	1.00	0.01	-0.79	-13.11	3	33.82	2.85	0.24	0.10
	EB	a =	0.00	0.01	-0.79	-13.11	3	33.82	2.85	0.24	0.10
	White		–	0.35	-0.56	-17.01	2	38.77	7.80	0.02	0.01
TW+t	**White**		–	0.01	1.19	14.50	2	-24.26	0.00	1.00	0.27
Tracheid	BM		–	0.00	1.21	14.21	2	-23.68	0.58	0.75	0.20
Width	Delta	δ =	3.00	0.00	1.19	15.21	3	-22.82	1.44	0.49	0.13
with	OU	α =	0.06	0.00	1.19	15.14	3	-22.69	1.57	0.46	0.12
Callitroid	Trend	slope =	100.00	0.00	1.20	14.98	3	-22.35	1.90	0.39	0.10
Thickening	Lambda	λ =	0.00	0.00	1.19	14.50	3	-21.41	2.85	0.24	0.07
	Kappa	κ =	1.00	0.00	1.21	14.21	3	-20.83	3.43	0.18	0.05
	EB	a =	0.00	0.00	1.21	14.21	3	-20.83	3.43	0.18	0.05

Supplementary Table 2 continued

Trait	Model	Parameter		σ^2	z0	lnL	k	AICc	Δ AICc	rel.LL	AICc weight
TW-t	**BM**			0.00	1.37	14.39	2	-24.04	0.00	1.00	0.38
Tracheid	OU	α =	0.01	0.00	1.37	14.48	3	-21.36	2.68	0.26	0.10
Width	Trend	slope =	0.03	0.00	1.37	14.47	3	-21.35	2.69	0.26	0.10
without	Delta	δ =	1.36	0.00	1.37	14.47	3	-21.35	2.69	0.26	0.10
Callitroid	Lambda	λ =	0.98	0.00	1.37	14.40	3	-21.21	2.83	0.24	0.09
Thickening	Kappa	ϰ =	1.00	0.00	1.37	14.39	3	-21.19	2.85	0.24	0.09
	EB		0.00	0.00	1.37	14.39	3	-21.19	2.85	0.24	0.09
	White			0.02	1.35	12.19	2	-19.63	4.41	0.11	0.04
PAD	**White**		–	0.01	0.54	21.88	2	-39.02	0.00	1.00	0.65
Pit	OU	α =	0.29	0.00	0.54	21.92	3	-36.25	2.77	0.25	0.16
Aperture	Lambda	λ =	0.00	0.00	0.54	21.88	3	-36.17	2.85	0.24	0.16
Diameter	Delta	δ =	3.00	0.00	0.54	19.47	3	-31.34	7.67	0.02	0.01
	Kappa	ϰ =	0.00	0.00	0.52	19.47	3	-31.33	7.68	0.02	0.01
	Trend	slope =	100.00	0.00	0.55	18.43	3	-29.26	9.76	0.01	0.00
	BM		–	0.00	0.55	16.65	2	-28.54	10.47	0.01	0.00
	EB	a =	0.00	0.00	0.55	16.65	3	-25.69	13.32	0.00	0.00
BPD	**White**			0.00	1.19	24.50	2	-44.26	0.00	1.00	0.60
Bordered	Lambda	λ =	0.33	0.00	1.19	24.74	3	-41.87	2.38	0.30	0.18
Pit	OU	α =	0.58	0.01	1.19	24.50	3	-41.41	2.85	0.24	0.14
Diameter	Kappa	ϰ =	0.00	0.00	1.18	23.36	3	-39.12	5.14	0.08	0.05
	Delta	δ =	3.00	0.00	1.19	22.44	3	-37.28	6.98	0.03	0.02
	Trend	slope =	100.00	0.00	1.20	21.57	3	-35.54	8.71	0.01	0.01
	BM			0.00	1.20	19.97	2	-35.20	9.06	0.01	0.01
	EB	a =	0.00	0.00	1.20	19.97	3	-32.35	11.91	0.00	0.00
MaxH	**BM**		_	0.00	1.09	-3.26	2	11.28	0.00	1.00	0.27
Maximum	Delta	δ =	3.00	0.00	1.05	-2.47	3	12.55	1.27	0.53	0.14
Height	OU	α =	0.04	0.01	1.06	-2.58	3	12.75	1.47	0.48	0.13
	Trend	slope =	100.00	0.00	1.07	-2.61	3	12.81	1.53	0.47	0.12
	White		_	0.09	1.08	-4.05	2	12.86	1.58	0.45	0.12
	Lambda	λ =	0.90	0.00	1.09	-2.96	3	13.52	2.24	0.33	0.09
	Kappa	ϰ =	0.80	0.01	1.08	-3.15	3	13.91	2.63	0.27	0.07
	EB	a =	0.00	0.00	1.09	-3.26	3	14.13	2.85	0.24	0.06

Supplementary Table 3. Full PGLS results for species position in ordinal niche space, Outlying Mean Index (OMI). Results are ranked by AICc weights, and significant results according to *P* values are marked in bold. Lambda refers to the phylogenetic correction of the regression, which is estimated using the residuals of the Y-axis.

	Intercept	Slope	Lambda	Sigma	R_squared	Pval	LogLk	AIC	AICc	deltaAICc	rel.LL	AICc weights
OMI ~ PNO18	**-0.098**	**0.197**	**0.861**	**0.001**	**0.998**	**0.000**	**79.701**	**-155.403**	**-154.653**	**0.000**	**1.000**	**1.000**
OMI ~ AI	**0.412**	**0.262**	**0.000**	**0.006**	**0.737**	**0.000**	**34.809**	**-65.617**	**-64.867**	**89.785**	**0.000**	**0.000**
OMI ~ Axis2	**0.317**	**0.026**	**0.000**	**0.006**	**0.737**	**0.000**	**34.807**	**-65.614**	**-64.864**	**89.788**	**0.000**	**0.000**
OMI ~ PNO8	**-0.121**	**0.389**	**1.000**	**0.009**	**0.707**	**0.000**	**34.615**	**-65.231**	**-64.481**	**90.172**	**0.000**	**0.000**
OMI ~ PNO17	**0.023**	**0.166**	**0.000**	**0.009**	**0.418**	**0.003**	**27.269**	**-50.538**	**-49.788**	**104.865**	**0.000**	**0.000**
OMI ~ PNO9	**0.824**	**-0.380**	**0.960**	**0.013**	**0.335**	**0.009**	**26.738**	**-49.475**	**-48.725**	**105.928**	**0.000**	**0.000**
OMI ~ Axis3	**0.370**	**-0.027**	**0.799**	**0.012**	**0.307**	**0.014**	**26.188**	**-48.375**	**-47.625**	**107.027**	**0.000**	**0.000**
OMI ~ PNO1	**-0.241**	**0.487**	**1.000**	**0.015**	**0.233**	**0.037**	**25.455**	**-46.910**	**-46.160**	**108.492**	**0.000**	**0.000**
OMI ~ PNO7	**0.986**	**-0.471**	**0.000**	**0.010**	**0.287**	**0.018**	**25.340**	**-46.681**	**-45.931**	**108.722**	**0.000**	**0.000**
OMI ~ Axis1	0.360	-0.006	1.000	0.017	0.040	0.412	23.327	-42.654	-41.904	112.748	0.000	0.000
OMI ~ PNO15	0.278	0.053	1.000	0.017	0.032	0.465	23.247	-42.495	-41.745	112.908	0.000	0.000
OMI ~ PNO19	0.421	-0.026	1.000	0.017	0.022	0.544	23.152	-42.304	-41.554	113.099	0.000	0.000
OMI ~ PNO6	0.326	0.046	1.000	0.017	0.020	0.563	23.132	-42.264	-41.514	113.138	0.000	0.000
OMI ~ PNO3	0.461	0.338	1.000	0.017	0.016	0.612	23.088	-42.177	-41.427	113.226	0.000	0.000
OMI ~ PNO5	1.196	-0.578	0.000	0.012	0.094	0.201	23.069	-42.138	-41.388	113.265	0.000	0.000
OMI ~ FCT	**0.300**	**-0.087**	**0.000**	**0.009**	**0.466**	**0.001**	**28.085**	**-52.169**	**-51.419**	**0.000**	**1.000**	**0.484**
OMI ~ TW-t	**-0.183**	**0.393**	**0.001**	**0.009**	**0.440**	**0.002**	**27.632**	**-51.263**	**-50.513**	**0.906**	**0.636**	**0.308**
OMI ~ TW+t	**-0.067**	**0.355**	**1.000**	**0.014**	**0.316**	**0.012**	**26.542**	**-49.084**	**-48.334**	**3.085**	**0.214**	**0.104**
OMI ~ PAD	**0.039**	**0.575**	**0.000**	**0.010**	**0.339**	**0.009**	**26.062**	**-48.124**	**-47.374**	**4.045**	**0.132**	**0.064**
OMI ~ BPD	**-0.365**	**0.602**	**0.000**	**0.010**	**0.283**	**0.019**	**25.287**	**-46.574**	**-45.824**	**5.596**	**0.061**	**0.030**
OMI ~ MaxH	0.257	0.096	0.954	0.015	0.141	0.112	24.307	-44.615	-43.865	7.555	0.023	0.011

Supplementary Table 3 continued

Model	Intercept	Slope	Lambda	Sigma	R_squared	Pval	LogLk	AIC	AICc	deltaAICc	rel.LL	AICc weights
FCT ~ OMI Axis 2	**-0.320**	**-0.196**	**0.000**	**0.053**	**0.699**	**0.000**	**-5.602**	**15.205**	**15.955**	**0.000**	**1.000**	**0.778**
FCT ~ AI	**-1.029**	**-1.928**	**0.000**	**0.058**	**0.648**	**0.000**	**-7.082**	**18.164**	**18.914**	**2.959**	**0.228**	**0.177**
FCT ~ ATR	**-7.630**	**5.224**	**0.001**	**0.063**	**0.572**	**0.000**	**-8.932**	**21.864**	**22.614**	**6.659**	**0.036**	**0.028**
FCT ~ PWarmQ	**1.080**	**-0.785**	**0.527**	**0.075**	**0.333**	**0.010**	**-10.408**	**24.816**	**25.566**	**9.611**	**0.008**	**0.006**
FCT ~ OMI	**0.636**	**-3.860**	**0.575**	**0.077**	**0.315**	**0.012**	**-10.475**	**24.951**	**25.701**	**11.549**	**0.003**	**0.003**
FCT ~ MaxTWarmM	**-9.881**	**6.258**	**0.642**	**0.082**	**0.233**	**0.036**	**-11.324**	**26.647**	**27.397**	**11.442**	**0.003**	**0.003**
FCT ~ Iso	-2.726	-6.582	1.000	0.106	0.132	0.126	-11.766	27.532	28.282	12.327	0.002	0.002
FCT ~ MinTColdM	-0.283	-0.669	1.000	0.108	0.096	0.196	-12.149	28.299	29.049	13.094	0.001	0.001
FCT ~ PDryQ	1.900	-1.253	0.000	0.076	0.389	0.004	-12.328	28.656	29.406	13.451	0.001	0.001
FCT ~ OMI Axis 1	-0.782	0.044	1.000	0.111	0.052	0.349	-12.605	29.210	29.960	14.005	0.001	0.001
FCT ~ PS	-0.143	-0.412	1.000	0.111	0.044	0.390	-12.685	29.369	30.119	14.164	0.001	0.001
FCT ~ OMI Axis 3	-0.783	-0.036	1.000	0.113	0.019	0.572	-12.926	29.852	30.602	14.647	0.001	0.001
FCT ~ MeanTWetQ	-0.285	-0.408	0.947	0.107	0.017	0.600	-12.963	29.925	30.675	14.720	0.001	0.000
FCT ~ MAT	0.207	-0.809	1.000	0.113	0.014	0.624	-12.971	29.943	30.693	14.738	0.001	0.000
FCT ~ MeanTDryQ	-0.458	-0.277	1.000	0.114	0.004	0.791	-13.069	30.139	30.889	14.934	0.001	0.000
FCT ~ PColdQ	-0.940	0.064	0.999	0.113	0.003	0.826	-13.081	30.163	30.913	14.958	0.001	0.000
FCT ~ PAD	**0.879**	**-3.014**	**0.742**	**0.083**	**0.267**	**0.023**	**-10.579**	**25.157**	**25.907**	**0.000**	**1.000**	**0.652**
FCT ~ TW-t	1.094	-1.370	0.860	0.096	0.103	0.180	-12.213	28.426	29.176	3.268	0.195	0.127
FCT ~ MaxH	-0.275	-0.478	0.993	0.108	0.081	0.239	-12.309	28.618	29.368	3.460	0.177	0.116
FCT ~ BPD	-0.347	-0.371	0.947	0.108	0.004	0.807	-13.087	30.174	30.924	5.016	0.081	0.053
FCT ~ TW+t	-0.927	0.111	0.985	0.112	0.001	0.915	-13.099	30.197	30.947	5.040	0.080	0.052

Supplementary Table 3 continued

Model	Intercept	Slope	Lambda	Sigma	R_squared	Pval	LogLk	AIC	AICc	deltaAICc	rel.LL	AICc weights
TW+t ~ MeanTWetQ	**0.575**	**0.505**	**0.755**	**0.017**	**0.406**	**0.003**	**19.264**	**-34.529**	**-33.779**	**0.000**	**1.000**	**0.455**
TW+t ~ MAT	**-0.061**	**1.010**	**0.000**	**0.015**	**0.359**	**0.007**	**18.735**	**-33.471**	**-32.721**	**1.058**	**0.589**	**0.268**
TW+t ~ PWarmQ	**0.800**	**0.174**	**1.000**	**0.022**	**0.310**	**0.013**	**17.744**	**-31.488**	**-30.738**	**3.041**	**0.219**	**0.099**
TW+t ~ OMI Axis 3	**1.204**	**-0.047**	**0.000**	**0.016**	**0.240**	**0.033**	**17.115**	**-30.230**	**-29.480**	**4.299**	**0.117**	**0.053**
TW+t ~ OMI Axis 1	1.181	-0.027	0.000	0.017	0.193	0.060	16.543	-29.087	-28.337	5.442	0.066	0.030
TW+t ~ MaxTWarmM	-0.573	1.204	0.000	0.017	0.183	0.068	16.425	-28.850	-28.100	5.679	0.058	0.027
TW+t ~ PS	0.746	0.280	0.000	0.017	0.149	0.102	16.043	-28.085	-27.335	6.444	0.040	0.018
TW+t ~ MinTColdM	1.063	0.172	0.000	0.017	0.113	0.160	15.639	-27.278	-26.528	7.251	0.027	0.012
TW+t ~ AI	1.233	0.146	1.000	0.025	0.119	0.147	15.421	-26.842	-26.092	7.687	0.021	0.010
TW+t ~ PColdQ	1.432	-0.109	0.000	0.018	0.057	0.326	15.059	-26.118	-25.368	8.410	0.015	0.007
TW+t ~ OMI Axis 2	1.182	0.012	0.977	0.026	0.058	0.321	14.811	-25.623	-24.873	8.906	0.012	0.005
TW+t ~ Iso	1.505	1.062	0.001	0.018	0.029	0.484	14.784	-25.569	-24.819	8.960	0.011	0.005
TW+t ~ MeanTDryQ	1.459	-0.209	0.898	0.024	0.039	0.416	14.669	-25.338	-24.588	9.191	0.010	0.005
TW+t ~ ATR	1.164	0.028	0.677	0.022	0.000	0.940	14.318	-24.635	-23.885	9.893	0.007	0.003
TW+t ~ PDryQ	1.202	0.000	0.691	0.022	0.000	0.999	14.315	-24.629	-23.879	9.900	0.007	0.003
TW+t ~ OMI	0.885	0.889	1.000	0.022	0.316	0.012	17.815	-31.630	-30.880	14.729	0.001	0.000
TW+t ~ MaxH	**0.858**	**0.309**	**0.000**	**0.011**	**0.675**	**0.000**	**25.180**	**-46.359**	**-45.609**	**0.000**	**1.000**	**0.625**
TW+t ~ TW-t	**0.075**	**0.825**	**1.000**	**0.016**	**0.667**	**0.000**	**24.665**	**-45.330**	**-44.580**	**1.029**	**0.598**	**0.374**
TW+t ~ BPD	**0.263**	**0.783**	**0.000**	**0.016**	**0.214**	**0.046**	**16.793**	**-29.587**	**-28.837**	**16.772**	**0.000**	**0.000**
TW+t ~ PAD	0.868	0.600	0.000	0.017	0.166	0.084	16.226	-28.451	-27.701	17.908	0.000	0.000
TW+t ~ FCT	1.200	-0.002	0.668	0.022	0.000	0.969	14.315	-24.631	-23.881	21.729	0.000	0.000

Supplementary Table 3 continued

Model	Intercept	Slope	Lambda	Sigma	R_squared	Pval	LogLk	AIC	AICc	deltaAICc	rel.LL	AICc weights
TW-t ~ PWarmQ	**0.932**	**0.188**	**0.874**	**0.019**	**0.376**	**0.005**	**18.797**	**-33.594**	**-32.844**	**0.000**	**1.000**	**0.437**
TW-t ~ MeanTWetQ	**0.683**	**0.552**	**0.496**	**0.016**	**0.412**	**0.003**	**18.648**	**-33.296**	**-32.546**	**0.298**	**0.861**	**0.376**
TW-t ~ OMI Axis 2	**1.315**	**0.030**	**0.001**	**0.017**	**0.354**	**0.007**	**16.339**	**-28.678**	**-27.928**	**4.917**	**0.086**	**0.037**
TW-t ~ AI	1.404	0.179	1.000	0.024	0.183	0.068	16.315	-28.631	-27.881	4.963	0.084	0.037
TW-t ~ MAT	0.460	0.736	0.756	0.020	0.180	0.070	16.020	-28.039	-27.289	5.555	0.062	0.027
TW-t ~ OMI Axis 3	1.381	-0.029	0.785	0.021	0.147	0.105	15.691	-27.382	-26.632	6.212	0.045	0.020
TW-t ~ MeanTDryQ	1.678	-0.251	0.943	0.024	0.059	0.315	14.967	-25.935	-25.185	7.659	0.022	0.009
TW-t ~ ATR	2.357	-0.742	0.001	0.018	0.250	0.029	14.924	-25.847	-25.097	7.747	0.021	0.009
TW-t ~ PDryQ	1.155	0.106	0.778	0.022	0.074	0.260	14.903	-25.807	-25.057	7.787	0.020	0.009
TW-t ~ OMI Axis 1	1.370	-0.009	1.000	0.026	0.036	0.434	14.747	-25.494	-24.744	8.100	0.017	0.008
TW-t ~ PS	1.240	0.084	1.000	0.026	0.032	0.460	14.708	-25.416	-24.666	8.178	0.017	0.007
TW-t ~ MinTColdM	1.312	0.078	1.000	0.026	0.024	0.529	14.623	-25.246	-24.496	8.348	0.015	0.007
TW-t ~ MaxTWarmM	0.889	0.332	0.953	0.025	0.015	0.614	14.540	-25.081	-24.331	8.514	0.014	0.006
TW-t ~ Iso	1.493	0.411	1.000	0.027	0.009	0.694	14.483	-24.967	-24.217	8.628	0.013	0.006
TW-t ~ PColdQ	1.407	-0.016	0.965	0.026	0.003	0.833	14.425	-24.850	-24.100	8.744	0.013	0.006
TW-t ~ OMI	1.024	0.963	0.899	0.019	0.381	0.005	18.904	-33.809	-33.059	11.884	0.003	0.003
TW-t ~ TW+t	**0.396**	**0.809**	**1.000**	**0.015**	**0.667**	**0.000**	**24.846**	**-45.693**	**-44.943**	**0.000**	**1.000**	**0.985**
TW-t ~ MaxH	**1.072**	**0.276**	**0.782**	**0.017**	**0.469**	**0.001**	**20.191**	**-36.382**	**-35.632**	**9.311**	**0.010**	**0.009**
TW-t ~ BPD	**-0.250**	**1.352**	**0.000**	**0.015**	**0.500**	**0.001**	**18.776**	**-33.553**	**-32.803**	**12.140**	**0.002**	**0.002**
TW-t ~ PAD	**0.786**	**1.052**	**0.000**	**0.016**	**0.399**	**0.004**	**17.030**	**-30.060**	**-29.310**	**15.633**	**0.000**	**0.000**
TW-t ~ FCT	1.302	-0.090	0.597	0.020	0.153	0.098	15.401	-26.801	-26.051	18.892	0.000	0.000

Supplementary Table 3 continued

Model	Intercept	Slope	Lambda	Sigma	R_squared	Pval	LogLk	AIC	AICc	deltaAICc	rel.LL	AICc weights
PAD ~ OMI Axis 2	**0.513**	**0.021**	**0.000**	**0.009**	**0.461**	**0.001**	**27.754**	**-51.508**	**-50.758**	**0.000**	**1.000**	**0.535**
PAD ~ AI	**0.586**	**0.199**	**0.000**	**0.010**	**0.416**	**0.003**	**26.995**	**-49.991**	**-49.241**	**1.518**	**0.468**	**0.251**
PAD ~ PWarmQ	**0.273**	**0.117**	**0.000**	**0.010**	**0.350**	**0.008**	**25.978**	**-47.956**	**-47.206**	**3.552**	**0.169**	**0.091**
PAD ~ ATR	**1.224**	**-0.507**	**0.000**	**0.010**	**0.324**	**0.011**	**25.597**	**-47.194**	**-46.444**	**4.314**	**0.116**	**0.062**
PAD ~ PDryQ	**0.271**	**0.136**	**0.000**	**0.011**	**0.275**	**0.021**	**24.935**	**-45.870**	**-45.120**	**5.638**	**0.060**	**0.032**
PAD ~ MinTColdM	0.442	0.130	0.000	0.012	0.139	0.116	23.307	-42.613	-41.863	8.895	0.012	0.006
PAD ~ MeanTWetQ	0.291	0.200	0.000	0.012	0.115	0.155	23.048	-42.096	-41.346	9.413	0.009	0.005
PAD ~ MaxTWarmM	1.449	-0.621	0.000	0.012	0.106	0.174	22.947	-41.894	-41.144	9.614	0.008	0.004
PAD ~ PColdQ	0.346	0.087	0.000	0.012	0.079	0.244	22.663	-41.326	-40.576	10.182	0.006	0.003
PAD ~ Iso	0.808	0.910	0.000	0.012	0.047	0.374	22.337	-40.673	-39.923	10.835	0.004	0.002
PAD ~MAT	0.241	0.240	0.000	0.012	0.044	0.388	22.311	-40.623	-39.873	10.886	0.004	0.002
PAD ~ OMI Axis 1	0.537	-0.004	0.000	0.012	0.011	0.670	21.987	-39.975	-39.225	11.534	0.003	0.002
PAD ~ PS	0.587	-0.030	0.000	0.013	0.004	0.802	21.919	-39.838	-39.088	11.670	0.003	0.002
PAD ~ MeanTDryQ	0.570	-0.026	0.000	0.013	0.001	0.887	21.894	-39.788	-39.038	11.720	0.003	0.002
PAD ~ OMI Axis 3	0.538	0.000	0.000	0.013	0.000	0.984	21.883	-39.766	-39.016	11.743	0.003	0.002
PAD ~ OMI	0.333	0.590	0.000	0.010	0.339	0.009	25.814	-47.629	-46.879	14.485	0.001	0.001
PAD ~ BPD	**-0.593**	**0.955**	**0.000**	**0.007**	**0.692**	**0.000**	**33.057**	**-62.113**	**-61.363**	**0.000**	**1.000**	**0.995**
PAD ~ TW-t	**0.025**	**0.379**	**0.000**	**0.010**	**0.399**	**0.004**	**26.723**	**-49.446**	**-48.696**	**12.668**	**0.002**	**0.002**
PAD ~ FCT	**0.493**	**-0.080**	**0.000**	**0.010**	**0.382**	**0.005**	**26.462**	**-48.923**	**-48.173**	**13.190**	**0.001**	**0.001**
PAD ~ MaxH	**0.395**	**0.133**	**0.000**	**0.011**	**0.272**	**0.022**	**24.900**	**-45.799**	**-45.049**	**16.314**	**0.000**	**0.000**
PAD ~ TW+t	0.210	0.276	0.000	0.011	0.166	0.084	23.603	-43.207	-42.457	18.907	0.000	0.000

Supplementary Table 3 continued

Model	Intercept	Slope	Lambda	Sigma	R_squared	Pval	LogLk	AIC	AICc	deltaAICc	rel.LL	AICc weights
BPD ~ PDryQ	**0.878**	**0.155**	**0.533**	**0.009**	**0.436**	**0.002**	**30.012**	**-56.024**	**-55.274**	**0.000**	**1.000**	**0.459**
BPD ~ OMI Axis 2	**1.164**	**0.017**	**0.000**	**0.008**	**0.423**	**0.003**	**29.729**	**-55.458**	**-54.708**	**0.567**	**0.753**	**0.346**
BPD ~ AI	**1.221**	**0.151**	**0.000**	**0.009**	**0.316**	**0.012**	**28.108**	**-52.216**	**-51.466**	**3.808**	**0.149**	**0.068**
BPD ~ PWarmQ	**0.971**	**0.094**	**0.000**	**0.009**	**0.300**	**0.015**	**27.885**	**-51.770**	**-51.020**	**4.254**	**0.119**	**0.055**
BPD ~ ATR	**1.681**	**-0.367**	**0.000**	**0.010**	**0.223**	**0.041**	**26.899**	**-49.799**	**-49.049**	**6.225**	**0.044**	**0.020**
BPD ~ PColdQ	0.953	0.107	0.526	0.011	0.190	0.062	26.581	-49.161	-48.411	6.863	0.032	0.015
BPD ~ MeanTWetQ	0.939	0.199	0.000	0.010	0.150	0.101	26.049	-48.097	-47.347	7.927	0.019	0.009
BPD ~ MaxTWarmM	1.931	-0.505	0.482	0.011	0.087	0.220	25.516	-47.033	-46.283	8.991	0.011	0.005
BPD ~ PS	1.342	-0.094	0.412	0.011	0.059	0.316	25.290	-46.581	-45.831	9.443	0.009	0.004
BPD ~ MinTColdM	1.122	0.084	0.000	0.010	0.077	0.250	25.264	-46.528	-45.778	9.496	0.009	0.004
BPD ~ MeanTDryQ	1.351	-0.128	0.416	0.011	0.042	0.402	25.115	-46.229	-45.479	9.795	0.007	0.003
BPD ~ OMI Axis 1	1.197	0.007	0.510	0.012	0.047	0.371	25.069	-46.139	-45.389	9.885	0.007	0.003
BPD ~ Iso	1.019	-0.598	0.445	0.011	0.031	0.472	24.986	-45.973	-45.223	10.051	0.007	0.003
BPD ~MAT	0.944	0.195	0.000	0.011	0.038	0.422	24.874	-45.747	-44.997	10.277	0.006	0.003
BPD ~ OMI Axis 3	1.194	-0.005	0.298	0.011	0.011	0.670	24.836	-45.672	-44.922	10.352	0.006	0.003
BPD ~ OMI	1.021	0.469	0.000	0.009	0.283	0.019	27.660	-51.319	-50.569	16.035	0.000	0.000
BPD ~ PAD	**0.795**	**0.724**	**0.000**	**0.006**	**0.692**	**0.000**	**35.677**	**-67.354**	**-66.604**	**0.000**	**1.000**	**0.989**
BPD ~ TW-t	**0.685**	**0.370**	**0.000**	**0.008**	**0.500**	**0.001**	**31.090**	**-58.179**	**-57.429**	**9.175**	**0.010**	**0.010**
BPD ~ FCT	**1.155**	**-0.053**	**0.000**	**0.010**	**0.225**	**0.040**	**26.926**	**-49.851**	**-49.101**	**17.503**	**0.000**	**0.000**
BPD ~ TW+t	**0.859**	**0.273**	**0.000**	**0.010**	**0.214**	**0.046**	**26.792**	**-49.583**	**-48.833**	**17.771**	**0.000**	**0.000**
BPD ~ MaxH	1.076	0.101	0.000	0.010	0.207	0.050	26.709	-49.419	-48.669	17.935	0.000	0.000

Supplementary Table 3 continued

Model	Intercept	Slope	Lambda	Sigma	R_squared	Pval	LogLk	AIC	AICc	deltaAICc	rel.LL	AICc weights
MaxH ~ AI	**1.195**	**0.604**	**1.000**	**0.056**	**0.325**	**0.011**	**0.468**	**3.064**	**3.814**	**0.000**	**1.000**	**0.360**
MaxH ~ MAT	**-1.969**	**2.458**	**0.000**	**0.041**	**0.302**	**0.015**	**-0.639**	**5.279**	**6.029**	**2.215**	**0.330**	**0.119**
MaxH ~ PS	**0.202**	**0.559**	**1.000**	**0.060**	**0.227**	**0.039**	**-0.818**	**5.635**	**6.385**	**2.571**	**0.276**	**0.100**
MaxH ~ MinTColdM	**0.620**	**0.609**	**1.000**	**0.060**	**0.224**	**0.041**	**-0.852**	**5.705**	**6.455**	**2.641**	**0.267**	**0.096**
MaxH ~ ATR	3.149	-1.549	1.000	0.061	0.200	0.055	-1.145	6.291	7.041	3.227	0.199	0.072
MaxH ~ OMI Axis 2	0.983	0.052	1.000	0.062	0.174	0.076	-1.452	6.905	7.655	3.841	0.147	0.053
MaxH ~ MeanTWetQ	0.131	0.768	0.736	0.051	0.148	0.104	-1.620	7.240	7.990	4.176	0.124	0.045
MaxH ~ OMI Axis 1	1.071	-0.048	0.828	0.054	0.128	0.133	-1.712	7.424	8.174	4.360	0.113	0.041
MaxH ~ PWarmQ	0.430	0.281	1.000	0.063	0.129	0.132	-1.957	7.914	8.664	4.850	0.088	0.032
MaxH ~ Iso	1.975	3.030	0.908	0.059	0.064	0.295	-2.328	8.656	9.406	5.592	0.061	0.022
MaxH ~ PColdQ	0.829	0.112	0.961	0.064	0.022	0.543	-2.825	9.649	10.399	6.585	0.037	0.013
MaxH ~ OMI Axis 3	1.078	0.023	0.972	0.064	0.020	0.562	-2.884	9.768	10.518	6.704	0.035	0.013
MaxH ~ MeanTDryQ	0.865	0.181	0.909	0.061	0.005	0.777	-2.912	9.825	10.575	6.761	0.034	0.012
MaxH ~ MaxTWarmM	0.644	0.303	0.879	0.060	0.002	0.860	-2.946	9.892	10.642	6.828	0.033	0.012
MaxH ~ PDryQ	1.089	-0.002	0.901	0.061	0.000	0.994	-2.958	9.915	10.665	6.851	0.033	0.012
MaxH ~ OMI	0.549	1.485	0.884	0.055	0.147	0.105	-1.452	6.903	7.653	16.148	0.000	0.000
MaxH ~ TW+t	**-1.521**	**2.182**	**0.000**	**0.028**	**0.675**	**0.000**	**6.622**	**-9.244**	**-8.494**	**0.000**	**1.000**	**0.974**
MaxH ~ TW-t	**-1.247**	**1.700**	**0.766**	**0.041**	**0.470**	**0.001**	**2.941**	**-1.881**	**-1.131**	**7.363**	**0.025**	**0.025**
MaxH ~ PAD	**0.250**	**1.521**	**0.722**	**0.050**	**0.200**	**0.055**	**-1.044**	**6.089**	**6.839**	**15.333**	**0.000**	**0.000**
MaxH ~ BPD	-0.646	1.446	0.744	0.052	0.123	0.142	-1.888	7.777	8.527	17.021	0.000	0.000
MaxH ~ FCT	0.957	-0.163	0.911	0.059	0.078	0.246	-2.187	8.373	9.123	17.617	0.000	0.000

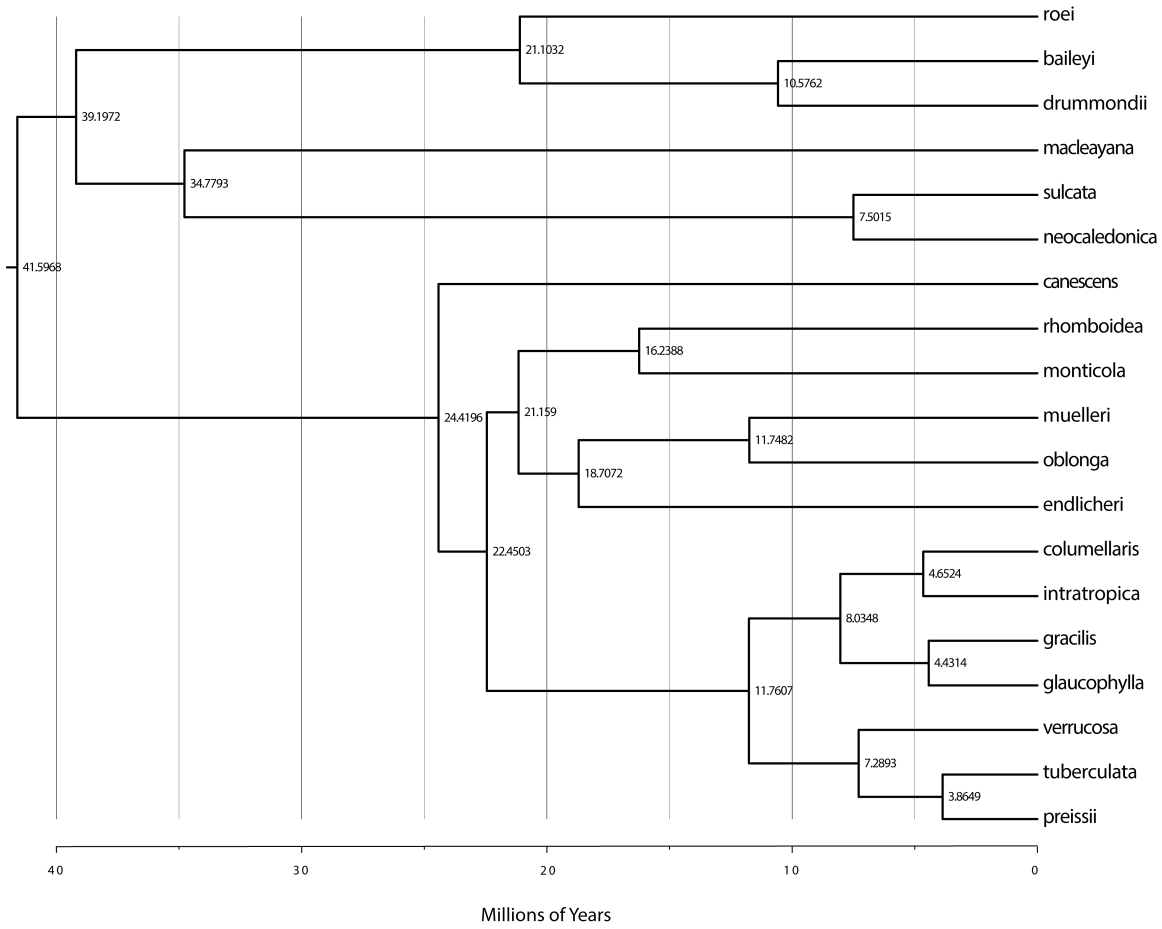

Supplementary Figure 1. BEAST maximum clade credibility (MCC) phylogeny used in for this study. Tips have been pruned to match the Heady (1997) woody trait sampling.

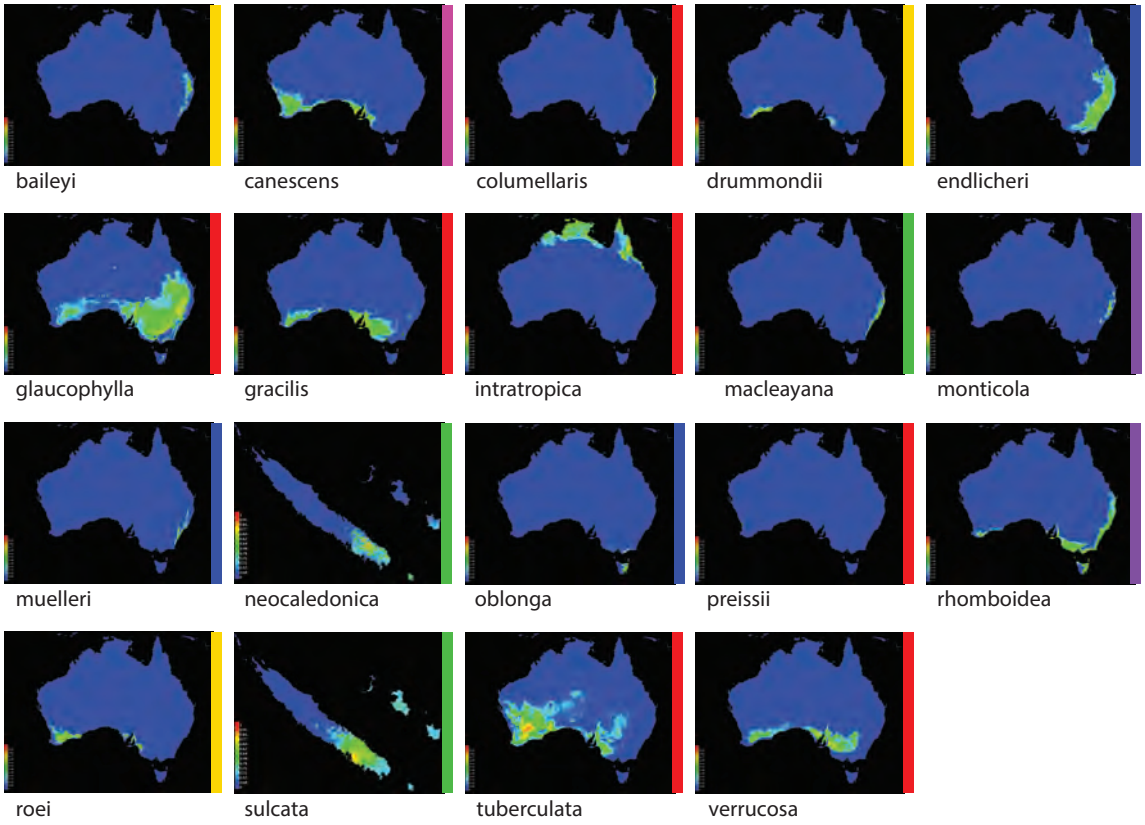

Supplementary Figure 2. Plots showing average MaxEnt predictions of suitable habitats for the 19 *Callitris* species studied. Means are based on 10 replicate runs, each with a different random seed. Colours indicate probability of habitat suitability with blue = 0 (unsuitable) to red = 1 (most suitable). Coloured bars at right hand side of each panel indicates the *Callitris* subclade. Niches were modelled with distributions edited to match Heady's (1999) woody trait sampling and are subsamples of actual ranges for some species (e.g. C. *glaucophylla, C. macleayana*).

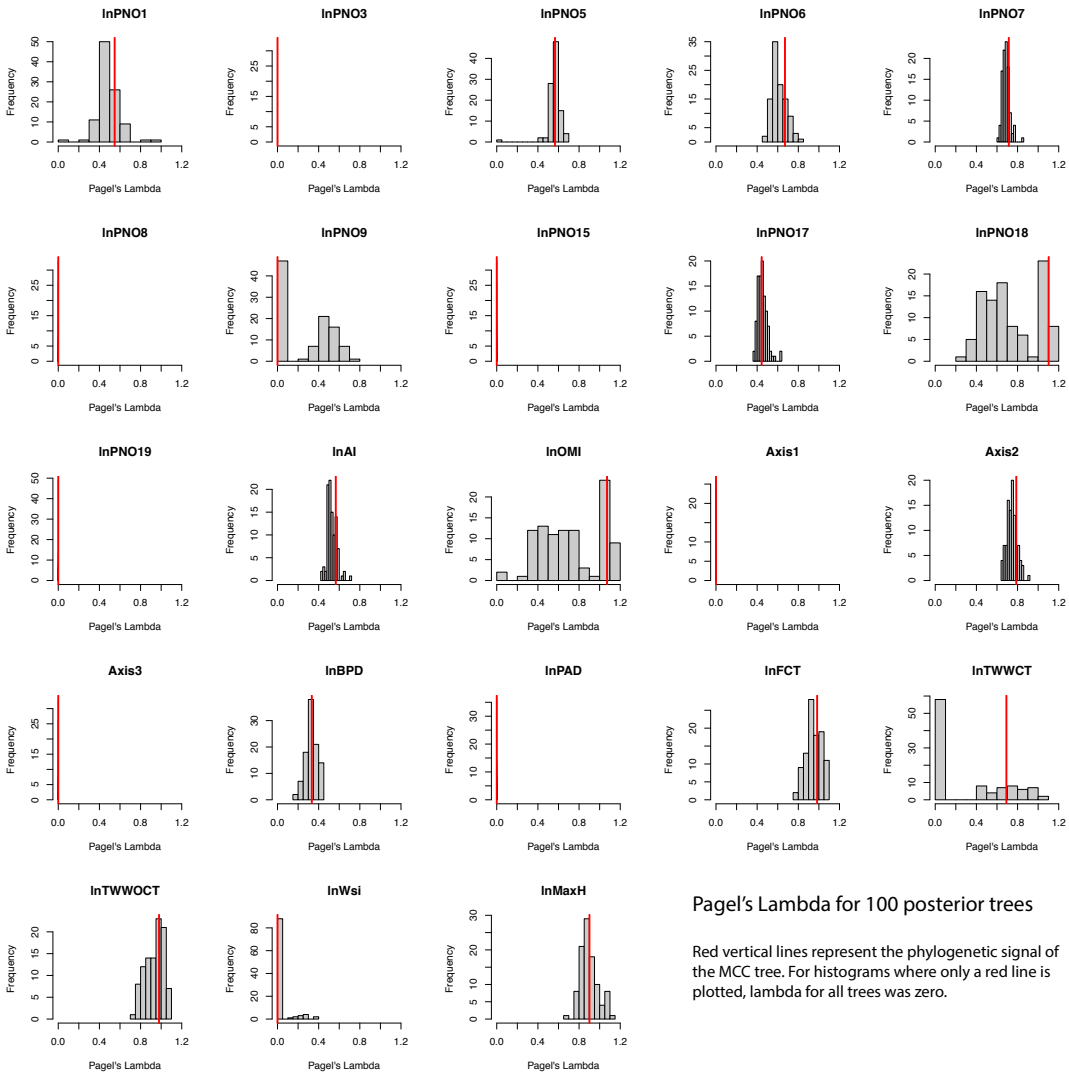

Supplementary Figure 3. Phylogenetic uncertainty according to Pagel's Lambda across 100 evenly sampled post-burnin posterior trees. Compared to the MCC tree there is considerable difference in phylogenetic signal in Precipitation of Warmest Quarter (Bio19), Outlying Mean Index (OMI) and Tracheid Width with Thickenings (TW+t).

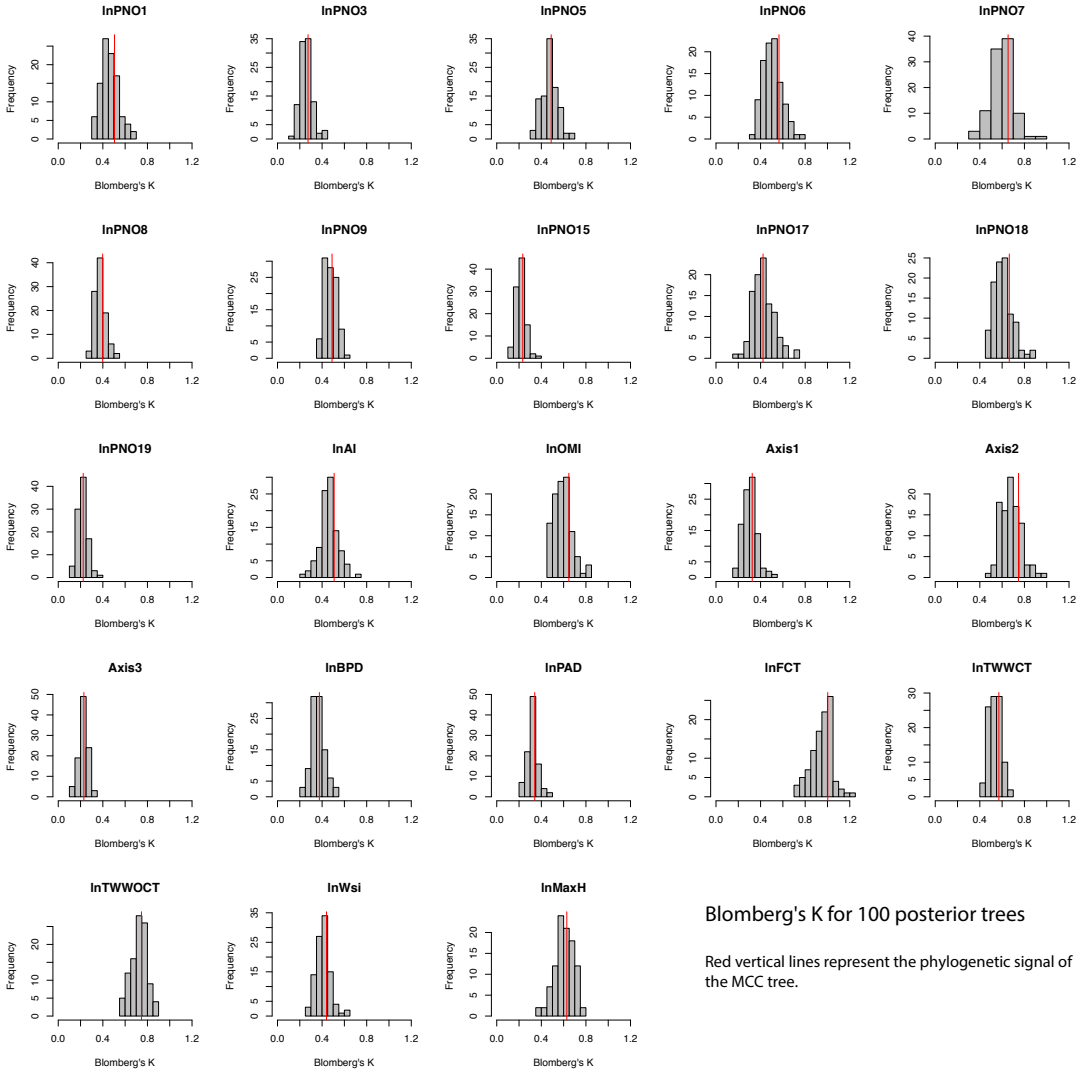

Supplementary Figure 4. Phylogenetic uncertainty according to Blomberg's K across 100 evenly sampled post-burnin posterior trees

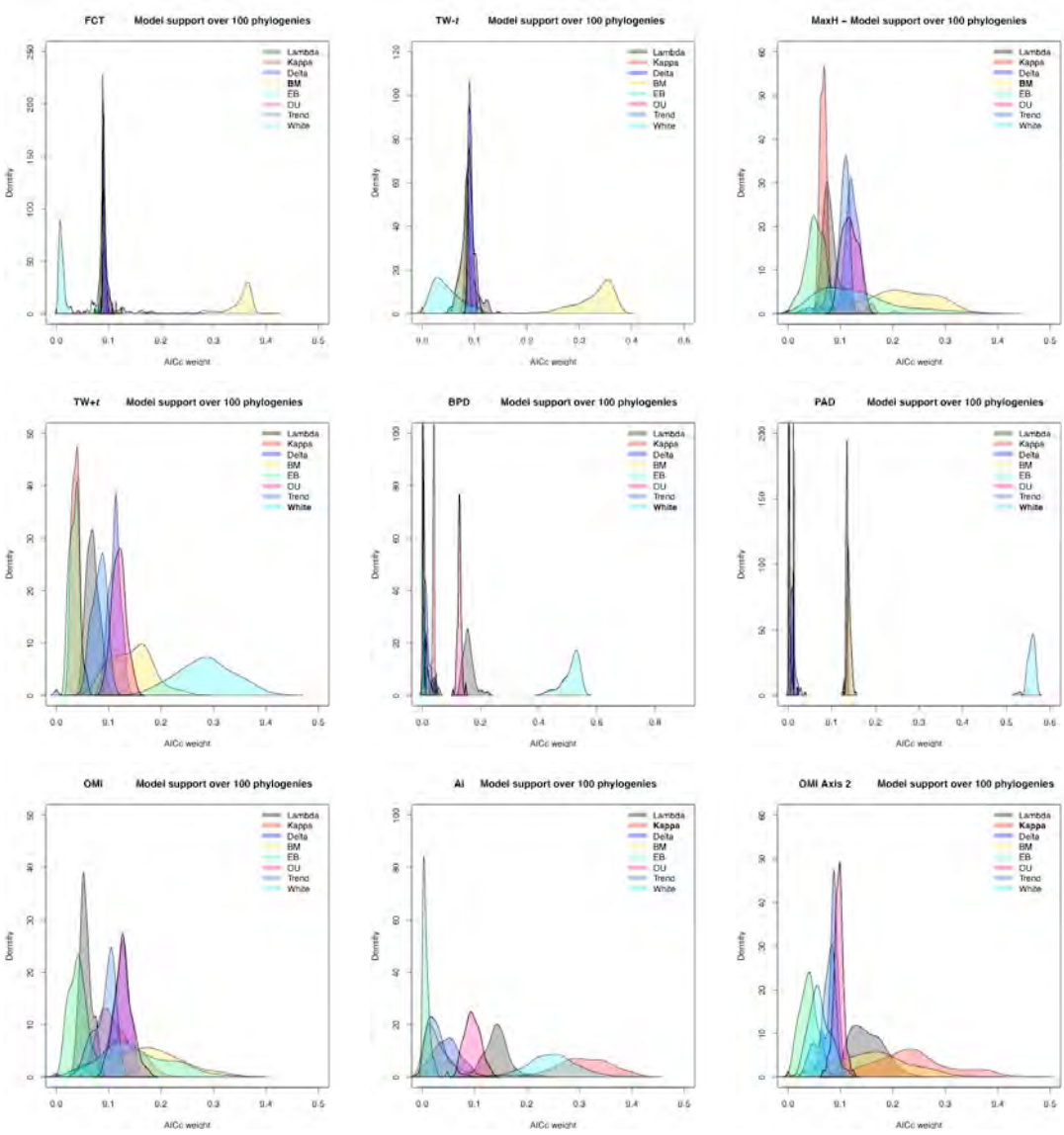

Supplementary Figure 5. Macroevolutionary models across 100 posterior trees. Plots show density curves of AICc weights for the eight models run.

Chapter 2

Not a radiation: *Callitris* climatic niche evolution and diversification

Not a radiation: *Callitris* climatic niche evolution and diversification

ABSTRACT

The evolution of extraordinary drought-tolerance traits in *Callitris* may have enabled it to diversify into novel arid niches. To investigate whether drought adaptation resulted in higher diversification we compared *Callitris* diversification with its nearest relatives, the southern hemishphere Callitroideae. We also investigated whether *Callitris* has a different climate niche from the Rest of the Callitroideae (RoC). Using sister-pair comparisons, we investigated whether species' niches overlapped in climatic niche or geographic range. Finally we modelled how future climate change will affect distribution of drought-adapted Australian *Callitris*. Our results indicate that *Callitris* does not have a higher rate of diversification than the RoC. *Callitris* and RoC climatic niches are partially overlapping and divergent. *Callitris* occupies a hotter, drier and flatter niche than the RoC. It also has a narrower climatic niche, reflecting the low elevation and topographic homogeneity of Australia. Sister-pair comparisons indicated that geographic overlap in Australian *Callitris* explained climatic niche divergence and similarity. Geographic isolation was frequently due to arid barriers. The lack of evidence for an increase in diversification associated with drought-adaption could be because extinctions were high as aridity intensified. Range fragmentation as a result of extinction due to aridity point to geographic speciation, which probably led to the evolution of extraordinary drought-tolerance in *Callitris*. Future climate change predictions suggest that a lack of climatic refugia will lead to range contractions and climatic niche extinctions. Despite its extraordinary drought-tolerance *Callitris* is not predicted to survive increasing aridification as temperatures increase because of low topographic relief in Australia.

INTRODUCTION

Water is critical to plant survival. The capacity to survive water stress is so important that it shapes distributional ranges, species assemblages and biomes (Bartlett et al. 2012; Vicente-Serrano et al. 2013; Donoghue and Edwards 2014; Cook et al. 2015; Greenwood et al. 2017; Trueba et al. 2017). Because plants are sessile, drought stress poses a potentially fatal threat to individuals, populations and species (Allen et al. 2015; Zwieniecki and Secchi 2015).

To evade warming drought stress, plants can track their suitable niche by shifting elevation because lower temperatures reduce evapo-transpiration demand (Kelly and Goulden 2008; Lenoir et al. 2008; Feeley et al. 2011; Wolf et al. 2016). Latitudinal range shifts can also offer an escape from hot climates because temperatures decrease towards the poles (Ordonez and Williams 2013; Boisvert-Marsh et al. 2014; Gonzalez-Orozco et al. 2016). Because plants can only track climatic niches via their progeny, range movement is limited by the high rates of climatic change, frequency of reproductive bouts, distance of propagule dispersal, physical or ecological barriers to establishment and local topography. Topography makes a difference because heterogeneous landscapes have a greater range of climatic niches (Thuiller et al. 2006; Stein et al. 2014). As environments become drier, heterogeneous landscapes provide microclimates and mesic refugia and therefore higher biodiversity (Ackerly et al. 2010). In low elevation regions with little landscape complexity, latitudinal or longitudinal (east-west) tracking are likely because neither elevation nor topographic refugia are available (VanDerWal et al. 2013; Fei et al. 2017).

Over macroevolutionary timescales, some lineages have evolved water-conserving traits that have allowed them to diversify into dry environments. These include reduced plant height in paper daisies (Nie et al. 2016); geophytic tubers in the Ceropegieae (Klak et al. 2017), geophytic bulbs in *Babiana* (Schnitzler et al. 2012), succulence in the Aizoaceae (Klak et al. 2017) and Cactaceae (Hernandez-Hernandez et al. 2014), modified leaf anatomy in *Triodia* (Toon et al. 2015), *Dioon* (Gutiérrez-Ortega et al. 2017) and the Cupressaceae (Pittermann et al. 2012) and CAM photosynthesis in the Agavoideae (Heyduk et al. 2016). Recent diversifications in arid-adapted Australian plant lineages

are likely to involve trait adaptations to drought (Byrne et al. 2008), especially since lineages experiencing aridification that are unable to shift their range or adapt, will become extinct.

Trees are particularly susceptible to drought because they operate close to the limit of water availability, and suffer hydraulic failure when water is limiting (Choat et al. 2012). The safety margin refers to the difference between 'normal', non-damaging water stress experienced in the field (minimum water potential) and the decrease in hydration that causes hydraulic failure. Conifers have larger safety margins than angiosperms because coniferous wood is constructed of small tracheids that are less vulnerable to drought-induced failure. Safety margins are largely independent of environment because all plants utilise the maximum amount of water available in their habitat, whether they are adapted to wet or dry climates. The majority of the world's conifers occupy moist niches (Fragnière et al. 2015), though two lineages have made the transition to semi-arid and arid environments – the pines (Pinaceae) and the cypresses (Cupressaceae). The most drought-tolerant trees in the world belong to the genus *Callitris*, a cupressoid conifer genus endemic to Australia (24 spp.) and New Caledonia (3 spp.).

Callitris is part of the southern hemisphere component of the Cupressaceae, the subfamily Callitroideae. The Cupressaceae is an ancient lineage. The oldest recorded Cupressaceae fossil has been dated to the Middle Jurassic (~170 million years ago (Ma)) (Spencer et al. 2015). Molecular evidence suggests a far earlier emergence in the Triassic or even the Permian, with dates varying between 209–282 Ma (Mao et al. 2012), 192–237 Ma (Yang et al. 2012), and 197–211 Ma (Lu et al. 2014). The Cupressaceae show an ancient divergence between the northern and southern hemispheres, which is assumed to represent the breakup of the supercontinent, Pangaea (Leslie et al. 2012; Mao et al. 2012). This divergence created the northern hemisphere Cupressoideae, and the southern hemisphere Callitroideae. Members of the Callitroideae are found on all of the major landmasses of the southern hemisphere, evidence of a long history of vicariance associated with the breakup of Gondwana and *in situ* diversification.

During the Cenozoic the world became cooler and drier. Late Miocene tectonic activity altered major ocean circulations (Potter and Szatmari 2009) and the climate worldwide, creating novel arid climates (Pound et al. 2012). This climate change initiated high extinction rates in conifers (Crisp and Cook 2011). The fossil record provides evidence that in the past Australian conifer diversity was far higher (Hill 2004). Genera now extinct from Australia but still extant on other landmasses include *Agathis* (Hill et al. 2008), *Austrocedrus* (Paull and Hill 2008) *Dacrycarpus* (Jordan 1995; Lewis and Drinnan 2013), *Dacrydium* (Macphail et al. 1995; Hill and Christophel 2001), *Fitzroya* (Paull and Hill 2010), *Libocedrus* (Whang and Hill 1999) and *Papuacedrus* and *Retrophyllum* (Carpenter et al. 2011).

Callitris is a relatively young clade, with a crown age of ~40 Ma (Crisp, in prep). The first unequivocal appearance of *Callitris* in the fossil record is *Callitris leaensis*, dated to the early Oligocene (~32–30 Ma) where it grew in the ever-wet forests of Tasmania (Paull and Hill 2010). A far younger fossil, *Callitris strahanensis*, is recorded from western Tasmania growing in wet forests during the early to Middle Pleistocene (~2.5–0.7 Ma) (Jordan 1995). Fossil pollen locates cupressoid conifers growing in mesic forests across southern Australia during the warm, wet Early Pliocene (Sniderman et al. 2016). By the Middle Pleistocene (0.7–0.1 Ma), these mesic forests had been replaced by arid shrublands on the Nullarbor, where cupressoids held out until the Last Glacial Maximum (LGM; 20 000 years ago). In south-eastern Australia, rainforests with now-extinct conifers alternated with moist sclerophyll forests until as recently as the Early Pleistocene (Sniderman 2011). Of the Australian conifers, only *Callitris* persisted in the increasingly arid interior, where it experienced severe bottlenecks and range contractions during the LGM (Sakaguchi et al. 2013). The subsequent pollen record suggests that woodland habitats increased following the LGM, and that *Callitris* populations increased (Dodson 1979). Increasing aridity over the last 2000 years has caused range contractions, as has human clearing in the last 200 years (Cupper et al. 2000).

Today, *Callitris* occupies much of the Australian continent (Fig. 1). They are found in subtropical rainforest, temperate forest, coastal margins, open woodlands, semiarid shrublands and desert rangelands. *Callitris* is are absent only from the three most arid areas of the country: a low elevation belt that crosses the country at approximately 20ºS,

comprised of the Great Sandy Desert, most parts of the Tanami Desert and the interior of Queensland; the Lake Eyre Basin, and the Nullarbor Plains.

Callitris are slow growing, long-lived trees. Dendrochronologists have used *Callitris* to reconstruct the Australian climate because its tree rings show a clear growth response to water availability (Haines et al. 2016). Their wide distribution across many habitat types makes them ideal to investigate the dynamics of the monsoon climate (Baker et al. 2008), the arid zone (Cullen and Grierson 2007), and the frequency of historical fires (O'Donnell et al. 2010). The imprinting of climate on the growth rings of *Callitris* is evidence of its adaptation to irregular rainfall in a range of climates.

Aims

Using a new phylogeny of the Callitroideae, constructed with sampling across species ranges and fossil calibrations, we investigate whether drought tolerance in *Callitris* enabled it to diversify into a different climate niche compared to its nearest relatives, the Rest of the Callitroideae (RoC), a paraphyletic group. Firstly we ask whether *Callitris* diversified faster than RoC using Lineage Through Time (LTT) analyses. Secondly, we investigate whether *Callitris* niche space is wider than in the RoC. We first use Principal Coordinates Analysis (PCA) and Ecological Niche Models (ENMs) methods to ask whether *Callitris* has diversified into more arid niches than the RoC, and if there is overlap between *Callitris*–RoC niches. We then investigate niche overlap in sister-species pairs to investigate whether *Callitris* niches are more diverged than RoC niches. Finally, we model *Callitris* niches under climate change models to see how climate change might affect their future distribution and survival.

METHODS

Callitroideae Phylogeny

This study uses a new and improved phylogeny of the southern hemisphere Callitroideae, focussing on the Australian and New Caledonian genus *Callitris* (Crisp, in prep). All species of *Callitris* recognised by Hill (1998) were sampled and the

phylogeny was estimated using Bayesian inference in BEAST ver. 1.8.0 (Drummond et al. 2012), using a relaxed clock. The data comprised DNA sequences obtained using the standard Sanger sequencing method from the chloroplast and three nuclear loci. For this study, the phylogeny was pruned to exclude replicate samples of species (Fig. 2). Callitroideae outgroups were not fully sampled and three absent taxa, *Libocedrus plumosa, Widdringtonia nodiflora* and *Widdringtonia whytei* were manually added to the tree. They were placed according to Farjon (2005) and added midway along the branch of their closest relative as their divergence dates are unknown. The phylogeny identifies a deep (~18.5) divergence between *Callitris canescens* populations from western and eastern Australia. They are therefore treated as two species in this study, *C. canescens* East and *C. canescens* West.

Did *Callitris* diversify faster than the RoC?

Lineages Through Time (LTT)

The phylogeny was used to define the phylogenetic relationships between study taxa, and for Lineages Through Time (LTT) analyses. LLT is a method of investigating the rate of divergence by counting the number of lineages throughout the tree. If diversification has been high, the slope of the LTT line is steep. Long, flat regions in a LTT plot can indicate either late radiation or a period of extinctions (Crisp and Cook 2009). We used Pybus and Harvey's gamma statistic (γ) (Pybus and Harvey 2000) to compare rates of diversification in the Callitroideae, the RoC and *Callitris*. The gamma statistic compares whether branches are longer towards the base of the tree ($\gamma < 0$) or the tips ($\gamma > 0$) relative to a pure-birth model in which branches are evenly spaced (= constant diversification). When $\gamma < 0$ it indicates late speciation or early extinctions, and when $\gamma > 0$, early speciation or late extinction. LTT plots were log transformed and the analysis performed using the R package phytools (Revell 2012).

Is the climatic niche of *Callitris* different from RoC?

Species Occurrence Data

Collection data for all extant southern hemisphere Callitroideae were downloaded from the Global Biodiversity Information Facility (GBIF; http://www.gbif.org/), Australia's Virtual Herbarium (AVH; http://avh.chah.org.au/), Herbarium of the Centre IRD Noumea (NOU; http://herbier-noumea.plantnet-project.org), New Zealand Virtual

Herbarium (NZVH; www.virtualherbarium.org.nz). For some *Widdringtonia* species, vouchered databased collections are depauperate and therefore data from citizen science websites such as iSpot Southern Africa (http://www.ispotnature.org/communities/southern-africa) were accessed. Additional data for *Widdringtonia wallichii* were sourced from White et al. (2016). The data were checked manually for errors in coordinates. Any points plotting in the ocean were replotted based on locality description or removed if the location could not be accurately pinpointed. Recent records were favoured over older records because they were considered to have more accurate global positioning system (GPS) data.

WorldClim Layers and Spatial Projections

Nineteen WorldClim v1.4 (Hijmans et al. 2005) climate raster layers based on data from 1960-1990 were downloaded from WorldClim (http://worldclim.org/). Global Potential Evapo-Transpiration (PET) and Aridity Index (AI) layers were downloaded from the Consultative Group on International Agricultural Research Consortium for Spatial Information (CGIAR-CSI, http://www.cgiar-csi.org/data/global-aridity-and-pet-database). Altitude data was sourced from the Shuttle Radar Topography Mission (SRTM) digital topographic data at a 30-arc second resolution. STRM v2.1 layers were downloaded from the U.S. Geological Survey (USGS) at https://dds.cr.usgs.gov/srtm/version2_1/SRTM30/.

Environmental Niche Models (ENMs)

ENMs were used to model climatic niches in an explicitly geographic context. ENMs were created with the base Bioclim layers (Bio 1-19) in MaxEnt (Steven and Miroslav 2008). The Bioclim layers are temperature and precipitation variables that define the major contributors to the world's climates. Many of the Callitroideae are threatened or endangered and MaxEnt has been shown to perform well even when using a low presence number (Pearson et al. 2007). We ran ten cross-validated runs of MaxEnt models with default settings, using the complementary log-log (cloglog) transformation to estimate the probability of species occurrences (Phillips et al. 2017). Future climate models were run for the two emission scenarios for 2050 and 2070 using Bioclim v1.4 rasters. All Bioclim layers were clipped to the relevant landmass limits and projected into a region-specific equal areas projection using QGIS (QGIS). Data for Antarctica

are not included in v1.4 Bioclim data and it is therefore not in any future climate models.

The MaxEnt prediction layers were converted into suitable climatic ranges, using the ten percentile training presence Cloglog threshold to create binary layers, where cells with values above the threshold = 1, and those below = 0. This threshold excludes presences that fell into the lowest 10 percent of the MaxEnt training model for a species, and effectively means excluding outliers. This is desirable in terms of constructing a niche model with improved prediction accuracy, but it also excludes records from range edges, locations often associated with niche adaptation. As this study does not address the process of niche adaptation, this limitation was not a concern. Suitable habitat layers were used to calculate predicted range area, elevation and slope. Range area was calculated from suitable habitat raster layers in Whitebox (Lindsay 2016) in square metres, and converted to square kilometres. Elevational data were extracted from the STRM layer by creating clipping masks from suitable habitat layers. Slope was calculated in QGIS using the Zevenbergen & Thorne method (Zevenbergen and Thorne 1987), expressed as percentage slope. Latitude was estimated by creating centroids for the suitable habitat range. All spatial analyses were carried out in QGIS and R (R Core R-Core-Team 2017).

Climatic Niches in Geographic Space

To investigate overlap in geographic space, pairwise species comparisons were made between suitable habitat rasters for all sister pairs. Because callitroid species are all endemic to a single landmass, comparisons were calculated at a landmass level. Analyses were run in the R package ENMeval (Muscarella et al. 2014) using the function `calc.niche.overlap`, which can compare multiple raster layers. Geographic overlap was calculated for predicted suitable habitat for 1960-90.

Climatic Niches in Ordination Space

We used spatial data extracted from occurrence records to estimate niche overlap between sister-species and at clade level, comparing *Callitris* with the rest of the Callitroideae (RoC). We used Principal Coordinate Analysis (PCA) to define species niches within coordinate climate space, according to presences and background data.

Following Broennimann (2012) the environmental PCA space was gridded into a raster layer and species occurrences modelled as a density kernel. The density kernel is used a smoother species occurrences across each cell of the environmental ordination space. This method has the advantage of making it possible to compare niches within a non-geographic framework, and is ideal in this case because, with the exception of Antarctica, the Callitroideae span the continents of the southern hemisphere. It also facilitates accounting for species occupancy when calculating niche overlap, and therefore contributes extra information about niche utilisation. We used niche overlap analysis to compare clade-level and sister pair niche differentiation.

Background data for the southern hemisphere was created by generating 50 000 random points across the landmasses of southern hemisphere. Species occurrence climatic data was extracted from Bioclim layers, and from additional rasters containing PET, AI, Altitude and Slope data. We used all layers in the analysis as the range of climatic ranges across the southern hemisphere is vast, and while some variables are highly correlated, their covariation is likely to change across extensive climatic regions. Therefore, excluding variables may lead to a lack of information about niche-specific covariances. Point climatic data for background and species occurrences were extracted using the Point Sampling Tool in QGIS (QGIS). All analyses were carried out in the R package ecospat (Di Cola et al. 2017).

Species Position and Species Niche Breadth

Outlying Mean Index (OMI) is a two-table form of canonical analysis (Dolédec et al. 2000) which can be used to estimate species niche position and niche breadth within climatic ordination space. A first principal coordinate analysis (PCA) creates environmental ordinate space for all species based on climatic point data. The centroid of the first PCA represents the mean environmental conditions for all species. A second PCA, orthogonal to the first, defines species niche positions, which lie a marginal distance from the mean environmental conditions for all species. OMI analysis was performed on the same PCA of environmental space used in niche overlap analysis.

Callitris–RoC Niche Differences

We used non-parametric Mann-Whitney U ranked tests to investigate *Callitris*–RoC differences in climate niche space, species position, niche breadth, AI, suitable habitat area, altitude, slope and latitude. To investigate whether adaptation to drought was correlated with range area and/or altitude, we used phylogenetic generalised least squares (PGLS) (Grafen 1989; Martins and Hansen 1999). We tested the correlation under three different tree branch modification methods lambda(Pagel 1999) (λ), which tests whether the correlation is predicted by the phylogeny or not; delta (δ), which tests for changes in the rate of correlated traits; and kappa ($\varkappa$), which tests whether trait correlation is associated with speciational or gradual evolution.

Niche Overlap in Sister Groups

We compared niche overlap between the *Callitris* and their nearest relatives, the rest of the Callitroideae (RoC) conifers using Schoener's D (*D*) and Warren's I (*I*) indexes. Schoener's D was developed in an ecological framework, and used to compare the frequency of species' niche utilisation (Schoener 1970). It therefore interprets the frequency of occupancy as having ecological significance, and uneven sampling ('utilisation') is considered to be biologically meaningful. Warren's *I* incorporates *D* with Helliger's distance, treating sampling densities as probability distributions to avoid direct ecological implications associate with frequency of use (Warren et al. 2008). For both indexes, niches are identical when equal to one, and have no overlap when equal to zero.

Niche Equivalency and Similarity in Sister Groups

Niche equivalency compares two species' niche overlap to a null model of overlap, constructed by randomly sampling the combined overlap of both species across climatic space. Overlap is measured with *D* or *I*. Niche similarity tests whether niches are similar by making reciprocal random draws of overlap from the each species' niche. If they describe the species' niche better than the null distribution of the combined niche, they are considered to be more similar. In other words, niche equivalency considers whether niches are clustered in ordination space, and niche similarity considers whether niches overlap. Significance for *D* and *I* was estimated by permutation testing using 1000 replicates. One-sided permutation tests were used to investigate if niches were more or less equivalent or similar than the null distribution. If the observed was greater than the

null distribution, the niches were more equivalent or similar than expected, indicating niche conservatism. When the observed value was lower, the niches were less similar than expected, indicating niche divergence.

Effect of climate change on future distribution of the Callitroideae

Future Climate Models

Future climate models for 2050 and 2070 from the Coupled Model Intercomparison Project Phase 5 (CMIP5) were downloaded from Worldclim (http://www.worldclim.org/CMIP5v1). The CMIP5 project couples different models of atmospheric, land, ocean, sea-ice and geological data to create global climate models (GCMs) for different emission scenarios, time periods and baseline data (Taylor et al. 2012). We used the Australian Community Climate and Earth System Simulator ACCESS 1.0 GCM (Bi et al. 2013), conditioned on the Bioclim v1.4 climate layers, under two Representative Concentration Pathways (RCP) scenarios. RCP scenarios model greenhouse gas emissions resulting from CO2 emissions, other greenhouse gases associated with pollution levels and land use intensity (IPCC).

We used two RCP scenarios to model suitable habitat niches in Australian *Callitris* under moderate and extreme climate change:

1. RCP 4.5: Intermediate greenhouse gas emissions, equivalent to a global temperature increase of 1.1–2.6 ºC by the end of the 21st century. Under this scenario, CO2 concentrations rise from the present ~ 400 ppm to 580–720 ppm.

2. RCP 8.5: Very high emissions equivalent to a global temperature increase of 2.6–4.8°C by the end of the 21st century. Under this scenario, CO_2 concentrations will rise to 720 to > 1000 ppm.

ACCESS 1.0 model predictions have been shown to perform well in predicting recent past climates in the southern hemisphere, and particularly in Australia (Moise et al. 2015). Predicted range size was based on suitable habitat estimated as described above. We compared predicited suitable habitat ranges for 1960-90 to ranges predicted by 2050 and 2070 future climate models unfor both emission scenarions. The 1960-90 ranges were taken as the baseline range, and the change in predicted geographic range expressed as a percentage.

RESULTS

Did *Callitris* diversify faster than the RoC?

Lineages Through Time

Lineages through time show did not show higher diversification in *Callitris* than in RoC (Fig. 2). The γ-statistic for all three groups was non-significant. Gamma was positive for the Callitroideae ($\gamma = 1.2983$, $P = 0.194$) and the RoC ($\gamma = 1.6419$, $P = 0.101$), showing a trend towards recent diversification or earlier extinctions, but negative for *Callitris* ($\gamma = -1.2873$, $P = 0.198$) reflecting a trend towards recent extinction or early diversification. The LTT plots show that the RoC and *Callitris* have had higher diversification in the last ~10 Ma. Long branches from this period suggest previous high extinctions.

Is the climatic niche of *Callitris* different from RoC?

Callitroideae ENMs and Suitable Habitat

The average area under the curve (AUC) for all MaxEnt models ranged from 0.84 to 1.00, indicating that models were able to predict test presences with high accuracy. Lower AUC values were associated with species that have large geographical ranges and/or widely dispersed presences. The majority of the predictions matched the observed presence data, but with some key exceptions: seven of the 24 Australian *Callitris* species (*Callitris canescens* East and West, *C. drummondii, C. gracilis, C. rhomboidea, C. roei*, and *C. tuberculata*) occur on the eastern or western side of Australia, but were predicted to occur on both sides.

PCA Climatic Niches

The first two axes of the PCA ordination space accounted for 71% of the variability in the climatic data (Table 1, Fig 3). Axis 1 (43%) was associated with the Maximum Temperature of Warmest Month (Bio5), Potential Evapo-Transpiration (PET) and the Mean Temperature of Warmest Quarter (Bio10). Axis 2 (27.9%) was associated with

the Minimum Temperature of the Coldest Month (Bio6), Mean Annual Precipitation (Bio12), and Precipitation of Wettest QuarterBio16) (Fig. 3).

Callitris–RoC Niche Differences

Differences between *Callitris* and RoC climatic niches were associated with PCA Axis 1 (Mann–Whitney U test: $P = 0.000$), but not PCA Axis 2 (Mann–Whitney U test: $P = 0.224$) (Fig. 4). *Callitris* and RoC had different species position (OMI) in ordination space (Mann–Whitney U test: $P = 0.000$), and *Callitris* had narrower niches than RoC (Mann–Whitney U test: $P = 0.034$). *Callitris* had more arid niches (Mann–Whitney U test: $P = 0.000$) at lower altitudes ($P = 0.000$) and species occurred on shallower slopes ($P = 0.000$). There were no significant differences between the two in latitude ($P = 0.501$) or range size ($P = 0.161$) (Table 1, Fig. 4).

PGLS analysis revealed that drier niches tended to be larger (Table 2), but the association was quite weak ($r^2 = 0.22$). All models found significant correlations between range area and AI, but AICc weights could not discriminate between the three 'best' models. The lambda model had the highest AICc weight ($\lambda = 0$, $P = 0.003$, *AICCw* = 0.37), indicating that phylogenetic relationships did not predict the evolution of large, dry niches. The second most probable model was a speciational model in which both AI and Altitude (Alt) were associated with range size ($\varkappa = 0$, P (AI) = 0.004, P (Alt) = 0.02, *AICCw* = 0.29). Three species had much smaller ranges than predicted by the regression: *Callitris preissii, Libocedrus chevalieri* and *Widdringtonia wallichii*. The last two species are critically endangered (IUCN). Altitude was weakly associated with range size ($r^2 = 0.14$) and was a poor model according to AICc weights (Table 2).

Callitris–RoC Geographic and Climatic Niche Overlap

Schoener's *D* and Warren's *I* interpret presence data differently. The Broennimann PCA method uses presences to create a density smoother indicating regions of high occupancy in climatic niche space. As overlap was calculated on data containing information about occupancy, results in text are presented for Warren's *I*. For reference, both measures are presented in Table 3. *Callitris* and RoC had very low geographic overlap ($I = 0.001$). Geographic overlap is only found in New Caledonia, where *Callitris* and *Libocedrus* species co-occur. Climatic niche overlap was much higher than

geographic overlap ($I = 0.56$). *Callitris*–RoC niches were not identical ($P = 0.038$), but they were more similar than expected ($P = 0.001$), reflecting niche overlap in *Callitris* and *Widdringtonia*, and the New Caledonian *Callitris* and *Libocedrus* species (Fig. 3).

Sister Species Overlap

Five out of nine *Callitris* sister-pairs had less equivalent climatic niches than expected (Table 3, Fig. 5), indicating niche divergence: *C. canescens* East–*C. canescens* West (Fig 5B); *C. columellaris*–*C. intratropica* (Fig. 5C)*; C. drummondii*–*C. baileyi* (Fig. 5D); *C. muelleri*–*C. oblonga* (Fig. 5F) and *C. tuberculata*–*C. preissii*, (Fig. 5H). In four of these pairs at least one sister species has a dry niche. *C. tuberculata*–*C. preissii* were less equivalent and less similar than expected. This sister-pair have no overlap in geographic ($I = 0.000$) or climatic space ($I = 0.000$), yet the nearest collections in this dataset lie only 30 km apart, and the predicted suitable habitat ranges are even closer. Two pairs (*C. glaucophylla*–*C. gracilis* and *C. rhomboidea*–*C. monticola* (Fig. 5E and 5G) were more similar than expected in their climatic niches. *C. glaucophylla*–*C. gracilis* share dry niches. Their geographic overlap is relatively low ($I = 0.26$) because *C. glaucophylla* has an extensive range that encompasses all but the most southerly range of *C. gracilis*. *Callitris rhomboidea*–*C. monticola* share moist niches along the coastal ranges. In contrast, the New Caledonian pair *Neocallitropsis pancheri*–*C. neocaledonica* (Fig. 5I) had high geographic and climatic overlap, yet their niches were neither conserved nor diverged, indicating little niche differentiation.

In the RoC, the sister pair *Diselma*–*Fitzroya* (Fig. 5J) had divergent niches ($P\ (I) = 0.027$) because they occur on different landmasses: *Diselma* is endemic to Tasmania and *Fitzroya* to Chile and Argentina. Within the RoC, the New Zealand *Libocedrus* species (Fig. 5L) had the highest geographic niche overlap ($I = 0.213$), but were the most diverged sister-pair ($P\ (I) = 0.007$). *Libocedrus bidwillii* encompasses most of the climatic niche space of *L. plumosa*, which has a smaller, mostly North Island climatic niche. *Widdringtonia wallichii* and *W. schwarzii* climatic niches were more similar than expected ($I = 0$, $P = 0.049$) despite no geographic overlap. *Libocedrus* sister pairs in New Caledonia had neither diverged nor more conserved climatic niches (Table 3).

Regression of geographic and climatic niches found that niche divergence in Australian *Callitris* was largely due to low geographic overlap ($df = 6$, $t = 3.43$, $P = 0.014$), but not in *Callitris* with New Caledonian species included ($P = 0.062$) or RoC ($P = 0.382$).

Effect of climate change on future distribution of the Callitroideae

Callitris Future Climatic Niches

Mean annual temperature across the current *Callitris* range is predicted to increase up to 3 ºC, from 17.1 ºC to a maximum 20.1 ºC under the highest emission 2070 models. Under RCP 4.5 models annual precipitation is predicted to increase mildly (+29 mm), and under RCP 8.5 to decrease mildly (-31 mm). However, any increases in precipitation will be counteracted by temperature increases, indicating that current *Callitris* niches will be more arid by 2050/70. As a result Australian *Callitris* species are predicted to experience moderate to severe range contraction as temperatures increase (Fig. 6). Lower emission models generally predict smaller declines in suitable habitat area, but the results are variable among models and species. Species in central Australia are predicted to move southwards, creating disjunct ranges as they diminish in area. South-eastern Australia is predicted to have a climate more like southwestern Australia today, and niche contraction is predicted for the majority of south-eastern species, especially those in semi-arid areas (Fig. 7). By 2070, under the highest emission scenario, *C. gracilis* will no longer have a suitable climatic niche in Australia. Conversely, some southwestern species (*C. arenaria, C. canescens* West and *C. drummondii*) are predicted to have expanding disjunct niches in the southeast, separated by the major barrier of the Nullarbor Plain. *Callitris preissii* is predicted to experience an increase in niche space as a result of a suitable but disjunct niche developing in the coastal Kimberley region. Species occupying moist coastal regions and ranges in the south-east are predicted to move south along the coast and/or into isolated niches in the coastal ranges. *Callitris* species closer the equator (*C. intratropica* and the New Caledonian species) are predicted to experience lower rainfall. These data predict that *C. neocaledonica* will have no climatic niche within the next 30 years, regardless of emission scenario. This is due to predictions of higher annual temperature ranges in future New Caledonian niches. *Neocallitropsis* has large predicted niche loss for the same reason, and is predicted have disjunct niches on the highest peaks in New Caledonia. *Callitris intratropica* is predicted to have a more northerly range, with largest declines in the Cape of York.

DISCUSSION

Did *Callitris* diversify faster than the RoC?

Drought exposes species to threats of population declines (Allen et al. 2015), range shifts (Brodribb and Cochard 2009; Fei et al. 2017), and ultimately, if traits do not evolve under selection, to extinction (Barreda and Palazzesi 2007; Jimenez-Moreno et al. 2013; Pokorny et al. 2015). However some studies have found that adaptation to drought results in an increase in diversification rates as species occupy new or empty niche space (Good-Avila et al. 2006; Arakaki et al. 2011; Gutiérrez-Ortega et al. 2017). Conifers in particular have had high extinction rates associated with aridification (Crisp and Cook 2011; Fragnière et al. 2015), yet lineages through time analyses show that the Callitroideae had a positive, albeit non-significant rate of diversification, indicating a trend towards later diversification. This more recent diversification (positive γ-statitistic) may have been driven by recent diversification in *Callitris* as found by Larter et al. (2017). However, we did not find recent diversification in *Callitris* (positive but non-significant γ) in this study. The phylogeny used in the Larter et al. (2017) study had a younger crown age for *Callitris* (~30 Ma vs ~41 Ma in this study) and fewer Callitoideae outgroups. Also, for example, *Callitris glaucophylla* was misidentified as *C. columellaris*, all of which might explain the different results in diversification for *Callitris*. Diversification in the *Callitris* clade alone showed a non-significant negative gamma, indicative of a trend of extinctions towards the present. Thus the evolution of drought-tolerance was not associated with higher diversification rates in *Callitris* compared to the RoC. This is in contrast to studies of other plant groups that found an association between aridity and increased speciation (Good-Avila et al. 2006; Arakaki et al. 2011; Gutiérrez-Ortega et al. 2017) (Klak et al. 2004), even in Cupressaceae (Pittermann et al. 2012).

Is the climatic niche of *Callitris* different from RoC?

If drought adaptation in *Callitris* has allowed it to occupy a novel climatic niche, we might expect *Callitris* to have a broader climatic niche that RoC. However, based on PCA analyses of climatic niche space, RoC has a broader climatic niche than *Callitris*.

Although drought-adaptation in *Callitris* did not result in a broader climatic niche for *Callitris,* climatic niches in *Callitris* and RoC nevertheless were not equivalent, suggesting niche divergence. Though RoC and *Callitris* overlap in climatic niche space, *Callitris* is concentrated in a hotter, drier section of the RoC niche and therefore has a narrower climatic niche. Differences in climatic niche were a result of significant differences in altitudinal ranges. The RoC inhabit warm-wet or cool-wet climates in mountainous or coastal regions across a wide latitudinal range. Low elevation in *Callitris* reflects the low topography of Australia.

Niche Divergence in Sister Pairs

Out of the five sister pair comparisons of the RoC, only *Libocedrus* in New Zealand and *Diselma–Fitzroya* had divergent niches, suggesting niches may be conserved. However, low species diversity within genera in the RoC reduces the number of available sister pair comparisons, making patterns difficult to interpret.

In the Australian *Callitris*, five out of eight sister pair comparsons had divergent climatic niches. This is largely due to geographic divergence. Nearly all sisters with divergent climatic niches are drought-adapted (the exception is *C. muelleri–C. oblonga*). Drought-adapted sisters were frequently separated by arid barriers. *Callitris canescens* East and *Callitris canescens* West occur on either side of the dry Nullarbor plain, but ENMs place their suitable habitat on both sides of the Nullarbor. *Callitris canescens* (~ 19 Ma divergence) could have been separated by the uplift of the Nullarbor karst approximately 15-14 Ma (Miller et al. 2012) but it is more likely that the subsequent aridification of the Nullarbor has left the sisters on either side of the continent in slightly different climatic niches. Furthermore, *C. columellaris* and *C. intratropica* are separated by an arid belt south of the monsoonal subtropics. *Callitris intratropica* may have niche-tracked a monsoon-like climate northwards as the interior of Australia become more arid (Herold et al. 2011) and/or adapted *in situ* as the modern monsoonal climate developed (Christensen et al. 2017). The most diverged sister pair is *C. tuberculata* and *C. preissii*, which have no climatic or geographic overlap. Yet their ranges are in very close geographic proximity, perhaps a result of the steep climatic gradients of the south-western Australia (Cook et al. 2015).

Three of the eight Australian *Callitris* sister pair comparisons had climatic niches that were equivalent or more similar than expected. Two drought-adapted sister pairs (*C. arenaria–C. pyramidalis* and *C. glaucophylla–C. gracilis*) were more similar than expected in their climatic niches because of high geographic overlap. The youngest sister pair (*C. arenaria* and *C. pyramidalis*) have an approximate divergence date of ~3 Ma and have the highest climatic and geographic overlap of all Australian species. Though they are sisters in terms of extant species, recent extinctions may have eradicated all other close relatives in regions that suffered intense aridification. Higher geographic overlap in *C. rhomboidea–C. monticola* might also represent niche convergence to mesic landscapes. This may indicate another possible outcome to aridity - niche convergence. There are therefore, contradictory patterns in climatic niche evolution, which cannot be explained by drought-adaptation in *Callitris*. Interpretation is further complicated by a lack of evidence on ancestral ranges of *Callitris*.

Effect of climate change on future distribution of the Callitroideae

Several *Callitris* species (*C. glaucophylla, C. macleayana, C. intratropica, C. oblonga* and *C. rhomboidea*) currently have disjuct populations, likely to have been created by climate change. Under future climate models of increased temperatures, a continuing pattern of range retraction, disjunctions and extinction of climatic niches is predicted. Suitable climatic niches are predicted to retreat from the arid centre, contracting to the north and south, with a bias towards the east in southern Australia. Future climate models suggest that the rate of aridification associated with climate change may lead an increased risk of extinctions in drought-adapted Australian *Callitris*, which have few areas of refuge from increasing temperatures.

It is becoming increasingly clear that hydraulic traits are essential to drought-adaptation and diversification into arid niches (Gleason et al. 2012; Choat 2013; Costa-Saura et al. 2016). *Callitris* species from the dry regions of Australia are extraordinarily drought-tolerant, recording the lowest cavitation resistance (P_{50}) values known (Brodribb and Hill 1998; Bouche et al. 2014; Larter et al. 2015). Larter et al. (2017) found that the evolution of drought-tolerant hydraulic traits led to a 'radiation' in *Callitris*, implying a 'key innovation' followed by the colonisation of novel niches. However, our data does not support higher diversification in *Callitris* relative to the RoC. *Callitris* has

diversified into dry niches, but the lack of evidence for higher diversification we found may be explained by counteracting high extinction rates.

Diversification in *Callitris* appears to be associated with the development of arid geographic barriers. Local extinctions in regions of extreme aridity were likely to cause range fragmentation leading to disjunct populations. Because *Callitris* are long-lived, slow-growing trres with low dispersal ability range movement was likely to be limited. Instead, local adaptation and extinctions could have selected for drought-tolerance traits as regional climates differentiated. It is therefore likely that the evolution of drought-tolerance traits and speciation in *Callitris* occurred hand-in-hand.

Conclusion

Divergent climatic niches separated by arid barriers such as the Nullarbor or the dry interior of Australia, suggest frequent geographic speciation in *Callitris*. However, drought-adaptation has not led to higher diversification. Rather the high selection imposed on hydraulic traits has led to high local extinctions, and possibly species extinctions. Evidence of high conifer extinction in the fossil record (Hill and Brodribb 1999; Hill 2004), the pattern of strong ecological associations in hydraulic traits (Heady and Evans 2000; Larter et al. 2017), and evidence of aridity-related genetic bottlenecks (Sakaguchi et al. 2013) in the context of increasing aridification in Australia (Fujioka et al. 2005; Fujioka et al. 2009; Quigley et al. 2010), all support the hypothesis that aridification led to diversification in Australian *Callitris* via geographic speciation, at the price of high extinction. Lastly, future climate models reiterate a pattern of niche divergence/convergence in response to increasing aridity. These models further suggest that *Callitris* will face a significant threat of extinction due to increasing temperatures and low topography in Australia, despite their evolution of extraordinary drought adaptation.

.

Table 1. Results of PCA and means of variables extracted from suitable habitat ranges predicted by ENMs. Results are arranged by group (*Callitris*–RoC) and species, showing species positions on OMI Axes 1 and 2, species niche position (OMI) and niche breadth (Tol) according to Outlying Mean Index analysis; and mean values for Aridity Index (AI), suitable range area, percent coverage of the landmass occupied, altitude, slope expressed as a percentage, latitude and the region of endemism for each species.

Group	Species	Code	OMI Axis1	OMI Axis2	Niche Position (OMI)	Niche Breadth (Tol)	Aridity Index (AI)	Suitable Range Area (km^2)	Landmass Coverage (%)	Mean Altitude (m)	Slope (%)	Mean Latitude	Region
Callitris	*Callitris acuminata*	Cac	1.63	-1.35	10.52	0.27	0.47	37941	0.49	144	1.57	-31.15	Australia
Callitris	*Callitris arenaria*	Car	2.85	-0.87	11.87	0.61	0.29	74297	0.96	221	0.61	-31.10	Australia
Callitris	*Callitris baileyi*	Cb	0.66	-1.19	4.55	0.30	0.58	38658	0.5	448	3.37	-27.46	Australia
Callitris	*Callitris canescens East*	CcanE	0.88	0.36	5.26	0.23	0.35	43857	0.57	90	0.95	-34.31	Australia
Callitris	*Callitris canescens West*	CcanW	2.35	0.33	6.72	0.76	0.28	295874	3.84	277	1.03	-31.33	Australia
Callitris	*Callitris columellaris*	Ccol	-1.42	-2.90	16.11	0.68	1.06	14164	0.18	39	1.43	-26.92	Australia
Callitris	*Callitris drummondii*	Cd	0.44	0.01	5.25	0.17	0.40	43203	0.56	163	1.29	-33.64	Australia
Callitris	*Callitris endlichei*	Ce	0.42	0.91	3.35	0.94	0.59	412824	5.36	513	3.84	-29.21	Australia
Callitris	*Callitris glaucohpylla*	Cgl	2.50	0.06	8.15	2.11	0.28	1957251	25.39	312	1.16	-27.34	Australia
Callitris	*Callitris gracilis*	Cgr	1.36	0.85	3.91	0.41	0.31	295227	3.83	151	0.87	-33.81	Australia
Callitris	*Callitris intratropica*	Ci	0.60	-7.25	56.06	2.68	0.70	462910	6.01	206	1.84	-15.53	Australia
Callitris	*Callitris macleayana*	Cmac	-2.80	-3.20	22.11	8.05	1.17	57213	0.74	373	6.58	-25.48	Australia
Callitris	*Callitris monticola*	Cmon	-1.82	0.08	7.67	0.46	1.03	21113	0.27	806	6.43	-29.41	Australia
Callitris	*Callitris muelleri*	Cmue	-2.19	0.67	8.78	0.71	1.01	11298	0.15	470	5.09	-34.77	Australia
Callitris	*Callitris neocaledonica*	Cn	-6.46	-4.48	69.58	2.38	1.63	2567	13.64	701	16.33	-21.98	New Caledonia
Callitris	*Callitris oblonga*	Co	-1.64	1.94	8.98	0.31	0.83	31061	0.4	626	4.31	-36.25	Australia
Callitris	*Callitris preissii*	Cpr	0.21	-1.65	15.21	0.03	0.60	521	0.01	21	0.96	-32.04	Australia
Callitris	*Callitris pyramidalis*	Cpy	1.20	-0.54	5.63	0.78	0.42	188726	2.45	174	1.22	-32.05	Australia
Callitris	*Callitris rhomboidea*	Crh	-1.28	0.90	4.20	2.31	0.82	228684	2.97	258	3.28	-33.09	Australia
Callitris	*Callitros roei*	Cro	1.28	0.59	4.02	0.08	0.32	108096	1.4	229	0.90	-32.97	Australia
Callitris	*Callitris sulcata*	Cs	-3.57	-4.76	43.90	0.73	1.32	3558	18.9	431	15.46	-21.91	New Caledonia
Callitris	*Callitris tuberculata*	Ct	2.97	0.17	9.35	1.54	0.22	433478	5.62	347	0.83	-30.22	Australia
Callitris	*Callitris verrucosa*	Cv	2.19	0.88	6.66	0.29	0.26	252928	3.28	154	0.72	-33.39	Australia
Callitris	*Neocallitrposis pancheri*	Np	-4.85	-3.11	38.65	2.41	1.73	1862	9.89	377	7.55	-21.97	New Caledonia

Table 1 continued

Group	Species	Code	OMI Axis1	OMI Axis2	Niche Position (OMI)	Niche Breadth (Tol)	Aridity Index (AI)	Suitable Range Area (km^2)	Landmass Coverage (%)	Mean Altitude (m)	Slope (%)	Mean Latitude	Region
RoC	*Diselma archeri*	Da	-7.42	4.03	72.58	1.80	2.47	10265	0.13	871	7.61	-42.39	Australia
RoC	*Fitzroya cupressoides*	Fc	-6.15	2.51	50.85	1.24	2.02	70237	0.48	668	14.15	-39.92	South America
RoC	*Libocedrus austrocaledonica*	La	-6.44	-4.78	72.22	2.65	1.61	3426	18.2	565	11.40	-21.80	South America
RoC	*Libocedrus bidwillii*	Lb	-7.32	2.28	62.60	7.60	2.60	71549	26.63	645	13.39	-41.25	New Zealand
RoC	*Libocedrus chevalieri*	Lc	-7.91	-4.05	94.30	0.11	2.09	74	0.39	1133	15.76	-21.92	New Caledonia
RoC	*Libocedrus plumosa*	Lp	-5.36	0.75	34.74	1.53	1.88	41370	15.4	184	4.93	-38.67	New Zealand
RoC	*Libocedrus yateensis*	Ly	-5.22	-5.31	61.70	1.13	1.72	3455	18.35	440	10.89	-21.52	New Caledonia
RoC	*Papuacedrus papuana*	Pp	-9.73	-3.86	139.74	5.81	2.22	96901	10.24	2217	16.61	-5.01	New Guinea
RoC	*Pilgerodendron uviferum*	Pu	-6.75	2.60	60.72	1.38	2.11	189572	1.28	639	15.74	-45.51	South America
RoC	*Widdringtonia nodiflora*	Wn	-0.48	-0.54	4.55	1.70	0.56	196944	2.12	1004	6.13	-27.38	Southern Africa
RoC	*Widdringtonia schwarzii*	Ws	-0.18	1.01	7.81	0.39	0.54	14079	0.15	764	8.76	-33.58	Southern Africa
RoC	*Widdringtonia wallichii*	Wwa	0.16	1.82	11.97	0.51	0.33	3396	0.04	1089	10.31	-32.32	Southern Africa
RoC	*Widdringtonia whytei*	Wwh	-4.10	-2.73	45.72	2.81	1.36	14669	0.16	1595	8.89	-15.72	Southern Africa

Table 2. PGLS regression results of range area (Range) regressed on Aridity Index (AI) and Altitude (Alt), according to Lambda (λ), Delta (δ) and Kappa (ϰ) tree branch modifications. ML Parameter = value of λ, δ or ϰ; Intercept = the intercept of the regression slope on the y-axis; AI = the slope of the regression for Aridity Index; Alt = the slope of the regression for Altitude; k = the number of parameters in each model; sigma = σ^2, the fitted variance of the random walk; P value = significance ($P < 0.05$); logLk = log likelihood; AICc = sample size corrected Akaike Information Criterion scores; ΔAICc = difference in AICc from the lowest AICc score; Relative LogLk = relative likelihood of AICc scores.

PGLS Model	ML Parameter	Intercept	AI	Alt	k	sigma	r^2	P value (AI)	P value (Alt)	logLk	AICc	ΔAIC	Relative logLk	AICc weights
Range ~ AI λ	0.00	10.19	-1.29	–	2.00	0.19	0.22	0.00	–	-77.12	158.59	0.00	1.00	0.37
Range ~ AI δ	3.00	10.90	-2.28	–	2.00	0.00	0.21	0.00	–	-89.09	182.52	23.93	0.00	0.00
Range ~ AI κ	0.00	12.64	-1.98	–	2.00	1.28	0.22	0.00	–	-79.50	163.35	4.75	0.09	0.03
Range ~ Alt λ	0.00	11.35	–	-0.15	2.00	0.21	0.00	–	0.69	-81.66	167.67	9.08	0.01	0.00
Range ~ Alt δ	3.00	4.81	–	0.91	2.00	0.00	0.11	–	0.04	-91.42	187.19	28.60	0.00	0.00
Range ~ Alt κ	0.00	4.42	–	0.95	2.00	1.34	0.14	–	0.02	-81.21	166.76	8.17	0.02	0.01
Range ~ AI+Alt λ	0.00	7.95	-1.49	0.37	3.00	0.19	0.24	0.00	0.31	-79.50	159.11	0.51	0.77	0.29
Range ~ AI + Alt δ	3.00	6.16	-2.08	0.73	3.00	0.00	0.28	0.01	0.08	-87.36	180.73	22.14	0.00	0.00
Range ~ AI + Alt κ	0.00	6.31	-1.85	0.86	3.00	1.20	0.33	0.00	0.02	-76.53	159.07	0.47	0.79	0.29

Table 3. Geographic and Climatic Niche Overlap results comparing *Callitris* and RoC and sister species pairs, showing Schoener's D and Warren's I indexes of overlap, and the results of niche equivalency and niche similarity tests using 1000 randomisations to produce a null model. One-tailed tests were run for either hypothesis of niche conservatism ('greater') or niche divergence ('less'). Results are arranged in rows by clade, *Callitris* sister-pairs and the Rest of Callitroideae (RoC) sister-pairs. Car = *Callitris arenaria*; Cpy = *C. pyramidalis* and CcanW = *C. canescens* East and West; Ccol = *C. columellaris*; Ci = *C. intratropica*; Cd = *C. drummondii*; Cb = *C. baileyi*; Cgl = *C. glaucophylla*; Cgr = *C. gracilis*; Cmue = *C. muelleri*; Co = *C. oblonga*; Crh = *C. rhomboidea*; Cmon = *C. monticola*; Ct = *C. tuberulata*; Cpr = *C. preissii*; Np = *Neocallitropsis pancheri*; Cn = *C. neocaledonica*; Da = *Diselma archeri*; Fc = *Fitzroya cupressoides*; La = *Libocedrus austrocaledonica*; Lc = *L. chevalieri*; Lb = *L. bidwillii*; Lp = *L. plumosa*; Wn = *Widdringtonia nodiflora*; Wwh = *W. whytei;* Wwa = *W. wallichii* (syn. *W. cederbergensis*); Ws = *W. schwarzii*.; CcanE

Sister-Pair	**Geographic Overlap**		**Climatic Niche Overlap**		**Niche Conservatism**				**Niche Divergence**			
					More equivalent than expected		*More similar than expected*		*Less equivalent than expected*		*Less similar than expected*	
					Equivalency		**Similarity**		**Equivalency**		**Similarity**	
	D	*I*	*D*	*I*	*P (D)*	*P (I)*	*P (D)*	*P (I)*	*P (D)*	*P (I)*	*P (D)*	*P (I)*
Callitris-RoC	0.001	0.001	0.397	0.557	**0.001**	1	**0.027**	**0.038**	1	**0.001**	0.977	0.964
Car-Cpy	0.329	0.525	0.503	0.639	**0.001**	0.513	**0.019**	0.051	1	0.54	0.974	0.941
CcanE-CcanW	0.025	0.064	0.306	0.406	0.426	1	0.088	0.155	0.578	**0.001**	0.91	0.841
Ccol-Ci	0.000	0.000	0.117	0.274	1	1	0.47	0.397	**0.001**	**0.001**	0.477	0.565
Cd-Cb	0.000	0.000	0.292	0.396	1	1	0.148	0.188	**0.002**	**0.001**	0.853	0.813
Cgl-Cgr	0.102	0.262	0.334	0.562	0.261	0.646	0.019	**0.010**	0.739	0.352	0.969	0.987
Cmue-Co	0.059	0.099	0.357	0.540	0.980	1	0.064	0.066	**0.027**	**0.001**	0.944	0.946
Crh-Cmon	0.074	0.242	0.455	0.664	0.079	0.072	**0.017**	**0.009**	0.924	0.929	0.984	0.99
Ct-Cpr	0.000	0.000	0.000	0.000	1	0.059	1	0.064	0.946	1	0.953	1
Np-Cn	0.612	0.719	0.481	0.565	0.31	0.632	0.136	0.236	0.715	0.383	0.857	0.773
Da-Fc	0.000	0.000	0.524	0.554	**0.001**	0.972	**0.005**	0.131	1	**0.027**	0.996	0.869
La-Lc	0.021	0.146	0.061	0.228	0.636	0.661	0.265	0.244	0.953	1	1	0.993
Lb-Lp	0.162	0.213	0.215	0.454	0.999	0.999	0.096	0.071	**0.007**	**0.007**	0.897	0.93
Wn-Wwh	0.031	0.113	0.282	0.418	0.073	0.165	0.171	0.177	0.931	0.849	0.829	0.824
Wwa-Ws	0.000	0.000	0.458	0.549	0.258	0.766	**0.049**	0.142	0.723	0.227	0.952	0.855

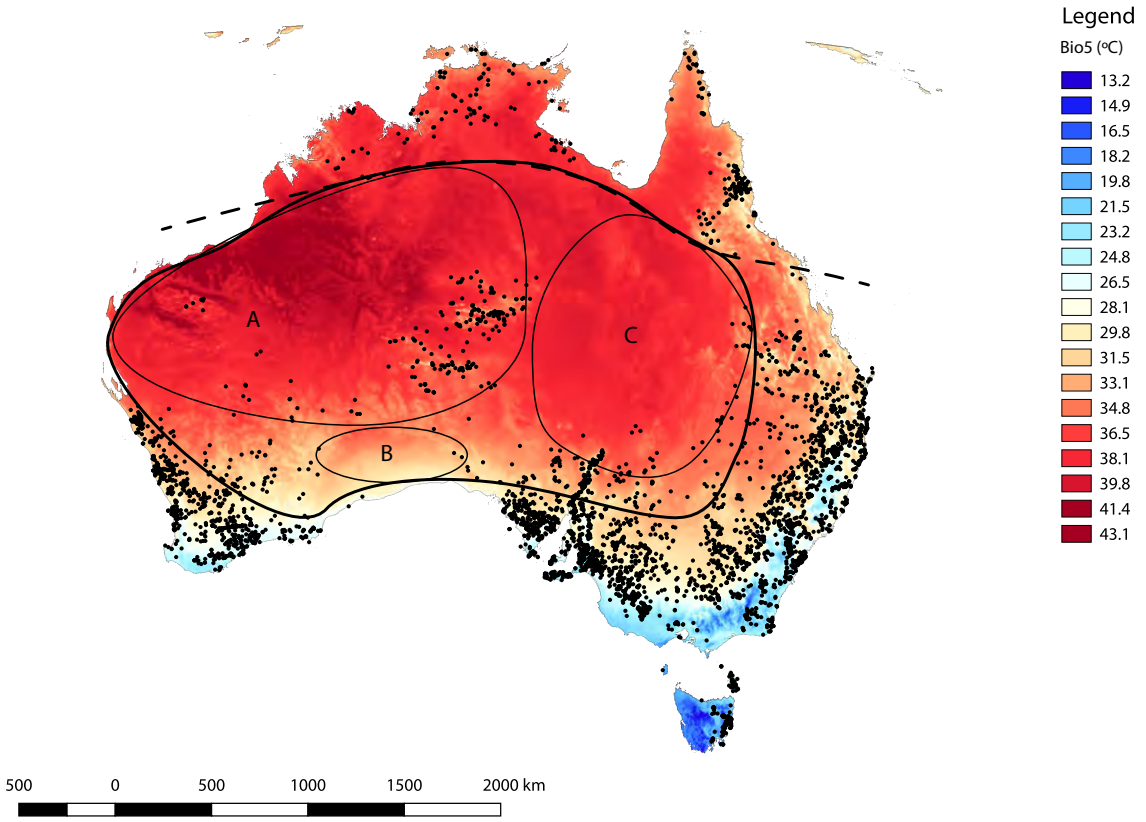

Figure 1. Map of Australia coloured according to the Maximum Temperature of the Warmest Month (Bio5), with collection data for Callitris species used in this study. The dashed line represents the southerly limit of the subtropical monsoon. Circles represent A) an arid region consisting of the Pilbara, the Little and Great Sandy Deserts, the Gibson Desert, the Tanami Desert and the Great Victorian Desert; B) the Nullarbor Plain and C) the Lake Eyre drainage basin. The shapes defining the arid regions are approximate.

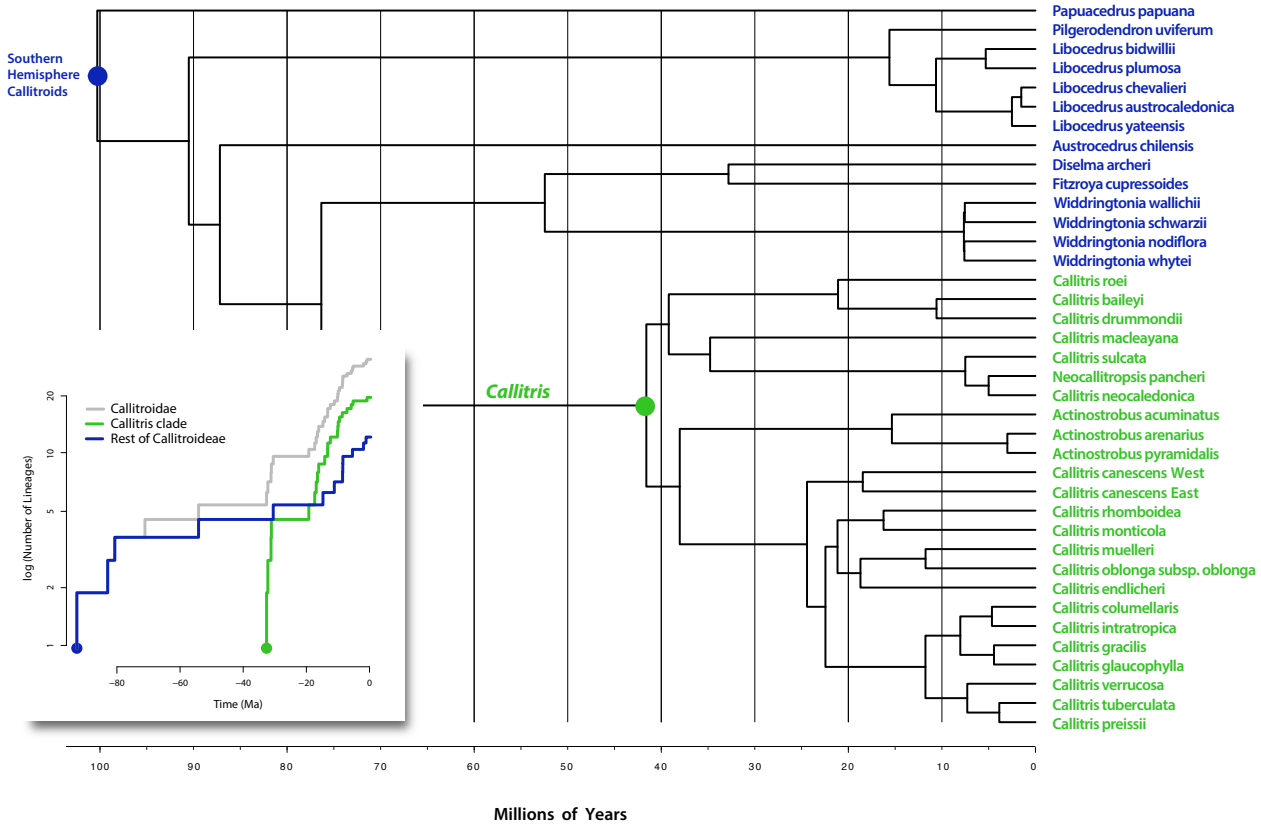

Figure 2. Callitroideae phylogeny used in this study and (inset) Lineages Through Time (LTT) plot. The Southern Hemisphere callitroids, the Callitroideae, are marked with a grey bar. *Callitris* species are shown in green, and the Rest of the Callitroideae (RoC) in blue. Circles at the crown of the RoC and *Callitris* correspond with the circles on the LTT plot.

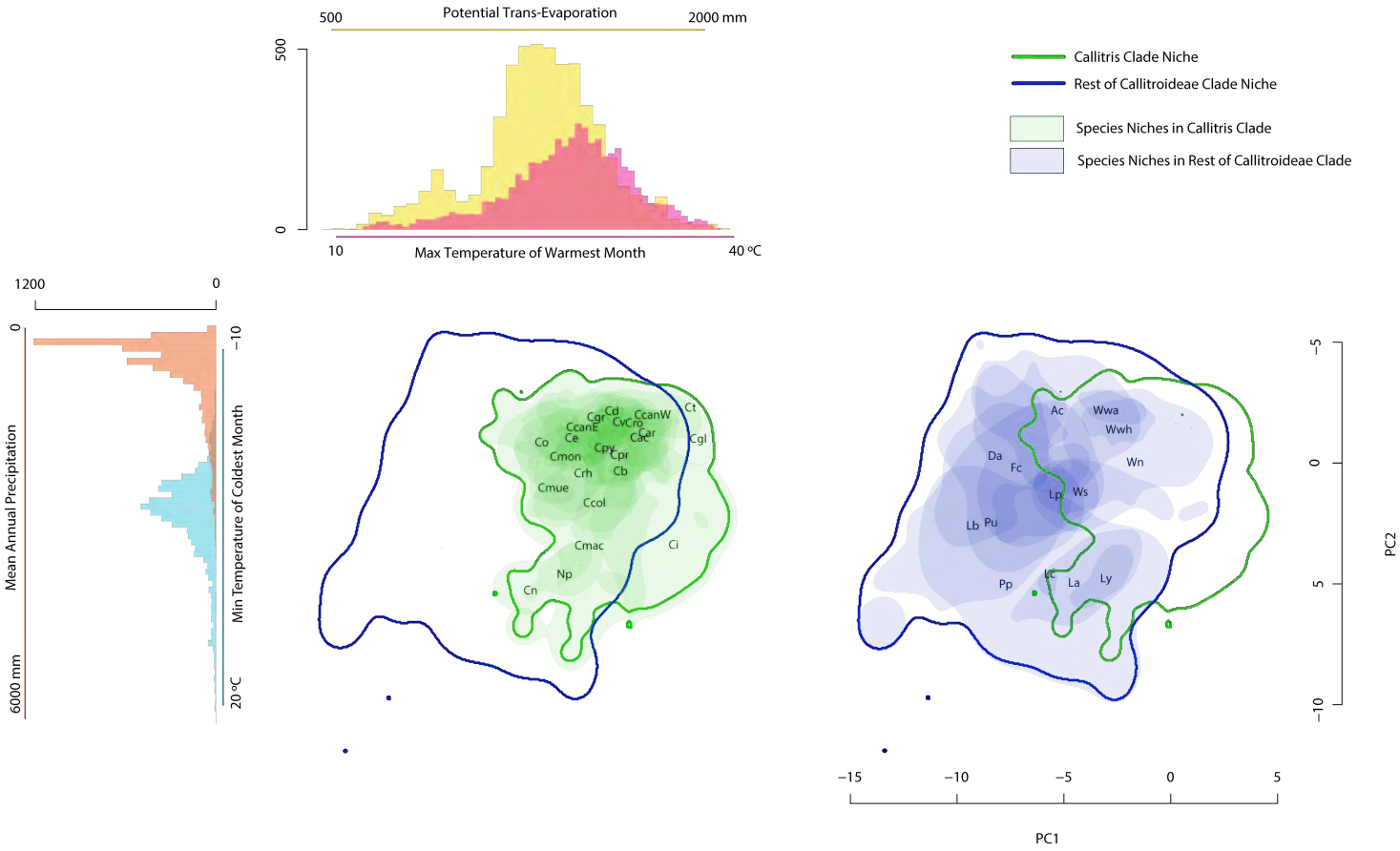

Figure 3. Plot of PCA climatic niches and overlap for the niche space of *Callitris* and RoC. Two identical plots of the PCA are shown to compare the niches of *Callitris* and the RoC, with a bold outline for each group on both plots, Green = *Callitris*; Blue = RoC. Coloured blobs represent species climatic niches within PCA space, identified by species codes. Species codes for drought-adapted *Callitris* species have been placed for legibility and do not accurately represent the PCA coordinates e.g. Ct, Ggl, Ci. The histograms represent the spread of values for the two most important variables for each axis.

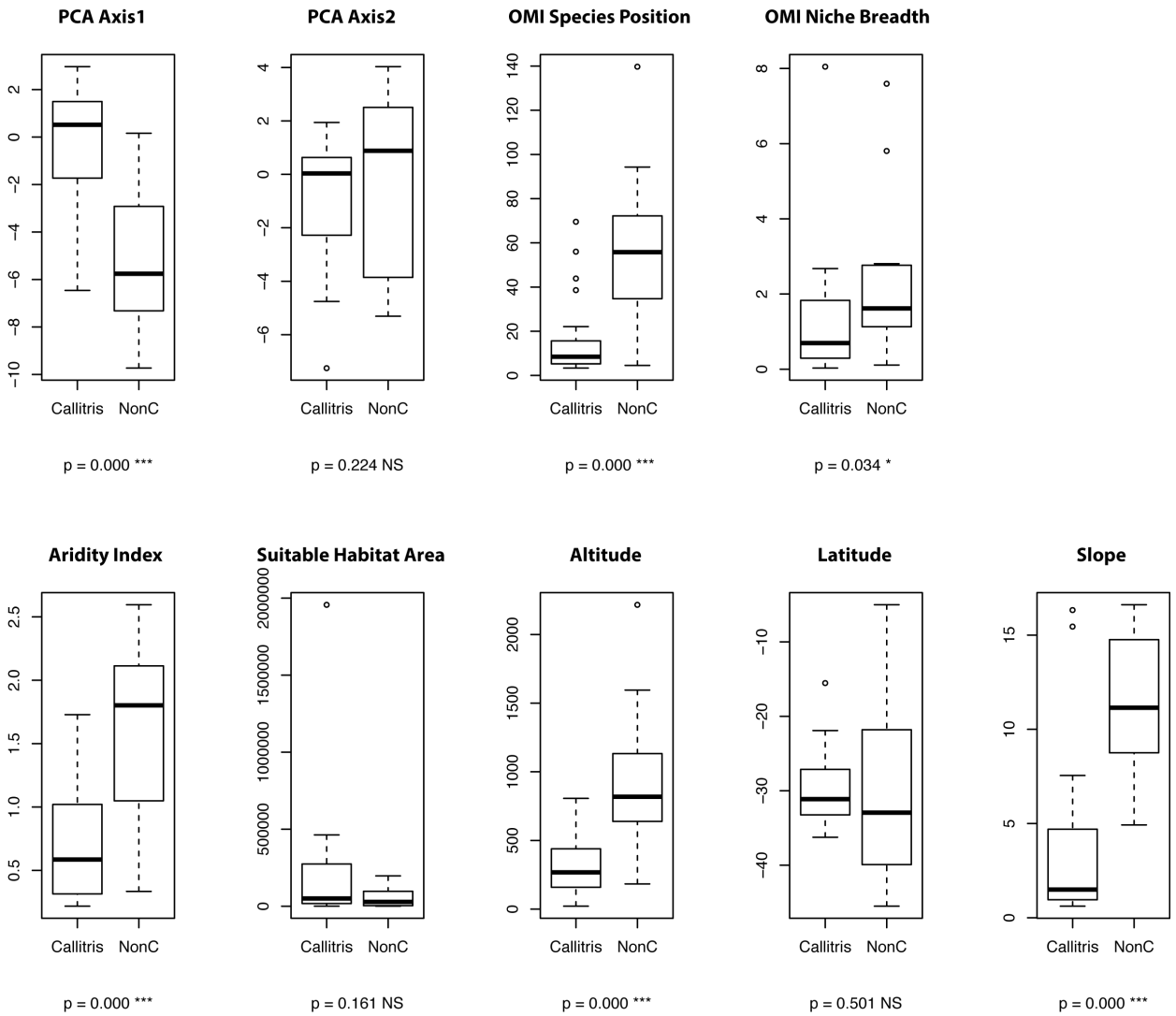

Figure 4. Boxplots of Mann-Whitney U tests comparing *Callitri*s and RoC differences in PCA climatic niche space and key variable

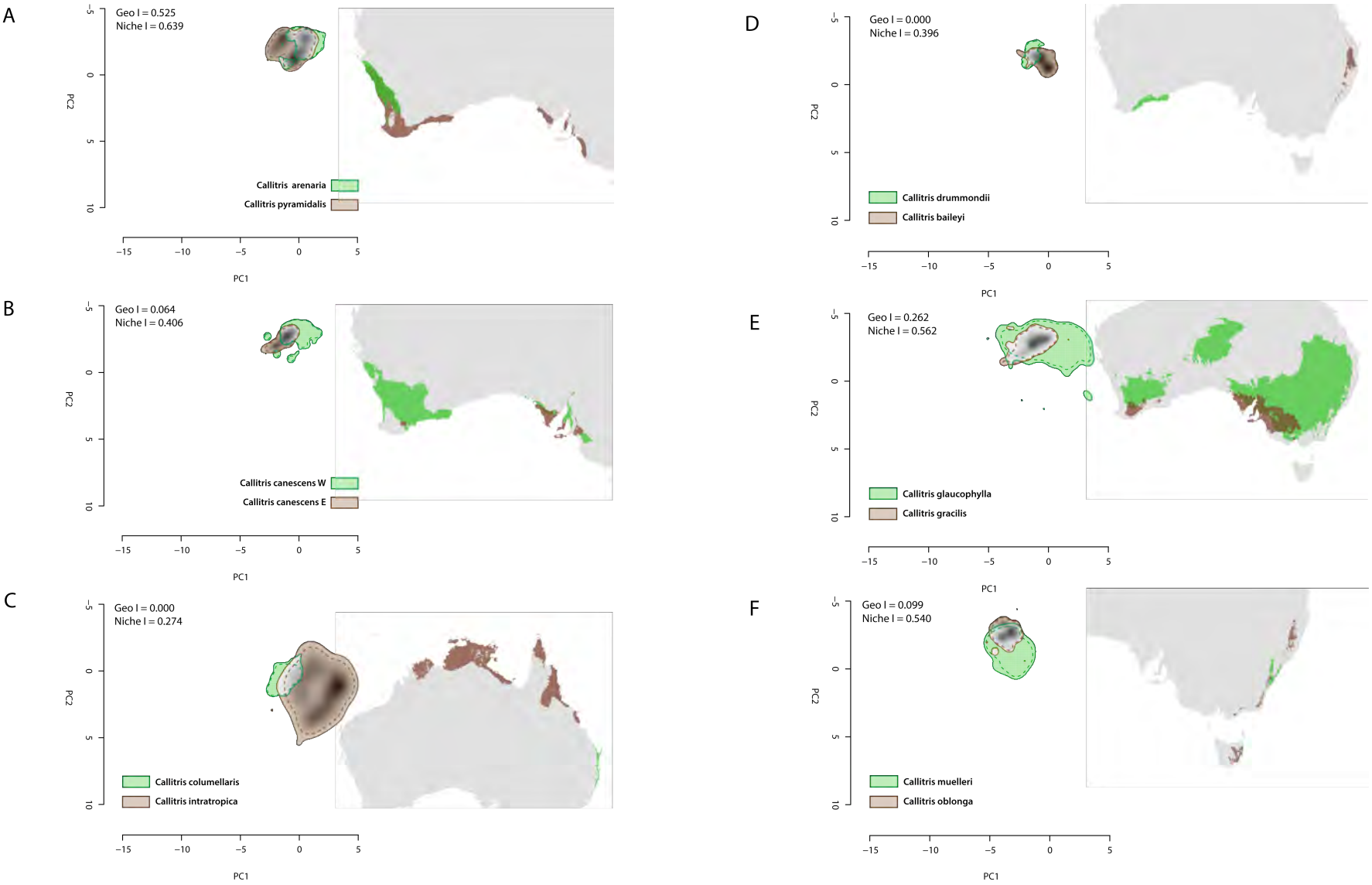
A
Geo I = 0.525
Niche I = 0.639
Callitris arenaria
Callitris pyramidalis
B
Geo I = 0.064
Niche I = 0.406
Callitris canescens W
Callitris canescens E
C
Geo I = 0.000
Niche I = 0.274
Callitris columellaris
Callitris intratropica
D
Geo I = 0.000
Niche I = 0.396
Callitris drummondii
Callitris baileyi
E
Geo I = 0.262
Niche I = 0.562
Callitris glaucophylla
Callitris gracilis
F
Geo I = 0.099
Niche I = 0.540
Callitris muelleri
Callitris oblonga
PC1
PC2

Figure 5. A-F

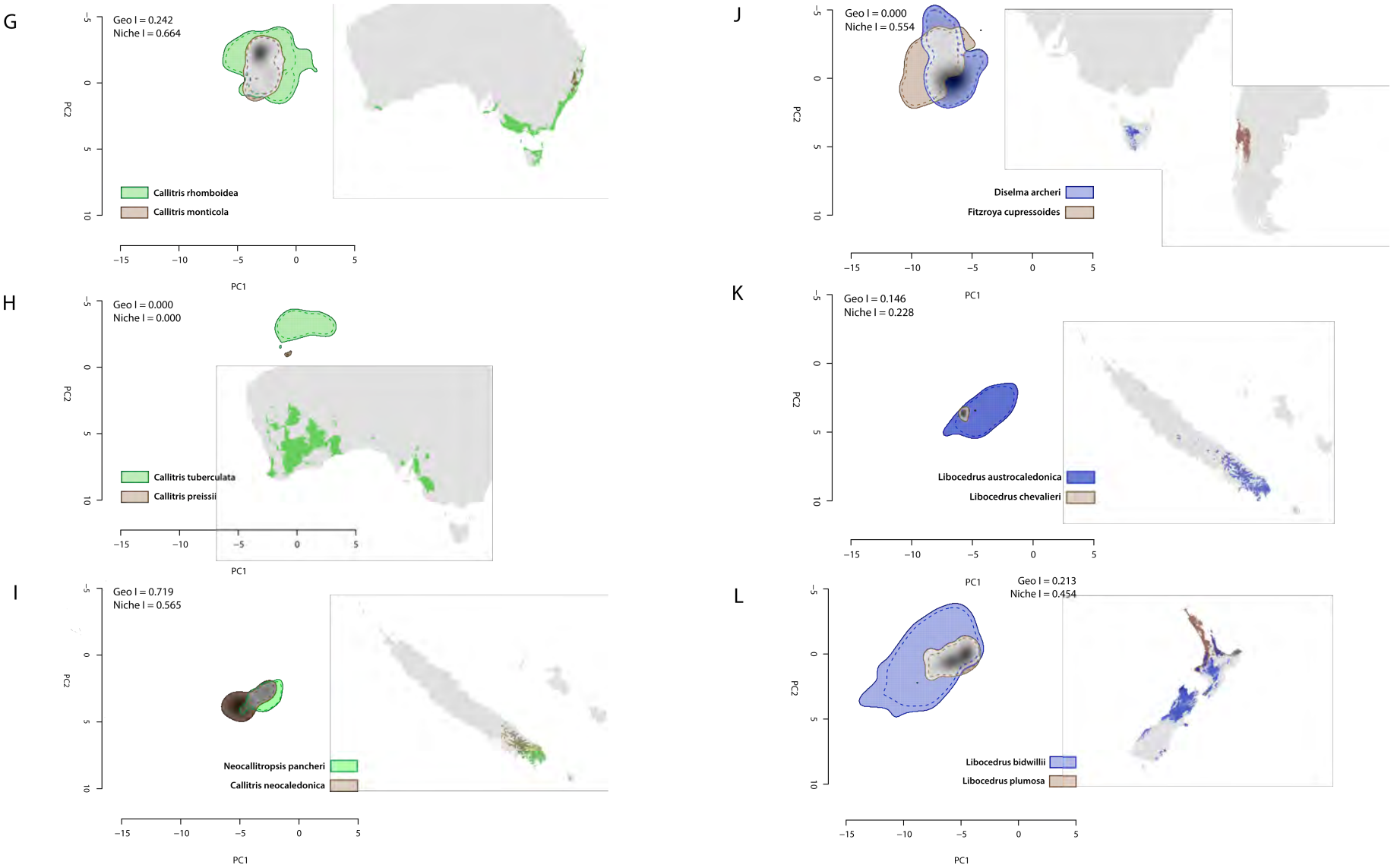
G
Geo I = 0.242
Niche I = 0.664
Callitris rhomboidea
Callitris monticola
H
Geo I = 0.000
Niche I = 0.000
Callitris tuberculata
Callitris preissii
I
Geo I = 0.719
Niche I = 0.565
Neocallitropsis pancheri
Callitris neocaledonica
J
Geo I = 0.000
Niche I = 0.554
Diselma archeri
Fitzroya cupressoides
K
Geo I = 0.146
Niche I = 0.228
Libocedrus austrocaledonica
Libocedrus chevalieri
L
Geo I = 0.213
Niche I = 0.454
Libocedrus bidwillii
Libocedrus plumosa
PC1
PC2

Figure 5. G-L

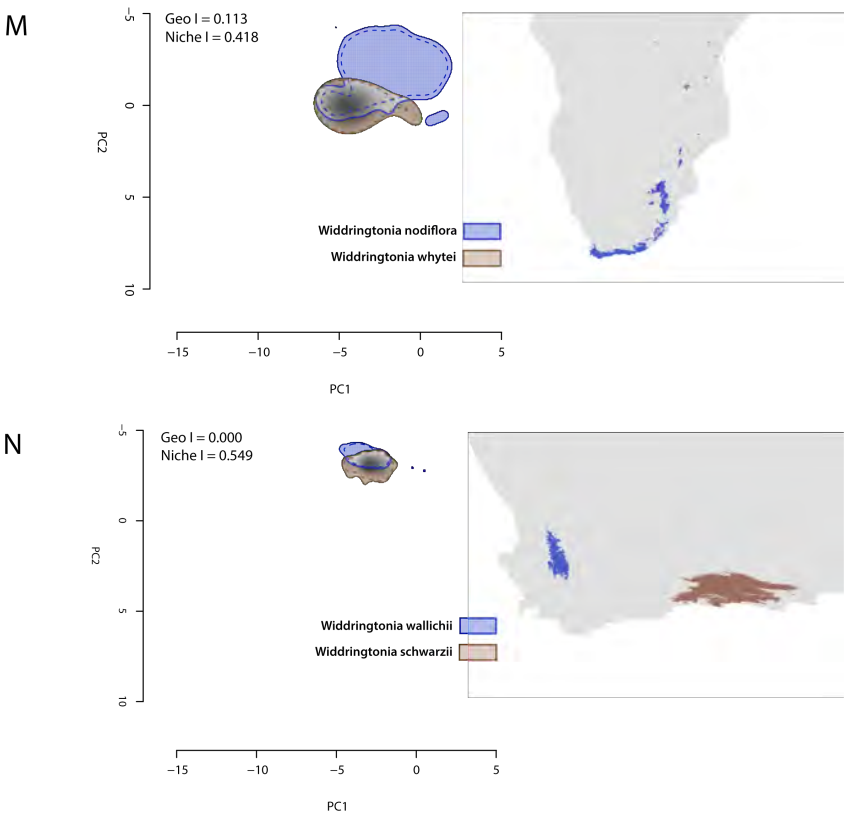

Figure 5. Geographic and climatic niche overlap in sister pairs. Plots show the climatic niches in PCA space (left), and their suitable predicted niche range (right), as predicted by MaxEnt models. *Callitris* pairs are coloured in green and brown, and RoC pairs in blue and brown. Regions of overlap in the PCA plot are shown in light gray. Occupancy is depicted in dark grey. Values for geographic and climatic niche overlap according to Schoener's *I* are in text. A) *Callitris arenaria–C. pyramidalis*; B) *C. canescens East–C.canescens West*; C) *C. columellaris–C. intratropica*; D) *C. drummondii–C. baileyi*; E) *C. glaucophylla–C. gracilis*; F) *C. muelleri–C.oblonga*; G) *C. rhomboidea–C. monticola*; H) *C. tuberculata–C. preissii*; I) *Neocallitropsis pancheri–Callitris neocaledonica*; J) *Fitzroya cupressoides–Diselma archeri*; K) *Libocedrus austrocaledonica–L. chevalieri*; L) *Libocedrus bidwillii–L. plumosa*; M) *Widdringtonia nodiflora–W. whytei*; N) *W. wallichi* (syn. *cedarbergensis*)*–W. schwarzii*.

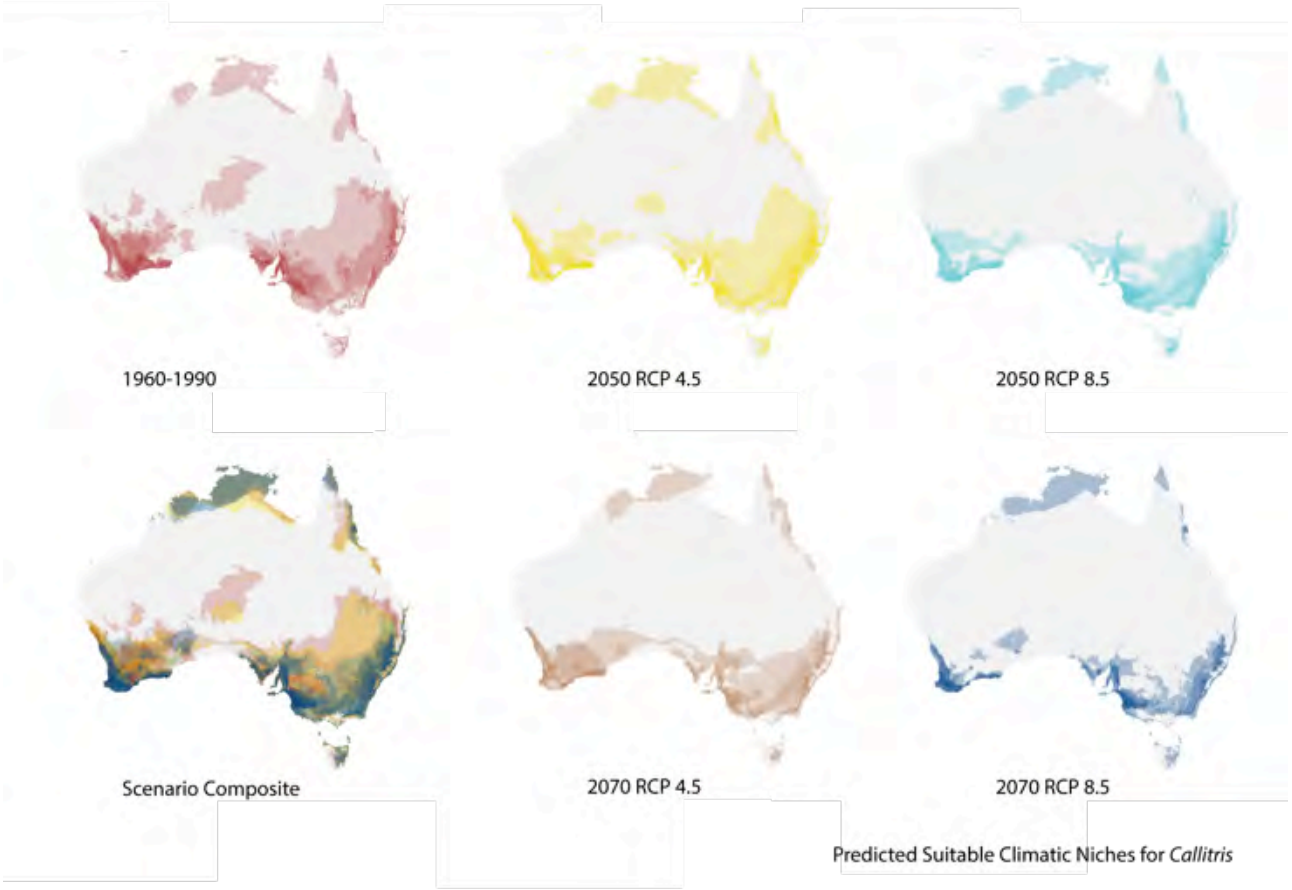

Figure 6. Maps of projected ranges for *Callitris* according to four future climate change scenarios as predicted by the ACCESS 1.0 climate model. Deep red = predicted suitable habitat ranges estimated in MaxEnt using the Bioclim variables (Bio1-19); Yellow = projected ranges under moderate emissions (RCP 4.5) by 2050; Brown = projected ranges under moderate emissions (RCP 4.5) by 2070. RCP 4.5; Cyan = projected ranges under high emissions (RCP 8.5) by 2050; Blue = projected ranges under high emissions (RCP 8.5) by 2070. All five models are overlaid in the composite image to show range changes over the different scenarios and periods modelled.

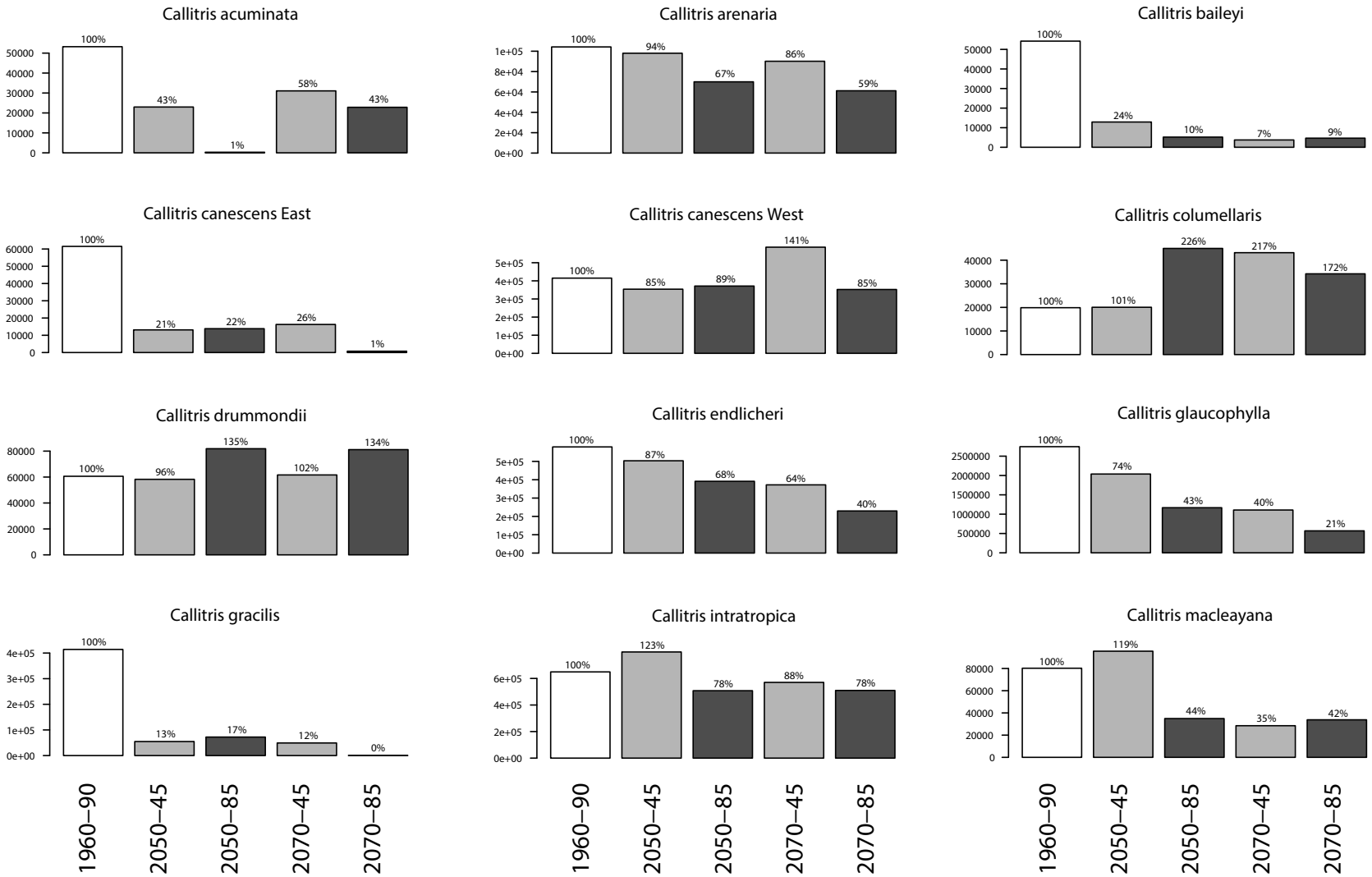
Callitris acuminata
100%
43%
1%
58%
43%
Callitris arenaria
100%
94%
67%
86%
59%
Callitris baileyi
100%
24%
10%
7%
9%
Callitris canescens East
100%
21%
22%
26%
1%
Callitris canescens West
100%
85%
89%
141%
85%
Callitris columellaris
100%
101%
226%
217%
172%
Callitris drummondii
100%
96%
135%
102%
134%
Callitris endlicheri
100%
87%
68%
64%
40%
Callitris glaucophylla
100%
74%
43%
40%
21%
Callitris gracilis
100%
13%
17%
12%
0%
Callitris intratropica
100%
123%
78%
88%
78%
Callitris macleayana
100%
119%
44%
35%
42%
1960–90
2050–45
2050–85
2070–45
2070–85

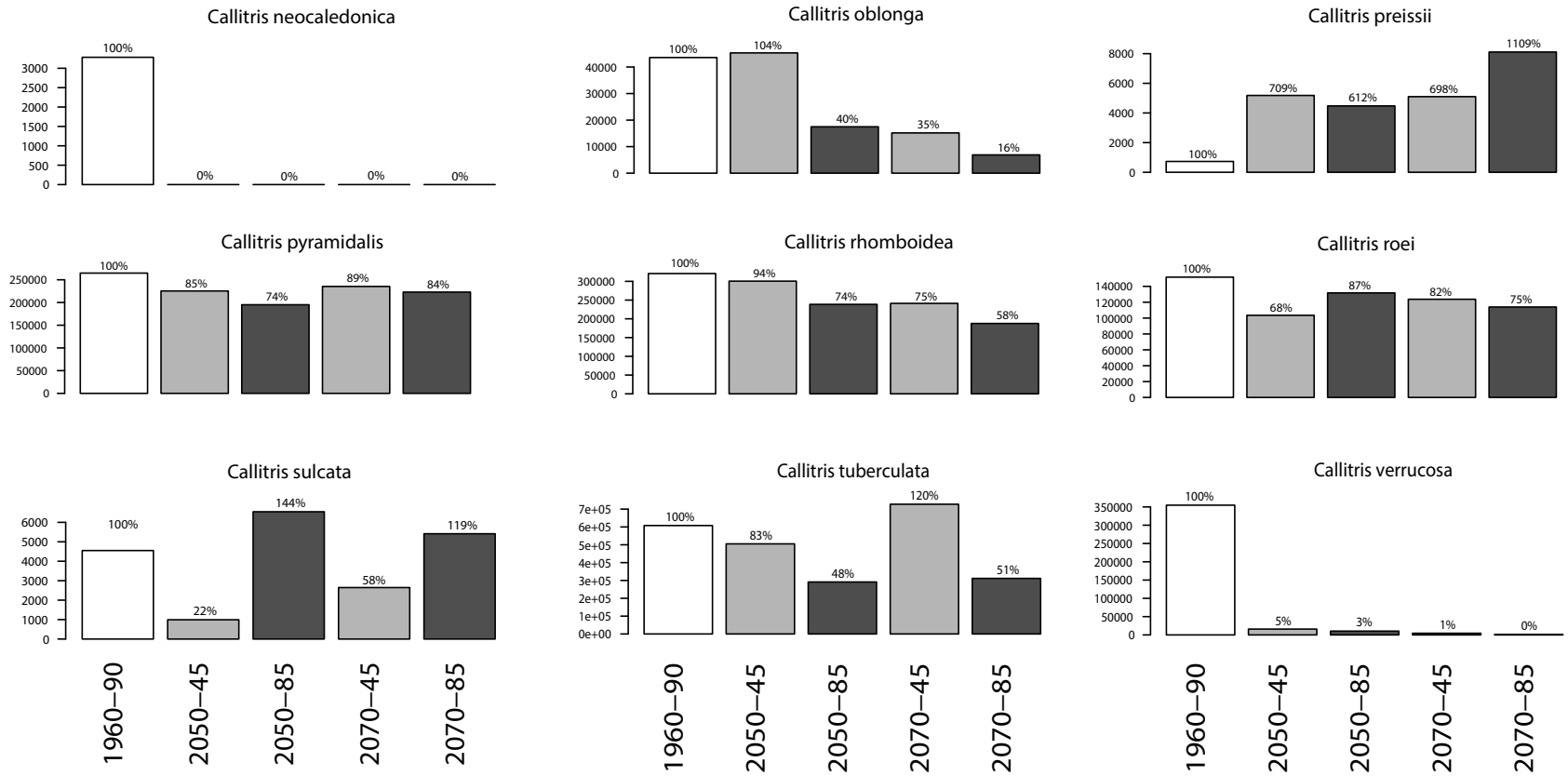

Figure 7. Barplots of predicted suitable climate range by 2050 and 2070 under two climate change emission scenarios. The present range is shown in white. Predictions for moderate emissions (RCP 4.5) are coloured in light grey, and high emissions in (RCP 8.5) in dark grey. Moderate and high emissions are grouped by year.

Chapter 3

Signal loss: Assessing the impact of extinctions on trait evolution models via simulations

Signal loss: Assessing the impact of extinctions on trait evolution models via simulations

ABSTRACT

Phylogenetic comparative methods (PCMs) use phylogenetic trees to investigate how traits evolve and influence diversification. One of the basic statistical assumptions of nearly all methods is that the phylogeny used in trait evolution studies is the 'true' tree. However, due to extinctions we are usually unable to sample the genomes of extinct taxa. If the lack of extinct data has an effect on phylogenetic tree reconstruction when using extant-only data, it might have flow-on effects to PCMs. We used simulations to test whether using phylogenetic reconstructions from extant-only taxa affected trait modelling analyses. To do this we simulated 100 'complete' trees (with extinct and extant taxa) under four extinction scenarios and then, using only the extant taxa, reconstructed phylogenies in BEAST 2. We simulated trait data under BM and single-optimum OU models and with two levels of trait variance to use in trait evolution models. We compared the effect of using the complete trees, complete trees with extinct taxa removed and BEAST MCC trees on lineages through time (LTT) and Pybus and Harvey's gamma, phylogenetic signal, ancestral character estimation, and evolutionary trait models. The commonly observed 'slowdown' in LTT plots may be artefact of BEAST priors, as it was not observed in the complete or pruned trees. MCC trees had more significant early diversifications than complete or pruned trees, higher than expected phylogenetic signal, and more inaccurate estimations of the root value. Evolutionary models misidentified BM traits on MCC trees as evolving under an Early Burst model, and OU traits were misidentified as evolving under a BM model. Extinction scenario had no effect on trait evolution models, implying that using extant-only data to reconstruct phylogenetic trees does have serious consequences for trait models.

INTRODUCTION

Reconstruction of the past is hampered by the large amount of evidence destroyed by the passage of time. In biology, fossils provide us with a window into the past of taxa

that went extinct. However, the vast majority of extinctions have left no fossil evidence, meaning we cannot reconstruct the past relying on fossils alone. DNA sequencing and its subsequent use in phylogenetic reconstruction offered an opportunity of filling the gaps left by extinctions, because ancestral genes persist in relatives even when their ancestors no longer exist. Thus theoretically, phylogenies could also be used to investigate the evolution of traits because traits are inherited (Ridley 1983; Harvey and Pagel 1991).

One of the basic statistical assumptions of evolutionary trait modelling methods is that the 'true' or 'known' phylogenetic tree is to be used (Felsenstein 1985). However, because of extinctions, the 'true' or complete tree can never be recovered. Thus extinctions represent an irremediable form of incomplete sampling when constructing phylogenies. Since the credible estimation of trait evolution rests on using the true tree, using a tree 'reconstructed' from extant species could have serious consequences for conclusions made about the phylogenetic and ecological factors that shape trait evolution.

Evolutionary biologists realised that Brownian Motion (BM) models used to describe stochastic movement patterns (Einstein 1906) could be used to model phylogenetic trees (Cavalli-Sforza and Edwards 1967; Felsenstein 1973), and trait evolution (Felsenstein 1985; Harvey and Pagel 1991; Maddison 1994; Pagel 1997) (Pagel 1999). Phylogenies could account for evolutionary relationships, while BM could be used to model the evolution of traits under the Darwinian premise of 'descent with modification', in which traits evolve gradually over time via inheritance and random genetic drift (Darwin 1859).

The most basic model used in trait modelling is the BM model. The BM model in trait evolution is altered by a single parameter, sigma (σ), which defines the variance of the random walk (Fig 1). The trait values found in the species at the tips of the phylogeny are the result of the cumulative sum of a random walk with a variance of σ over the time of the tree. Trait divergence fits a normal distribution with the trait mean equal to the value at the root. The random walk is non-directional, meaning that trait values can increase or decrease over time, and the walk is unbounded: traits can evolve into any area of trait space without any constraints. The rate of evolution is non-varying: traits do not evolve at a faster or slower rate in certain portions of the tree, i.e. the value of σ

does not alter across the tree. Therefore in a BM model traits diverge according to a normal distribution, a rate defined by σ, the time span of the tree, and the timing of species divergences in the tree (Felsenstein 1973).

The BM model is thought of as a 'neutral' or 'drift' model for several reasons. One reason BM models are 'drift' models refers to the use of phylogenetic trees, which are constructed with 'neutral' loci that are not under selection (Felsenstein 1973). Genes under selection would identify similarly adapted species as close relatives, rather than a single group with highly diverse phenotypes. Another reason refers to the non-directional character of the BM random walk, in which traits are free to wander into any area of trait space guided by the topology of the tree. Finally it refers to the gradual accumulation of trait changes over time in traits evolving under genetic drift, not selection.

A way to assess the influence of relatedness on trait evolution is phylogenetic signal (Pagel 1999; Blomberg and Garland 2002; Blomberg et al. 2003). Phylogenetic signal uses the phylogeny to predict trait values under the BM assumption of evolutionary drift. If traits have evolved under a BM model, the structure of the tree should predict the evolution of species' traits at the tips of the tree. Based on this Pagel (1999) developed Pagel's Lambda (λ), a tree branch-length transformation method that investigates whether the observed traits are more likely to have been produced by the phylogeny as it is (indicating that the traits fit a BM model, $\lambda = 1$), or whether shorter ($\lambda < 1$) or longer shorter ($\lambda > 1$) branches fit the trait data better. Phylogenetic signal tests whether species' relatedness accounts for their trait values, but does not investigate the underlying evolutionary processes that have shaped traits (Revell et al.). Therefore, high phylogenetic signal cannot always be interpreted as evidence of BM, because both real and artifactual factors can shape the tree.

Concepts of neutrality have led to the BM model sometimes being thought of as a null model of trait evolution (Crisp and Cook 2012). When traits fit a BM model, they are frequently thought to have evolved in the absence of selection or under stabilising selection. Conversely, when traits do not fit a BM model, it is seen as evidence that they have departed from the neutral phylogeny because of selective pressures. For this reason, traits fitting a BM model have sometimes been referred to as 'conserved', or 'constrained', and considered evidence for a lack of evolutionary innovation (Diniz et

al. 1998; Johnson et al. 1999; Prinzing et al. 2001; Webb et al. 2002; Wiens 2004). The BM model is also a 'null' model in comparison to evolutionary models with more parameters, such as Ornstein-Uhlenbeck (OU) models (Hansen 1997; Butler and King 2004)

One parameter that is not very often thought of as a parameter is the phylogenetic tree itself. It is probably the single most influential parameter as it acts as the scaffold for all trait evolution methods. The tree brings essential information about species relationships, but the topology of the tree also predicates the outcome of evolutionary trait models. Because the phylogeny has so much influence on trait models, researchers have incorporated posterior trees to account for 'phylogenetic uncertainty'. Phylogenetic uncertainty refers to the range of tree topologies, branch lengths and their variance produced from the Bayesian MCMC chain. If the range of tree topologies is large, using them in trait models will reduce the chance of finding a false significant result that is the result of one particular tree (de Villemereuil et al. 2012).

However, any given set of posterior trees will have been fitted using the same Bayesian priors, which means that the range of tree topologies may be limited depending on the starting phylogeny and model parameters used. Trees are usually constructed with sequence data from extant species only, therefore the interior nodes of the trees may not be accurately placed. Because of this the nodes of a tree have no special meaning other than marking points of species divergences given the data and the model. Thus phylogenetic trees are a map of genetic similarities and differences drawn from present species only.

Because we can rarely sample ancient genetic data, concerns about the effect of extinctions of trait modelling remain a moot point. And yet, if unsampled extinct data significantly alters the relationships and timing of divergences in trees (Yedid et al. 2012), it could have downstream effects on trait evolution models (Grafen 1989; Losos 2010).

In this study, we investigate the effect of extinction on tree reconstruction and trait modelling. To do this we simulated 'complete' trees (with extinct and extant taxa). We considered these trees to be the 'true' evolutionary trees. We modelled traits on the complete trees which gave us 'extinct' traits to use in modelling. The assumption

therefore is that the complete trees and traits accurately represent the full evolutionary history of the simulated group. We then reconstructed phylogenetic trees using only the extant species from the complete trees. We applied commonly used PCMs to the complete trees and the reconstructed trees and compared the outcome of modelling. If the result of PCMs on the reconstructed tree match those on the complete tree, then extinctions do not affect tree and trait reconstruction, because tree shape did not affect the outcome.

METHODS

To create data, we simulated trees with different levels of random (non trait-related) extinction events and then simulated DNA over the trees. This provided our complete trees and modelled DNA sequences of those trees. We then modelled traits on the trees under a BM model and a single OU model, giving us complete trait data for extinct and extant species. Because tree reconstructions rarely include extinct genetic data, we pruned out extinct sequences and reconstructed the trees in BEAST. We applied standard trait evolution methods using the complete tree and traits, the complete tree and traits pruned to exclude extinct taxa, and reconstructed BEAST trees and traits. We chose the most simple (and perhaps unlikely) models possible, using random extinctions, a strict molecular clock and BM and single-optimum OU traits.

Simulation methods

To create 'complete' phylogenies (with extinct and extant taxa), we simulated 100 trees under four extinction scenarios. We used multiple extinction scenarios because the loss of extinct sequence data earlier or later in history might affect tree reconstructions. DNA sequences were modelled over the complete phylogenies.

Tree Simulations

One hundred trees with 50 species were simulated under a birth-death process for four random extinction scenarios.

Extinction Scenarios

1. Random Extinction (Null) – Birth-death trees with a speciation rate ($\lambda = 1$), and an extinction rate ($\mu = 0.3$). Trees therefore have a diversification rate of 0.7 ($r = \lambda-\mu$) (Magallon and Sanderson 2001) without any large extinction events.
2. Random and Early Extinction Event (Early) – a single extinction event early in the tree, where 30% of the species survive. Simulates an estimated mass extinction level for plants at the Cretaceous–Paleogene (K–Pg) boundary (Wilf and Johnson 2004).
3. Random and Late Extinction Event (Late) – a single smaller extinction event, where 60% of the species survive, representing a Pleistocene-like extinction rate for conifers, based on the known records (Barnosky et al. 2011).
4. Random and Double Extinction Events (Double) – A combination of the Early and Late scenarios.

Four time intervals (T0, T1, T2, T3, moving back in time from T0, the present) were used to place mass extinction events (Early = T3; Late = T1). The simulated trees had 50 extant tips and *n* number of extinct species, so that trees with higher extinction rates have more extinct taxa rather than fewer tips. The same number of tips ensures that analyses are not confounded by differences in sample sizes. Trees were simulated using the `sim.bd.taxa` function in the R package TreeSim (Stadler 2017).

DNA Sequence Simulation

Using the R package PhyloSim (Sipos et al. 2011), DNA sequences were modelled over the simulated trees that included extinct species to create simulated nucleotide sequence data. These data were subsequently used to reconstruct trees in BEAST. A single gene of 1000 base pairs was modelled under a General Time-Reversible and Gamma (GTR+G) model (Tavare 1986; Felsenstein 2004). The GTR model allows for different nucleotide frequencies, and nucleotide substitution rates that can vary individually. The DNA simulation model had base frequencies of: T and C = 0.33333333; and A and G = 0.1666667, with a gamma distribution of $\alpha = 1$. Sequences of extinct taxa were pruned from the simulated DNA sequence fasta files, creating sequences for extant only taxa. These sequences were used to reconstruct the simulated trees in BEAST.

Phylogenetic Reconstruction

Using the nexus files for extant only species we reconstructed the simulated trees in BEAST 2 (Bouckaert et al. 2014). Nucleotide frequencies were estimated under a GTR+G substitution model, with a strict clock, and a uniform Birth-Death model estimated under BEAST default settings. The MCMC chain length was 10 million. The convergence of model parameters was confirmed in TRACER v 1.6 (Rambaut and Drummond 2013). All BEAST tree reconstructions had likelihood effective sample sizes (ESS) > 200, indicating good mixing of the MCMC chain. The first 25% burnin of the MCMC chain was removed and maximum clade credibility (MCC) trees estimated in Tree Annotator (Bouckaert et al. 2014). Node heights were estimated using Common Ancestor Heights.

The aim of this study was not to assess BEAST performance *per se*, or even to recover the original simulated trees with high accuracy. In actual studies the true tree is never known, and the BEAST settings used cannot truly be verified to recover the true tree. This approach therefore aims to mimic the unavoidable error introduced by not knowing the true evolutionary history of genes.

We compared the pruned TreeSim (pTreeSim) trees with the MCC trees using Robinson-Foulds distances (RFDs) (Robinson and Foulds 1981). RFDs compare tree topologies between trees with the same tip numbers, so comparisons between the extinct and extant trees were not possible. When two trees differ in the placement of a single branch edge then RFD = 2 (Fig. 1).

Trait Simulations

To simulate traits to use in evolutionary trait modelling, we simulated continuous traits for extinct and extant taxa on the complete TreeSim trees. A single trait was simulated under 1) a BM model and 2) an OU model on 100 trees for all four extinction scenarios. Traits for extinct taxa were removed when trait models were used with extant taxa only.

Models of Trait Evolution

Trait evolution models aim to discriminate between traits evolving under drift or selection. To test this we generated two trait datasets: traits evolving under a drift BM model, and traits evolving under a single-optimum OU model, indicating selection for a single trait optimum. Two levels of trait variance were modelled for BM and OU traits.

Traits evolving under a Brownian Motion (BM) model

For traits simulated under a BM model, root values ranging from 3-30 were generated with random deviates from the uniform distribution. Two BM data sets were generated, with two different variances, sigma (σ), in the BM random walk (Fig. 2). Under $\sigma = 0.1$, the variance of the random walk is low, representing a "slow" rate of trait evolution. Under $\sigma = 1$, variances are high with trait values at the tips more dispersed than under $\sigma = 0.1$, *i.e.* a "faster" rate of trait evolution. BM traits were simulated using the function `fastBM` in the R packages phytools (Revell 2012) and ape (Paradis et al. 2004).

Traits evolving under an Ornstein-Uhlenbeck (OU) model

The single-OU model is identical to a BM model, with the exception of two parameters: alpha (α) (the optimum value traits evolve to), and theta *(θ)* (the rate at which modelled values converge to alpha). In fact, the BM model is a particular case of an OU model with a single optimum, where alpha = 0. Single optimum OU models with low alphas will closely resemble a true BM model of evolution.

Single optimum OU traits were evolved using the same root and σ values as in BM trait modelling. Theta *(θ)*, the value representing an optimum adaptive trait value, was created using random deviates from the uniform distribution with minimum and maximum values extracted from an exponential distribution. Alpha (α), the rate at which traits evolve to reach the optimum trait value was set at $\alpha = 0.5$ (refer to Table 1 for a summary of simulations).

Evolutionary Analyses

Phylogenies

We used three phylogenies ('tree types') in evolutionary analyses:

1. The complete TreeSim trees, which include extinct and extant taxa, and two variant phylogenies derived from these trees represented by (2) and (3) below.
2. The pruned TreeSim (pTreeSim) trees with extinct taxa removed.
3. The BEAST MCC trees, which are the data commonly used in comparative studies.

All four extinction scenarios described above were applied to each of the three tree types.

Lineages Through Time (LTT)

Lineages Through Time (LTT) plots and the Pybus and Harvey γ statistic were used to assess the impact of extinctions on diversification, and the effect of tree type on the estimation of diversification. To estimate the number of lineages at different time points across a tree, LTT analyses were conducted with the `ltt` function in the R package phytools (Revell 2012). LTT plots show the number of lineages at different time points across a tree (Harvey et al. 1994; Nee 2006). As lineages accumulate the slope of the line increases, allowing easy visual comparison of lineage numbers and rates of diversification over time. A decrease in lineages as a result of extinction is represented by a fall in the slope of the LTT plot when extinct taxa are included. Because diversification is exponential, extinctions are seen as a flat section when extinct taxa are absent from the tree (Crisp and Cook 2009). LTT plots were log transformed.

The Pybus and Harvey γ statistic (Pybus and Harvey 2000) tests whether rates of diversification have been constant, the expectation under a pure birth model (the null hypothesis). When γ is negative it indicates that diversification has occurred early in the tree, and when γ is positive, that diversification is closer to the tips.

Phylogenetic Signal

Phylogenetic signal (Pagel 1997; Blomberg and Garland 2002; Blomberg et al. 2003) investigates whether species' relatedness accounts for their trait value. Phylogenetic signal was estimated with Pagel's Lambda (λ), using maximum likelihood (ML). When $\lambda = 1$, trait evolution is equivalent to a BM model because the timing of species divergences accounts for species' trait differences. When $\lambda = 0$, branch lengths are reduced to zero creating a single polytomy or 'star' phylogeny, indicating that species relationships have no effect on trait evolution. When lambda is low (< 1), species' traits are less alike than would be expected given a BM expectation and the phylogeny, and when very high (> 1), species' traits are more similar than expected given a BM model.

Lambda relies on the timing of species divergences to create a covariance matrix. It could therefore be susceptible to changes in tree topology, theoretically leading to an over- or underestimation of phylogenetic signal.

Lambda has been shown to be a robust method to measure the statistical dependence of traits on trees (Freckleton et al. 2002). For each trait data set we estimated phylogenetic signal for TreeSim trees, pTreeSim trees and MCC trees under four extinction scenarios. Significance was tested with 999 randomisations of the data. Phylogenetic signal tests were conducted in R using the `phylosig` function in the phytools package.

Ancestral Character Estimation

Ancestral Character Estimation (ACE) was used to investigate the effect of extinctions on the ability to predict ancestral characters. ACE was estimated under a BM model using the `ace` function in the R package ape. Under a BM model, the root value should be the mean of the trait values at the tip. If random extinctions distort the distribution of values at the tips, ACE accuracy should be affected. We were able to compare estimated root values against the true root values used to simulate trait data to access accuracy.

Evolutionary Modelling

We used macroevolutionary models within a ML framework to examine the effect of extinctions on trait evolution models. We used eight to models to fit to the data: Brownian Motion (BM) (Felsenstein 1973), Ornstein-Uhlenbeck (OU) (Butler and King), lambda (λ), kappa ($\varkappa$), delta (δ), (Pagel 1997) Early Burst (EB), (Harmon et al. 2010), Late Burst (LB) (Blomberg et al. 2003) and White Noise (WN). Models were fitted using maximum likelihood (ML). Model selection was performed using sample-size corrected second-order Akaike information criterion (AICc) weights. Models were fitted using the function `fitContinuous` in the R package geiger (Pennell et al. 2014).

RESULTS

Tree Simulations

The effect of modelling trees with extant data and selection of a strict clock affected the ages of the trees: nodes in all MCC trees were far younger than in the simulated trees (data not shown). BEAST reconstructed all sister pairs accurately, and most trees did not differ substantially in topology at shallower nodes. However, there were large differences in tree topology between the TreeSim trees and pTreeSim and MCC trees (Fig. 1A), but far fewer between pTreeSim and MCC trees, though they too differed in

the placement of deeper internal nodes (Fig. 1B). The mean RFDs of pTreeSim and MCC tree comparisons ranged from 8.34 (Late) – 9.02 (Double), with a maximum of 22 (Fig. 3), i.e. 11 branch differences between two trees tree with 50 taxa. Standard deviations were between 4.34 and 4.71. Extinction scenario made no difference to RFDs.

LTT & Gamma

Lineages through time plots demonstrated that the modelling of extinctions was successful, as large drops in lineage numbers are visible in the plots of simulated trees (Fig. 4). The steep slope of lineage accumulation indicated the high rate of diversification ($r = 0.7$) set in the simulation parameters. In all LTT plots of the MCC trees there was a noticeable decline in the gradient of the slope towards the present, representing a slowdown in the rate of diversification. In TreeSim trees, γ values had a wide distribution, regardless of extinction scenario, indicating that extinctions were random across individual trees (Fig. 5). Mean gamma for TreeSim and MCC trees were marginally below zero for all extinction models (Table 2). The range of gamma was larger when extinctions were large (Double) or occurred early (Early) in TreeSim trees (Fig. 5). In early extinctions mean gamma was marginally more negative, but 41% of the early extinction trees had a positive gamma (data not shown). For all extinction scenarios, the removal of extinct taxa (pSimTrees) resulted in a higher mean gamma. Regardless of extinction scenario, mean gamma for the MCC trees was always more negative than mean gamma of TreeSim trees, indicating even or early diversification (Table 2). There were no instances of late diversification, indicated by positive gamma in the MCC trees (Fig. 5), except for a single outlier in the early extinction. As a result, the proportion of significant gamma results was inflated for MCC trees (median $P = 0.01$) compared to simulated trees, especially when extinctions were very low, as in the Null extinction simulated trees (Fig. 5). In the case of Null TreeSim trees, diversification rates were non-significant in 84% of trees (median $P = 0.47$). In TreeSim trees only 16% had a significant ($P < 0.05$) gamma to the null expectation, whereas in MCC trees the number of significant results was 69% (Table 2).

Phylogenetic Signal

Because all BM and OU traits were modelled using trees with extinct taxa, we were able to observe the effect of different tree topologies on estimates of phylogenetic signal. As expected, TreeSim trees showed highly significant phylosignal ($\lambda = 0.88$ to

1.00), regardless of extinction scenario or whether traits were BM or OU (Table 3, Fig. 6). Phylogenetic signal was higher in pruned TreeSim trees with BM traits ($\lambda = 0.87$ to 1.04) than in TreeSim trees, but highest in the MCC trees ($\lambda = 0.98$ to 1.12), showing an upward trend across all extinction scenarios. Ninety to ninety-five percent of lambdas for BM traits on MCC trees were higher than one, indicating more similarity among traits than predicted by the tree under a BM model (Table 3). The highest lambda values were in MCC trees with Null Extinctions (maximum $\lambda = 1.12$). Phylogenetic signal was lower for OU traits on pruned ($\lambda = 0$ to 1.01) and MCC trees ($\lambda = 0.60$ to 1.05). Again, λ were elevated when using pruned or reconstructed trees (λ pTreeSim = 17 to 26%, λ MCC = 59 to 68%) (Table 3, Fig. 6), but the percentage of erroneously high lambdas in OU traits was not as extreme as for BM traits (Table 3). Only 1-3% of OU traits on pTreeSim and MCC trees had false, non-significant phylogenetic signal. Trait variance had no effect on phylogenetic signal (data not shown).

Ancestral Character Estimation

We measured the relative increase or decrease in the reconstructed root value compared to the true root value, expressed as a percentage, to estimate how accurately the root value was calculated. The type of tree used to estimate the ancestral root had a large impact on accurate reconstructions. Estimating the root value with extinct trait data (TreeSim trees) produced the closest values to the true root. Percentage differences in root values were highest under higher trait variance ($\sigma = 1$) for all extinction scenarios under a BM model (Fig. 7). Standard deviations of the ACE root values were consistently higher in OU than in BM models for all three tree types and across all four extinction scenarios (Table 4). Using either pruned pTreeSim trees or MCC trees root estimates were highly erroneous, but they were similarly erroneous, indicating the impact of lost trait data in extinct taxa. Root values in both OU datasets were overestimated by 500% in some cases (Fig. 7).

Evolutionary Modelling

Eight evolutionary models were fitted to traits simulated under BM and OU models. Traits were modelled on pruned simulated (pTreeSim) trees and MCC trees only, because it is not possible to fit evolutionary models on trees with extinct taxa in the function `fitContinuous`. Akaike Information Criterion weights (*AICcw*) were used to identify the best fitting model of the models tested. The results here refer to the median *AICcw* for each tree-trait combination. For all extinction scenarios, traits

simulated under a BM model were correctly identified as best fitting a BM model when using pTreeSim trees, but were incorrectly identified as evolving under an Early Burst model when modelled on MCC trees under all extinction scenarios (Fig. 8). Traits simulated under an OU model were equally likely to fit an OU or Late Burst model when modelled on pTreeSim trees for all extinction scenarios. When OU traits were modelled on MCC trees, traits fitted a BM model, however, AICc weights were low, showing that no single model was good at discriminating the pattern of OU trait data on MCC trees (Fig. 8).

DISCUSSION

Because DNA degrades rapidly after death, it is usually impossible to obtain DNA sequences of ancient extinct ancestors. The lack of ancient DNA can affect the accuracy of phylogenetic tree reconstructions and the evolutionary trait models that rely on those phylogenies. But does it really matter that we cannot account for extinct taxa? Do extinctions really have a dramatic or even a negligible effect on phylogenetic reconstructions and thus macroevolutionary trait models?

Extinctions affect tree reconstruction and measures of diversification

Despite the lack of sequence data of extinct taxa, BEAST was able to reconstruct sister species relationships perfectly, and shallow nodes were also placed with high accuracy. However, deeper relationships were less well resolved, and there were large rearrangements of MCC tree topology towards the base of the tree (Fig. 1).

The LTT plots for reconstructed MCC trees showed a noticeable slowdown in diversification toward the present. In contrast, the LTT plots for complete and pruned complete trees showed a steep gradient, expected under a low extinction birth-death model (Nee et al. 1994). Explanations for the slowdown observed in LTT for MCC trees are multitude, ranging from incomplete sampling (Nee et al. 1994), poor identification of recently diverged species (Purvis et al. 2011), density dependent diversification as a result of niche filling (Purvis et al. 2011; Price et al. 2014), species richness (Rabosky 2013), time for speciation (Etienne and Rosindell 2012), non-random extinctions (Rabosky 2009) or a combination of these factors (Moen and Morlon 2014; Gascuel et al. 2015).

The Pybus and Harvey γ statistic showed significantly negative gamma values associated with tree type, but not with extinction scenario. In fact, the largest difference in gamma was between simulated and MCC trees under the Null extinction scenario. These results suggest that the slowdown in diversification rates could be an artefact of tree reconstruction methods. When using only extant data, BEAST priors may have a smoothing or homogenising effect on branch lengths resulting in the observed slowdown. This may be related to the birth-death model and/or clock settings and suggests that branch lengths are longer than they should be toward the present. Because we used BEAST default settings, this result could be due to a simplified approach to phylogenetic analyses, but widespread commentary on slowdowns in diversification rates suggests the phenomenon is commonly observed (Rabosky 2009; Purvis et al. 2011; Etienne and Rosindell 2012; Rabosky 2013; Moen and Morlon 2014; Price et al. 2014; Gascuel et al. 2015). Thus the slowdown is likely to be a result of the model and the data used in tree reconstructions, implying that interpretations of diversification rates, the timing of extinctions and temporal triggers of trait evolution are all in question.

Extinctions affect tree topology which skews phylogenetic signal

The phylogenetic signal of traits on pTreeSim and MCC trees was higher than expected (i.e. lambda > 1) for both BM (90 to 95%) and OU (59 to 68%) traits (Table 3). This indicates that traits were more similar than predicted by the tree and that phylogenetic signal was influenced by tree topology. The removal of extinct taxa significantly changes tree topology and therefore evolutionary relationships among taxa. If traits have evolved under a pure BM model, sampling traits from the present actually represents a subsample of traits values. The combined effect of reconfigured species relationships and undersampling of the BM process is what most likely leads to higher phylogenetic signal than expected. When traits have evolved under a BM model across the timespan of the tree, the undersampling of extinct species in the phylogeny leads to the erroneous interpretation that trait evolution has been constrained.

Extinctions make ancestral character estimation of the tree root problematic

Concerns about the accuracy of ancestral trait reconstruction are long standing. These concerns range from methodological approaches used (Cunningham et al. 1998; Duchene and Lanfear 2015; King and Lee 2015), to inaccuracies due to evolutionary

processes shaping traits (Oakley and Cunningham 2000; Webster and Purvis 2002). For example, estimations of ancestral characters are known to be poor when the distribution of extant traits does not include the ancestral root value (i.e. trait evolution with a directional trend) (Oakley and Cunningham 2000). Because of directional trends in character evolution, it has been suggested that traits showing strong phylogenetic signal, and therefore assumed to fit a BM model, are more likely to produce reliable ancestral trait reconstructions (Litsios and Salamin 2012). But despite high phylogenetic signal, the estimation of root values on the MCC trees tends to be inaccurate (high standard deviations) even in Null extinction scenarios and BM traits with low variance. Also, and perhaps more concerning, is the common interpretation that traits with high phylogenetic signal are evolving under a BM model. Our results show that single-optimum OU traits can also show high phylogenetic signal. If OU traits are incorrectly assumed to be evolving in a BM manner because of high phylogenetic signal, root estimates can be overestimated by as much as 500% according to our simulations. The implication here is that it is impossible to know just how incorrect ancestral character estimation is because phylogenetic signal does not describe any particular evolutionary processes (Revell et al. 2008).

The different topology of trees lacking extinct taxa has a very large effect in ancestral character estimation (Cusimano and Renner 2014), but even when we used extinct taxa and traits, root estimates were poor for OU traits (as seen by large standard deviation values, Table 4). This is because there was no trait data available close to the root. Additionally, the strength of attraction to the trait optimum (α) affects how accurate trait reconstruction will be under an OU model because the optimum trait value is reached more or less rapidly depending on the strength of alpha (Butler and King 2004).

Implications of extinctions on tree reconstruction and evolutionary trait models

Model-based methods are recommended to pin down the most likely process of trait evolution. If evolutionary models can detect whether traits fit a BM or OU model, then ancestral estimates might be more accurate, giving valuable insights into trait change over time. However, we show that evolutionary models are just as susceptible to tree topology as the other methods investigated here (LTT and gamma, phylogenetic signal and ACE). In every extinction scenario, BM traits modelled on MCC trees were more likely to fit an Early Burst model, and OU traits to fit a BM or Late Burst model. This makes sense when we know that BM traits had high phylogenetic signal as a result of

undersampled extinct data, but in the absence of that information, interpretation can be bewildering. Perhaps more importantly, tree topology swamped any extinction signal in the data – every extinction scenario fitted the same models in the same way, though with small differences in variance.

This gives rise to the frightening thought that inferred early bursts of trait diversification could also be a tree-related phenomenon. It also suggests that traits appearing to evolve under a BM model can be evolving to an optimum with a trend. The difference between a pure BM model and an OU model with low alpha is slight, and model discrimination with small trees (< 200 taxa) can be poor (Cooper et al. 2016b), perhaps explaining this result. Unfortunately, had we not known that our 'BM' model was in fact a single-optimum OU model, we would again have made incorrect inferences about the process of trait evolution. We would have interpreted a trait evolving with a trend to an optimum to be a 'conserved' trait, and this could have been confirmed by its high phylogenetic signal. Any ancestral character estimation would therefore also seem to be valid, but the ancestral values could be highly erroneous depending on the strength of the trend.

Another consideration (not investigated here) is whether the evolutionary past has left a mark on diversification. If extinctions are non-random, or if speciation is not independent from traits like life history, growth habit or environment (Lanfear et al. 2013; Bromham et al. 2015), then molecular evolution may not be 'neutral'. If the reconstructed tree is in fact a reflection of trait-biased diversification, trait models will be unable to find any model other than a BM model because the loci used to reconstruct the tree are not independent of diversification. The assumption that a phylogenetic tree is evolving under BM model, or is neutral is in question in such cases.

Many researchers will have had unsettling thoughts about how the trees they use effect their interpretation of trait evolution (Losos 2011). This is exacerbated by the multiple sources of potential error in trait models (Cooper et al. 2016a; Cooper et al. 2016b). It has been shown that well placed fossil data improves the accuracy of trait modelling because 1) fossils can invalidate poor models of trait reconstructions (Meseguer et al. 2015; Puttick and Thomas 2015; Sherratt et al. 2015; Saladin et al. 2017; Schnitzler et al. 2017), and 2) fossils can rectify some of the evolutionary signal lost through extinction when used in models (Slater et al. 2012). Recent studies found model

inaccuracy when comparing extant-only data to fossil evidence in birds (Mitchell 2015), but not in mammals (Puttick and Thomas 2015), results that probably reflect different levels of trait disparity in the extant groups.

Unfortunately, many groups do not have a good fossil record, so the 'true' evolutionary tree cannot be recovered because of undersampling due to extinctions. If tree reconstruction obscures actual evolutionary processes because extinct taxa cannot be sampled, the downstream consequences for evolutionary trait modelling are serious. The effect of the gap between 'true' trees and reconstructed trees on trait models has not been investigated using simulations before. A previous study by Sanmartin (Sanmartin and Meseguer 2016) found that extinctions affect tree reconstruction and estimates of diversification rates. We found the same, but also that commonly used PCMs were affected by trees reconstructed from extant-only data. Phylogenetic signal, ancestral character estimation and evolutionary trait models were all unable to recover the initial evolutionary process shaping traits, even in the most conservative cases of a constant, random background extinction rate and traits evolving under BM. These results suggest that, depending on the extant study group, we may be analysing phylogenetic reconstruction methods far more than we are analysing diversification or trait evolution.

This problem with the way trait evolution models use phylogenies is two-fold. First, models assume the tree to be 'true' (Felsenstein 1985; Grafen 1989). Secondly, the entirety of the tree is used. Thus the relationships are taken as evolutionary fact, even though the effect of extinctions is to distort the actual evolutionary relationships between taxa and clades. Inaccurate relationships toward the base of the tree reflect diminishing signal in extant genetic data, rather than a plotted map of evolutionary history, suggesting that methods need to be developed that do not rely on the estimation of root values. Alternatively, estimations should be able to accommodate a wider range of scenarios towards the root of the tree.

Table 1. Extinction scenarios, trees and traits used in simulations.

Extinction Scenarios			
Null	**Early**	**Late**	**Double**
Background Extinctions = 30% extinct	Early Extinction Event = 70% extinct	Late Extinction Event = 40% extinct	Early and Late Extinctions = 70% + 40% extinct
Tree Types			
TreeSim	**pTreeSim**	**MCC**	
Simulated Tree with Extinct and Extant	Simulated Tree with Extinct removed	BEAST MCC Tree	
Trait Models		*Sigma*	
BM	**OU**	**σ**	
Traits evolve under under a Brownian Motion model	Traits evolve under a single-optimum Ornstein-Uhlenbeck (OU) model. The optium applies to the whole tree.	All trait datasets are fitted with one of two different variances of a random walk (σ); 0.1 or 1	

Table 2. Results of lineages throught time (LTT) gamma tests. Mean gamma, standard deviation (SD) of gamma and the number of trees with significant gamma, indicating non-constant diversification rates. TreeSim = simulated trees with extinct and extant taxa; pTreeSim = simulated trees with extinct taxa removed; MCC = BEAST maximum clade credibility tree. Null, Early, Late and Double refer to the levels of extinction modelled in simulated trees.

	Null			**Early**			**Late**			**Double**		
	Mean γ	*SD*	*n* Trees *P < 0.05*	*Mean γ*	*SD*	*n* Trees *P < 0.05*	*Mean γ*	*SD*	*n* Trees *P < 0.05*	*Mean γ*	*SD*	*n* Trees *P < 0.05*
TreeSim	-0.393	1.207	16	-0.882	2.015	38	-0.374	1.319	17	-0.313	1.754	25
pTreeSim	0.611	1.058	11	1.328	1.049	31	1.410	0.872	27	1.979	0.934	56
MCC	-2.446	0.834	69	-2.047	0.811	56	-0.257	0.731	59	-1.759	0.781	40

Table 3. Phylogenetic signal (λ) and *P* values for BM and OU trait data and four extinction scenarios, estimated on trees with extinct taxa included (TreeSim), extinct taxa removed (pTreeSim), and MCC trees (MCC). The number of samples where lambda was larger than one is shown in bold.

			λ TreeSim	**P (TreeSim)**	**λ pTreeSim**	**P (pTreeSim)**	**λ MCC**	**P (MCC)**
BM	Null	Min	0.97	0.00	0.87	0.00	0.99	0.00
		Max	1.00	0.00	1.04	0.00	1.12	0.00
		λ > 1 *(n)*	**0**	**–**	**62**	**–**	**90**	**–**
	Early	Min	0.98	0.00	0.97	0.00	0.98	0.00
		Max	1.00	0.00	1.01	0.00	1.04	0.00
		λ > 1 *(n)*	**0**	**–**	**57**	**–**	**95**	**–**
	Late	Min	0.97	0.00	0.98	0.00	1.00	0.00
		Max	1.00	0.00	1.01	0.00	1.10	0.00
		λ > 1 *(n)*	**0**	**–**	**47**	**–**	**95**	**–**
	Double	Min	1.00	0.00	0.96	0.00	1.00	0.00
		Max	1.00	0.00	1.01	0.00	1.04	0.00
		λ > 1 *(n)*	**0**	**–**	**57**	**–**	**95**	**–**
OU	Null	Min	0.88	0.00	0.00	0.00	0.69	0.00
		Max	1.00	0.00	1.01	1.00	1.05	0.47
		λ > 1 *(n)*	**0**	**–**	**26**	**–**	**68**	**–**
	Early	Min	0.90	0.00	0.18	0.00	0.62	0.00
		Max	1.00	0.00	1.01	1.00	1.04	0.01
		λ > 1 *(n)*	**0**	**–**	**24**	**–**	**65**	**–**
	Late	Min	0.97	0.00	0.00	0.00	0.60	0.00
		Max	1.00	0.00	1.01	1.00	1.03	0.01
		λ > 1 *(n)*	**0**	**–**	**17**	**–**	**59**	**–**
	Double	Min	0.99	0.00	0.29	0.00	0.74	0.00
		Max	1.00	0.00	1.00	0.43	1.03	0.01
		λ > 1 *(n)*	**0**	**–**	**21**	**–**	**60**	**–**

Table 4. Comparisons of the true root value and the root value estimated using ancestral character estimation (ACE). Results are displayed showing the standard deviation of percent differences in root values. Comparisons were made using three tree types (TreeSim: simulated tree with extinct trait data; pTreeSim: simulated tree with extinct traits removed; MCC: the BEAST reconstructed tree with extant traits), under four different extinction scenarios (Null, Early, Late, Double) and traits simulated under two models (BM and OU).

		Null		**Early**		**Late**		**Double**	
Trait Model	*TreeType*	*SD* ($\sigma = 0.1$)	*SD* ($\sigma = 1$)	*SD* ($\sigma = 0.1$)	*SD* ($\sigma = 1$)	*SD* ($\sigma = 0.1$)	*SD* ($\sigma = 1$)	*SD* ($\sigma = 0.1$)	*SD* ($\sigma = 1$)
BM	Root v TreeSim Estimate	4.38	10.27	5.53	14.45	6.70	14.99	4.09	16.27
	Root v pTreeSim Estimate	12.68	45.63	21.32	51.84	13.54	36.35	14.68	50.86
	Root v MCC Estimate	12.82	46.05	21.24	52.15	13.38	36.05	14.73	51.21
OU	Root v TreeSim Estimate	55.20	55.46	46.98	47.36	64.34	63.43	69.57	69.07
	Root v pTreeSim Estimate	101.34	101.34	106.14	106.90	102.44	102.05	106.71	106.66
	Root v MCC Estimate	101.39	101.39	106.12	106.77	102.44	102.04	106.71	106.61

A.

B.

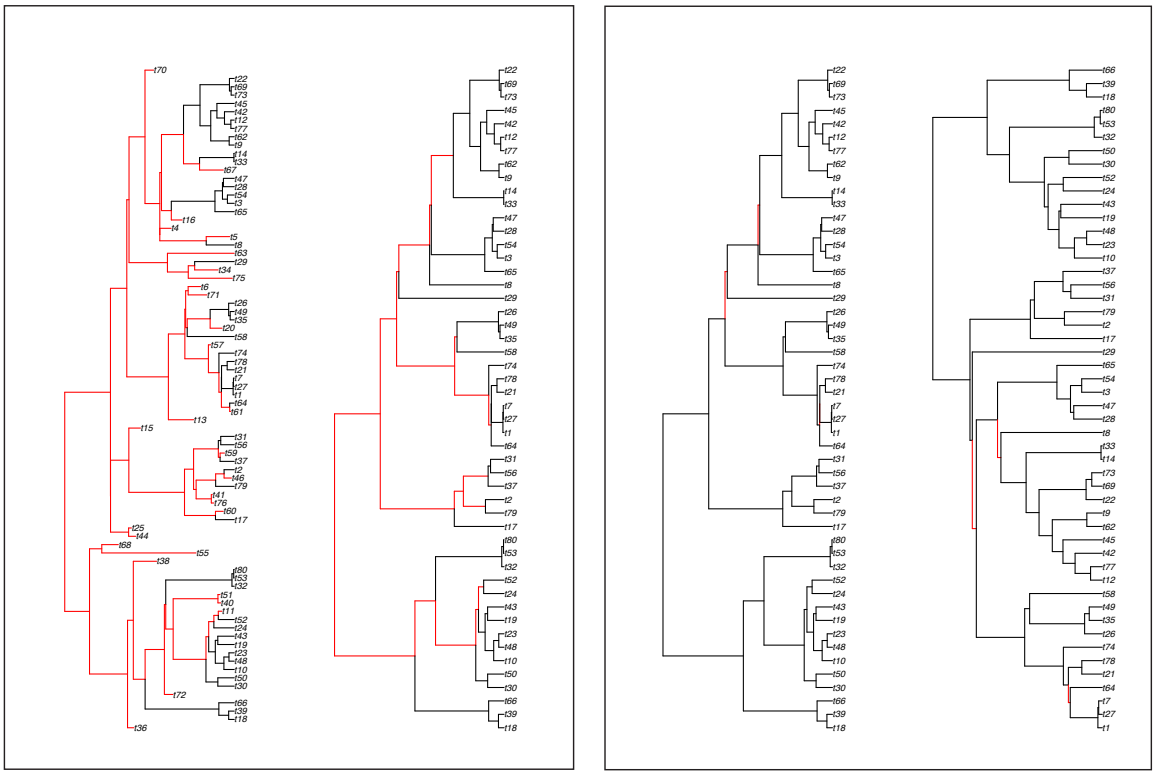

Figure 1. One of one hundred trees simulated under the null extinction scenario, showing differences in topology between A) TreeSim trees (with extinct taxa) and pruned TreeSim (pTree) trees, and B) pTreeSim trees and the MCC tree reconstructed in BEAST. Branches coloured in red indicate unique edges in the trees compared. For example, the Robinson-Foulds Distance (RFD) for the trees shown in B is 6, because there are three edge differences between the two trees. Plots were constructed using the function `phylo.diff` in the R package distory.

A. B.

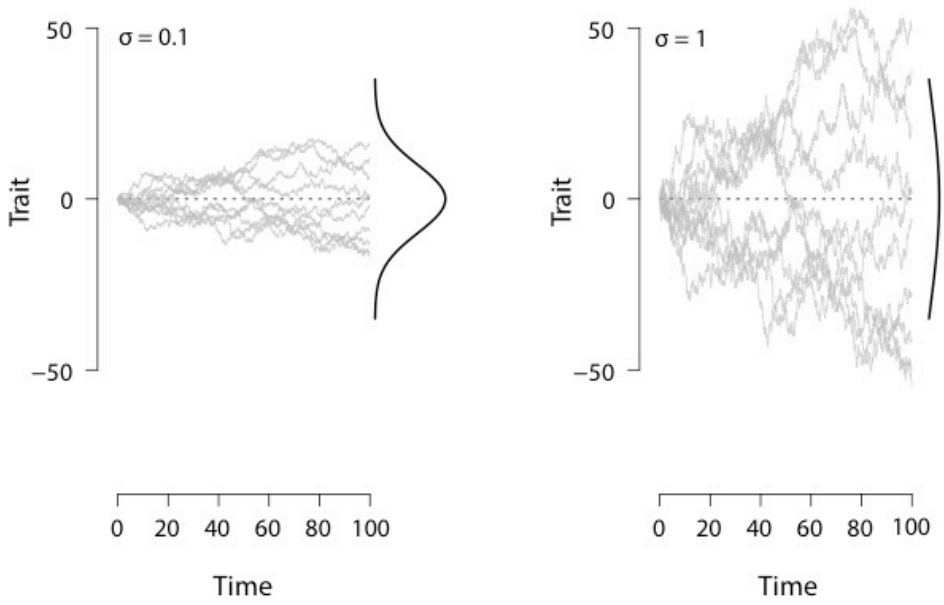

Figure 2. Plots demonstrating the effect of the variance parameter, sigma (σ) of the Brownian Motion random walk on trait values at the tips. A) Under low σ, the smaller variance of the random walk results in smaller variance at the tips. B) Trait variance is larger under higher σ. A density curve of the normal distribution is plotted to emphasise the effect of σ on trait distributions. The code to create the plots is from Wagenmakers, J and Gronau, Q.F., *A Compendium of Clean Graphs in R*., Version 2.0 http://shinyapps.org/apps/RGraphCompendium/index.php.

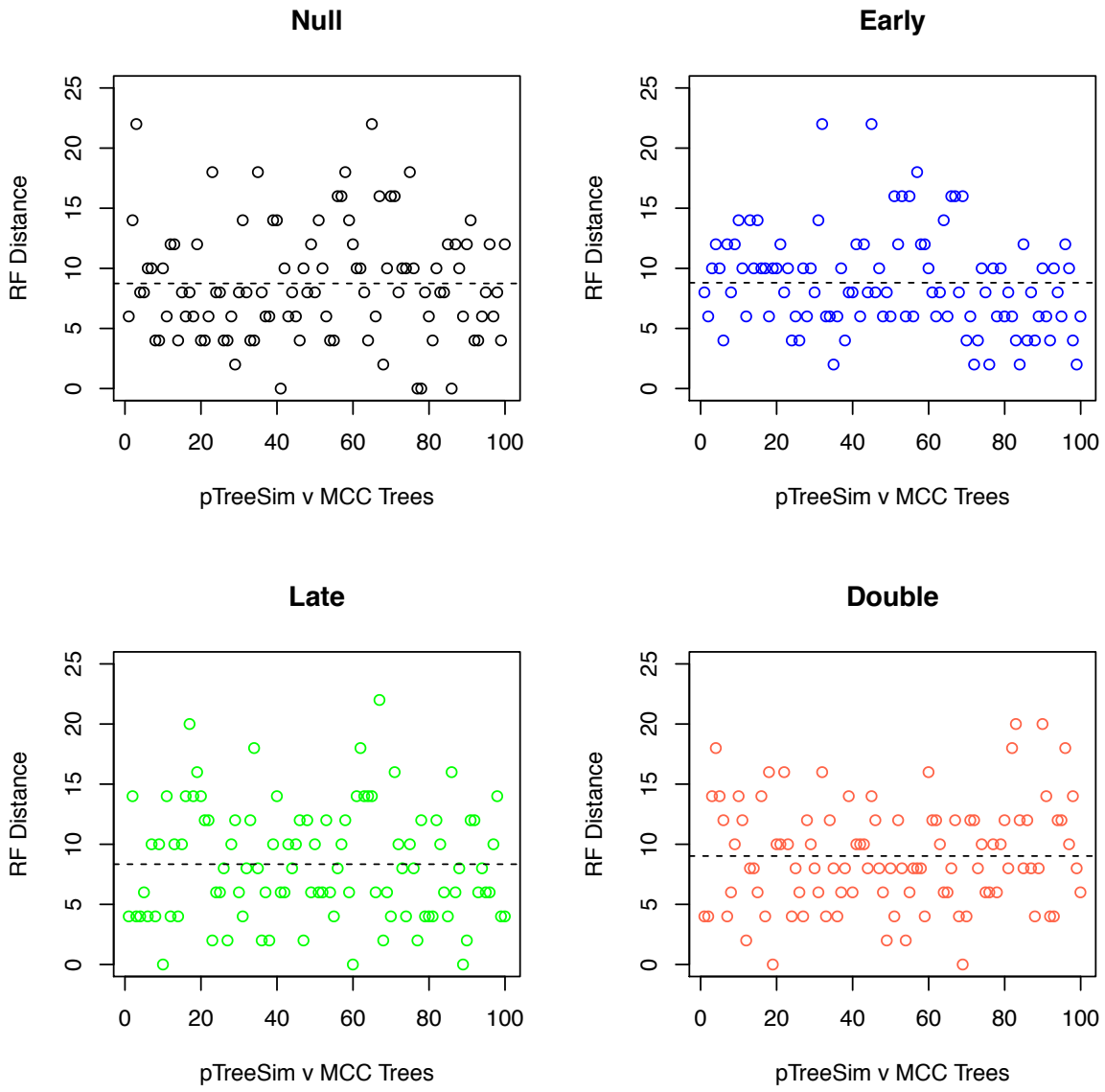

Figure 3. Robinson-Foulds distances (RFDs) comparing tree topology in pruned simulated (pTreeSim) and MCC trees for each extinction scenario. Dotted horizontal lines indicate the mean RFD.

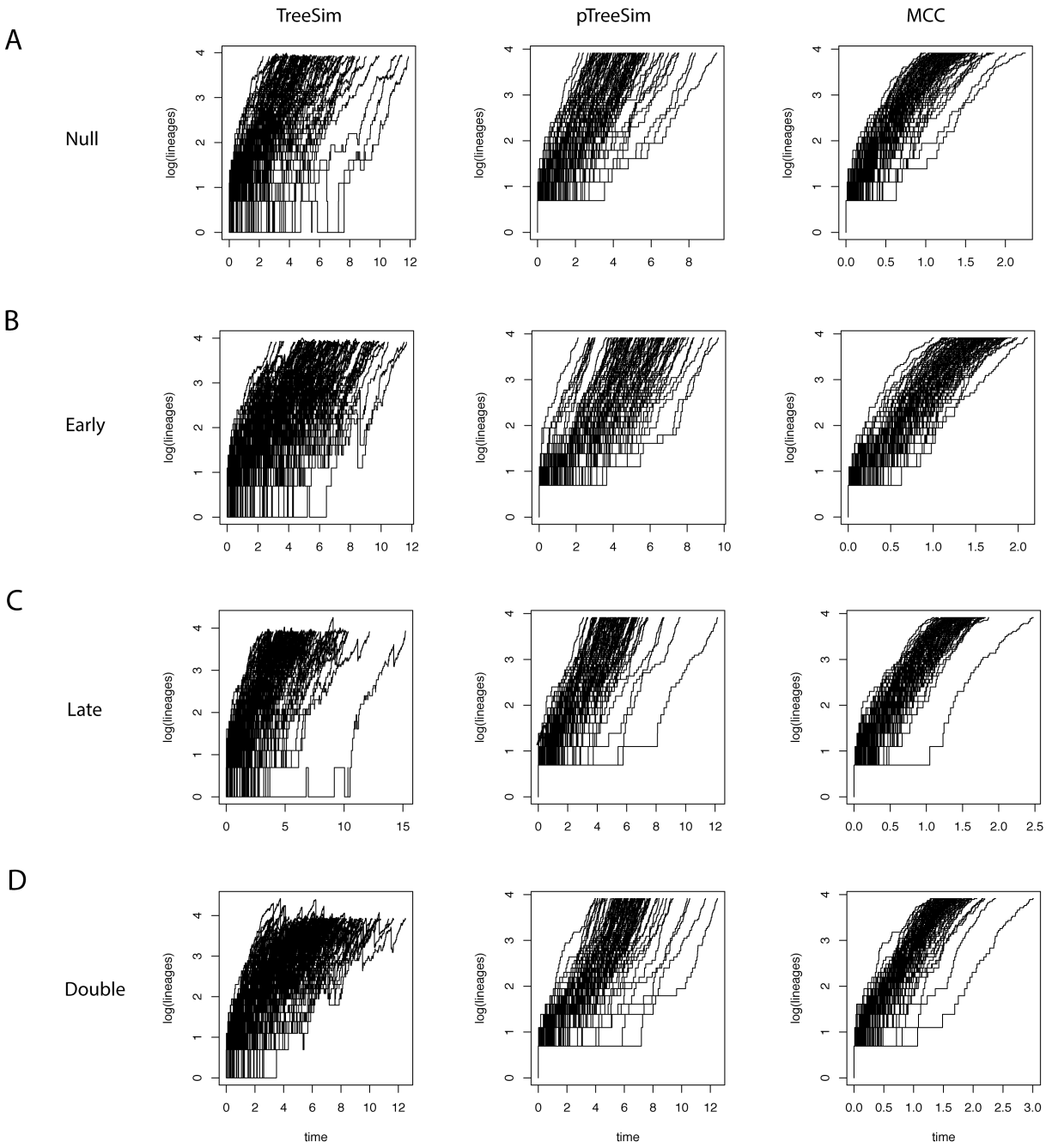

Figure 4. Lineage Through Time (LTT) plots for A) background Null extinctions; B) Early Extinction; C) Late Extinction and D) Double Extinction. For each extinction scenario individual plots show LTT for 100 trees with extinct species (TreeSim trees); simulated trees with extinct species removed (pTreeSim trees) and BEAST MCC trees. Extinctions can be seen in downward steps in the simulated (TreeSim) plots.

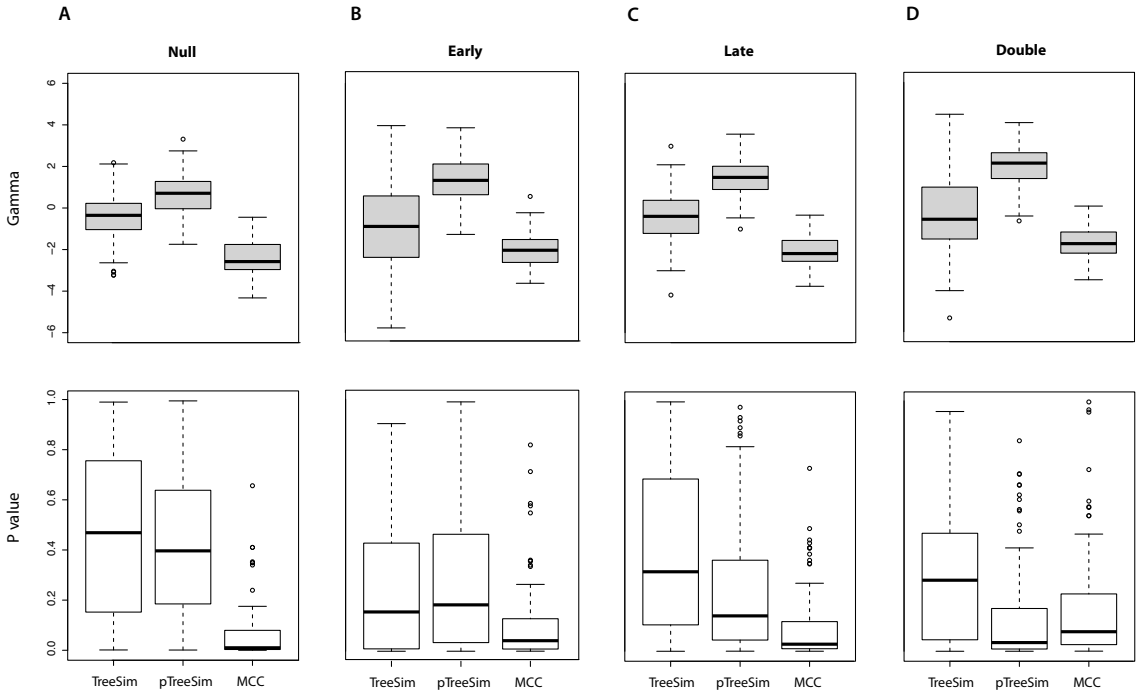

Figure 5. Boxplots of Pybus and Harvey's gamma for A) Null Extinction Event, B) Early Extinction, C) Late Extinction and D) Double Extinction. The upper panels are boxplots of the γ-statistic ordered by tree type (TreeSim, pTreeSim and MCC). The lower panels are *P* values for gamma. Each boxplot represents 100 trees with 50 tips.

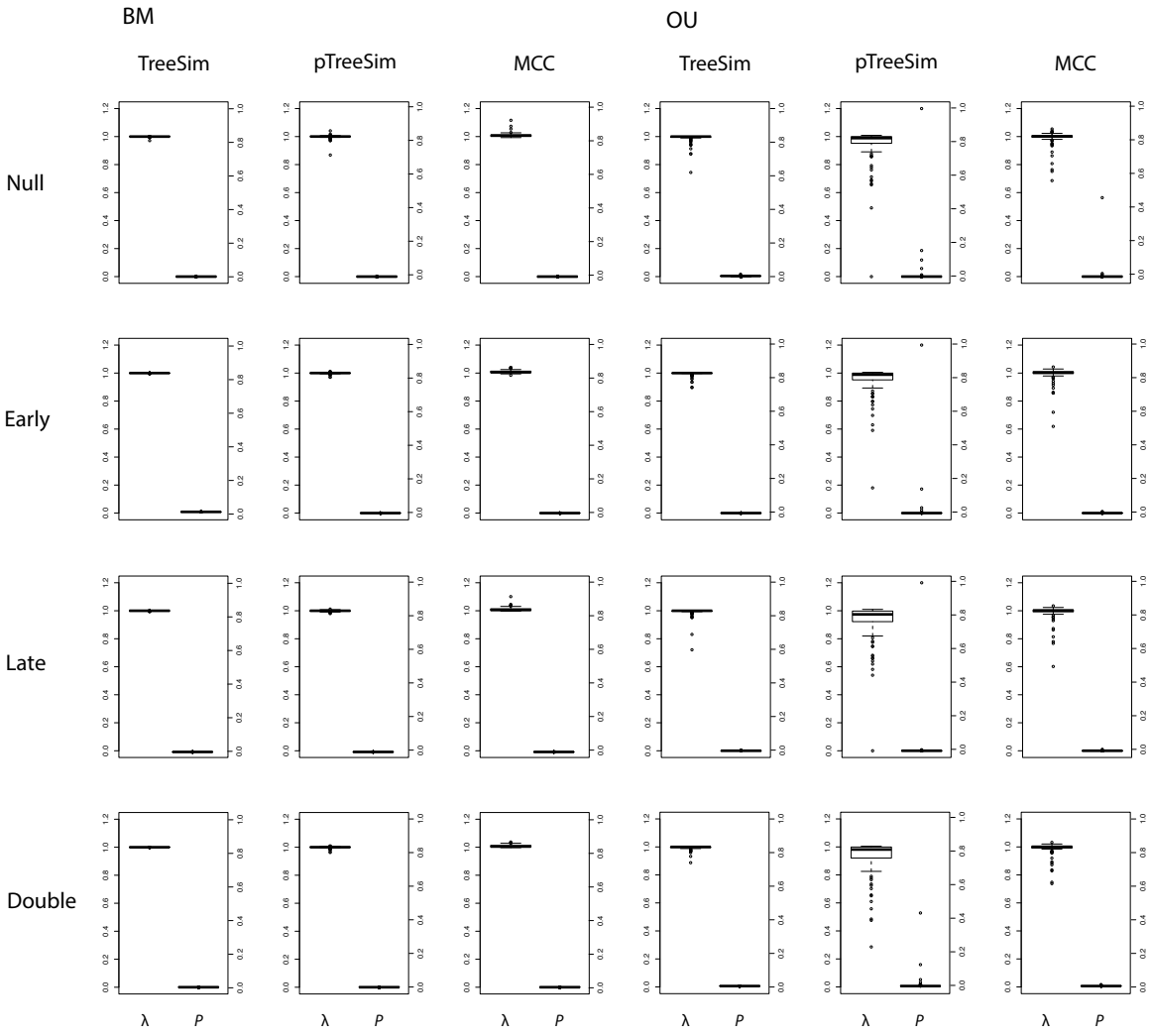

Figure 6. Boxplots of phylogenetic signal according to Pagels's Lambda (λ) Results are arranged by trait type (BM and OU); tree type (TreeSim, pTreeSim, MCC); and extinction scenario (Null, Early, Late, Double). For each boxplot frame, lambda (λ) is plotted on the left with the significance value of lambda *(P)* on the right.

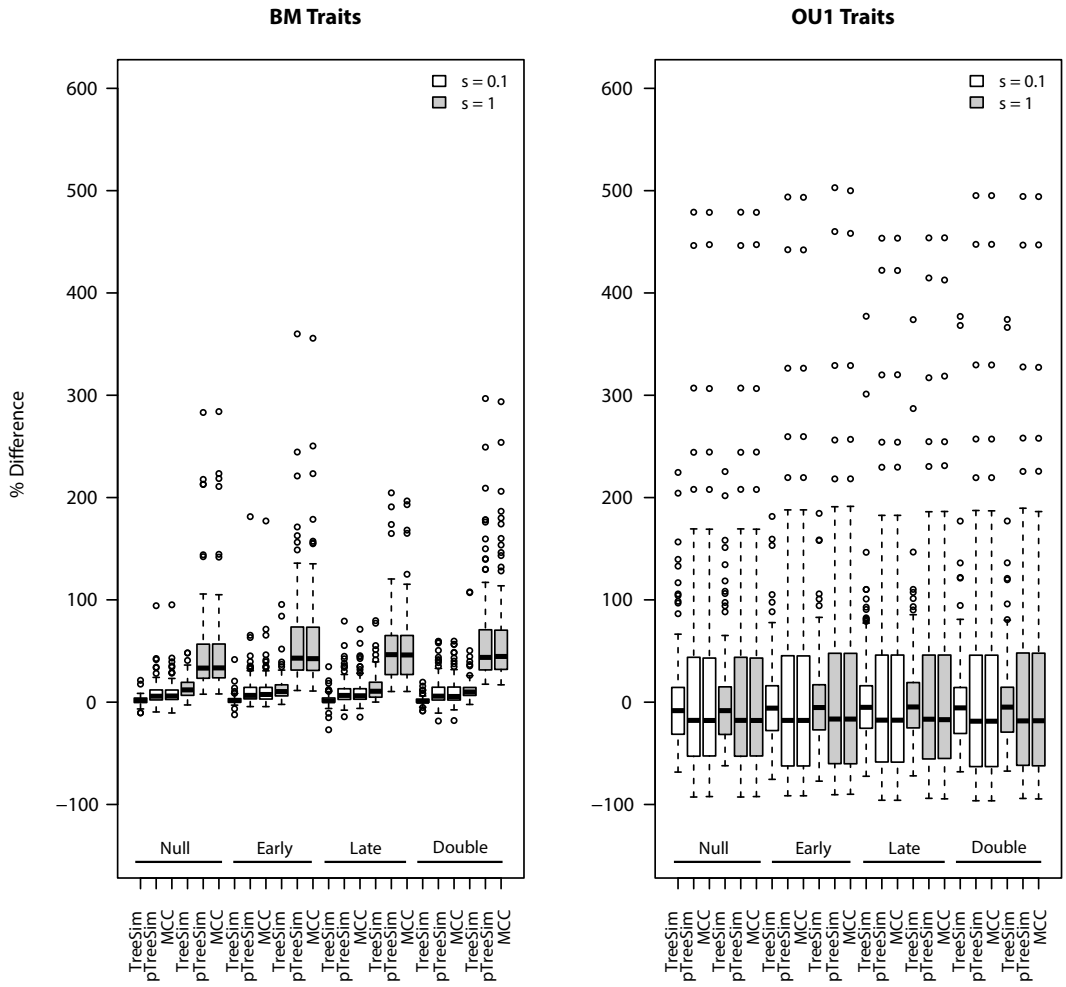

Figure 7. Boxplots of ancestral character estimation (ACE) of the root value for traits evolved under two different models: Brownian Motion (BM, left) and single-optimum Ornstein Uhlenbeck (OU, right). Each boxplot shows the difference between the true root and the estimated root expressed as a percent. Comparisons were made between extinction models (Null, Early, Late and Double, shown by bars at the bottom of each plot); the tree type (TreeSim, pTreeSim, and MCC) and the variance of the random walk used to simulate traits ($\sigma = 0.1$, the first three boxplots in each extinction model shown in white; and $\sigma = 1$, the last three boxplots in each extinction model shown in grey).

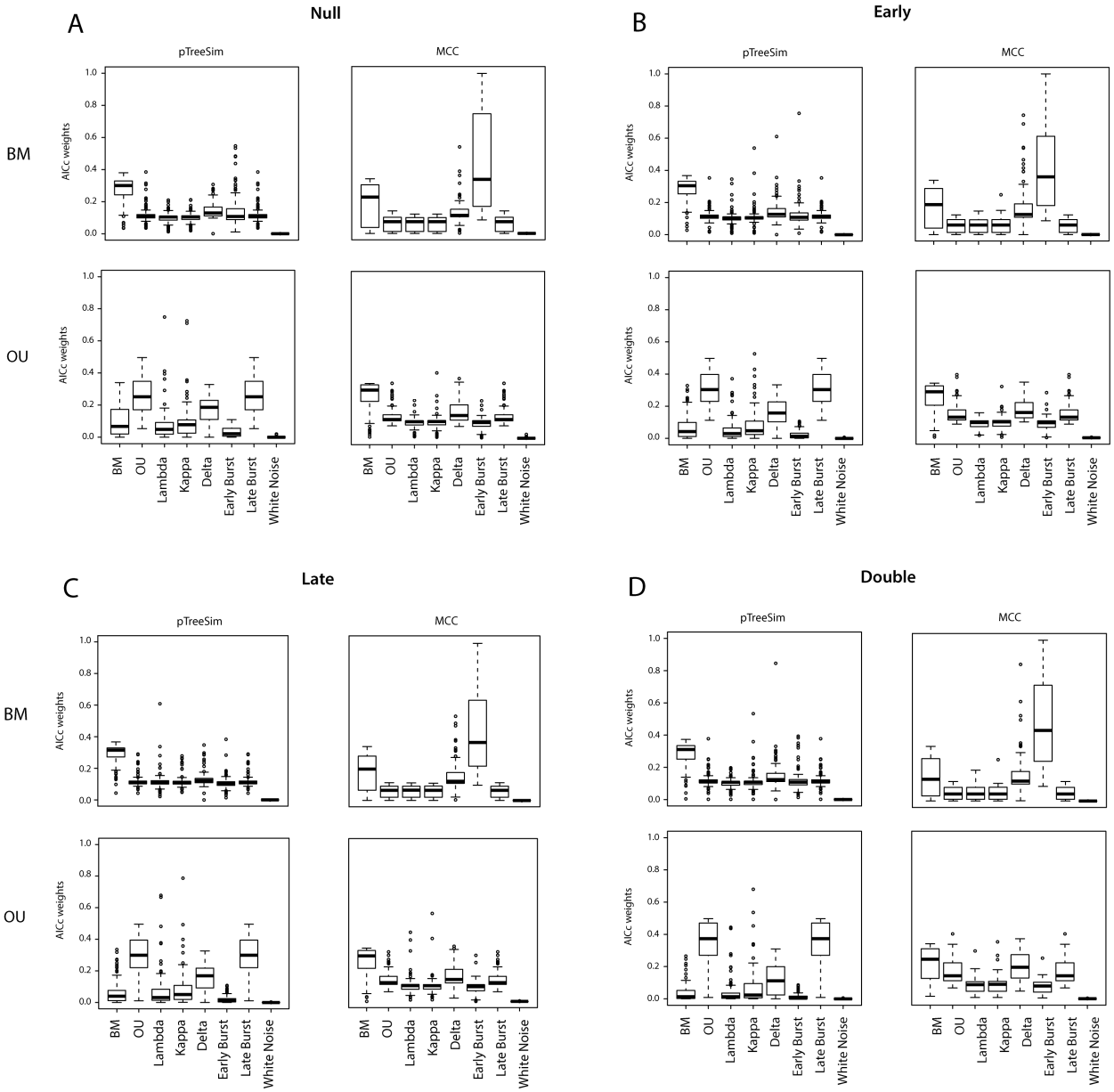

Figure 8. Boxplots of AICc weights comparing eight evolutionary models. A) Null; B) Early; C) Late and D) Double extinctions. The upper two boxes within each extinction group are trait evolution model results for BM simulated traits on pTreeSim trees (left) and MCC trees (right). The lower two boxes are trait evolution model results for OU simulated traits. Boxplots are organised by model type: Brownian Motion (BM), Ornsein-Uhlenbeck (OU), Lambda, Kappa, Delta, Early Burst, Late Burst and White Noise.

Concluding Remarks

CONCLUDING REMARKS

Callitris are endemic to Australia, a continent with ancient geology and low elevation that has been undergoing increasing aridification since the late Eocene. As seasonal climates were established (with both winter and summer rainfall zones), and Australia gradually became a more arid, distinct regional climatic niches developed. It is hard to image that a conifer lineage from ever-wet habitats 40 million years ago would become the most drought-tolerant tree species in the world.

Drought Adaptation and Diversification

It is hypothesised that aridity accelerates plant evolution (Stebbins 1952; Donoghue and Edwards 2014) and promotes higher species diversification (Klak et al. 2004; Crayn et al. 2006; Arakaki et al. 2011; Cornwell et al. 2014; Evans et al. 2014; Horn et al. 2014). *Callitris* species are the most drought-adapted tree species in the world, but adaptation to drought in *Callitris* did not result in a higher diversification, or an adaptive radiation.

Chloroplasts and gene flow

Callitris are long-lived, slow-growing trees that take an average of 30 (20–70 years) years to reach sexual maturity (Sakaguchi et al. 2013). Trees have lower mutation rates than short-lived plants due to their longer generation times, large genomes and increased stature (Lanfear et al. 2013). Conifer molecular evolutionary rates are slow relative to angiosperms but conifers have higher substitution rates, with a higher proportion of sites under positive selection (De La Torre et al. 2017), indicating higher fixation of beneficial mutations. In wind-pollinated *Callitris*, the chloroplast is inherited paternally (Sakaguchi et al. 2014). Chloroplasts are the sites of photosynthesis, where CO_2 is converted into sugars to use in growth. But, chloroplasts are sensitive to drought-stress, heat, CO_2 concentration and salinity (Ashraf and Harris 2013). These factors may damage photosynthetic apparatus and reduce growth. Plants that are more drought-adapted should have a selective advantage because their growth rates are not as constrained by drought. Thus, wind pollination might result in drought adaptation by the fixation of beneficial mutations. But high gene flow also leads to incomplete lineage sorting in drought-adapted *Callitris* (Sakaguchi et al. 2014), which could have reduced speciation rates.

Geographical speciation in Callitris

In Australian trees population-level genetic differences are strongly associated with range disjunctions (Broadhurst et al. 2017). The distributional patterns of *Callitris* suggest that arid barriers have caused population fragmentation and local adaptation. Strong ecological associations in traits such as callitroid thickening suggests that traits associated with drought are under high selection, and therefore could be drivers of speciation via local extinctions and local adaptation. Evidence of genetic clustering according to geographic range in *C. glaucophylla* and *C. gracilis* demonstrates that *Callitris* species do have a signature of geography in their genomes (Sakaguchi et al. 2015).

The phylogenetic encoding of geography

It appears that speciation in *Callitris* has a strong geographic signal. Hydraulic traits have strong ecological associations, suggesting that selection has been high as landscapes became more arid. Strong selection pressure on drought-tolerance traits, resulted in trait-biased extinctions and trait-dependent diversification. This means that the phylogeny of *Callitris* might not be neutral if speciation is the product of trait adaptation to geographically defined climatic niches. The simulations in Chapter 3 show that reconstructed phylogenies can produce erroneous results when used in phylogenetic comparative methods (PCMs) because of unsampled extinct taxa, even when extinction is random. Trait-biased extinctions associated with aridification might mean that the phylogeny and hydraulic traits, are correlated with geography, and not neutral at all. This could explain why traits like callitroid thickening fitted a BM model: because speciation has occurred as a result of selection on drought-tolerance traits. If the tree is not independent of geography or drought-tolerance it might explain why we could not infer an OU model, even though the frequency of callitroid thickening (FCT) is convergent with aridity.

This then is a classic example of how the assumption that the tree is neutral can lead to the misinterpretation of PCMs. FCT showed high phylogenetic signal and fitted a BM model. One interpretation could have been that FCT was not a trait evolving under strong selection, but just a trait evolving under drift, which has nothing to do with selection. Equally, the hydraulic traits that fitted a white noise would have been identified as highly labile and considered to be under selection because they 'departed from the null tree'. This also explains why FCT is a trait convergent with aridity, but also why single or multiple OU models did not fit the evolution of FCT – because the tree itself is an OU tree, not a BM tree.

Instead it seems likely selection for drought tolerance was so strong that it resulted in high extinction rates, which might have cancelled out increases in speciation rate. Because Australia has large, low-elevation topography, climate space in Australia is quite narrow. Once adapted to arid climates, *Callitris* could form extensive populations, with little variation in ecology to select against, resulting in low speciation rates.

Collectively, this research show that modelling the evolution of multiple hydraulic traits enabled me to identify callitroid thickening as the most important trait implicated in the evolution of extreme drought-tolerance in *Callitris*. It also explains a lack of a hydraulic trade-off and trait lability found by other studies. Hydraulic traits are integrated to achieve optimal conductance and minimum failure. However, in the case of trade-offs, multivariate methods failed because of inverse scaling. Thus investigating correlations between many individual hydraulic traits in an evolutionary context, uncovered traits critical to drought adaptation. (Un)fortunately, this study also highlights the weaknesses associated with trait modelling. The structure of the phylogeny is implicated in misinterpreting the evolution of drought-adapted traits in *Callitris,* but my simulations show that the effect could be far reaching. Because the models are heavily reliant on the tree, tree structure can lead to false conclusions of trait evolution. Without other forms of testing trait evolution such as convergence testing, it is impossible to verify whether the model of trait evolution is real or an artifact.

REFERENCES

Ackerly, D. D., S. R. Loarie, W. K. Cornwell, S. B. Weiss, H. Hamilton, R. Branciforte, and N. J. B. Kraft. 2010. The geography of climate change: implications for conservation biogeography. Diversity and Distributions 16:476-487.

Allen, C. D., D. D. Breshears, and N. G. McDowell. 2015. On underestimation of global vulnerability to tree mortality and forest die-off from hotter drought in the Anthropocene. Ecosphere 6:1-55.

Arakaki, M., P. A. Christin, R. Nyffeler, A. Lendel, U. Eggli, R. M. Ogburn, E. Spriggs, M. J. Moore, and E. J. Edwards. 2011. Contemporaneous and recent radiations of the world's major succulent plant lineages. Proceedings of the National Academy of Sciences of the United States of America 108:8379-8384.

Ashraf, M., and P. J. C. Harris. 2013. Photosynthesis under stressful environments: An overview. Photosynthetica 51:163-190.

Baker, P. J., J. G. Palmer, and R. D'Arrigo. 2008. The dendrochronology of *Callitris intratropica* in northern Australia: annual ring structure, chronology development and climate correlations. Australian Journal of Botany 56:311-320.

Barnosky, A. D., N. Matzke, S. Tomiya, G. O. U. Wogan, B. Swartz, T. B. Quental, C. Marshall, J. L. McGuire, E. L. Lindsey, K. C. Maguire, B. Mersey, and E. A. Ferrer. 2011. Has the Earth's sixth mass extinction already arrived? Nature 471:51-57.

Barreda, V., and L. Palazzesi. 2007. Patagonian vegetation turnovers during the Paleogene-early Neogene: Origin of arid-adapted floras. Botanical Review 73:31-50.

Bartlett, M. K., C. Scoffoni, and L. Sack. 2012. The determinants of leaf turgor loss point and prediction of drought tolerance of species and biomes: a global meta-analysis. Ecology Letters 15:393-405.

Bi, D. H., M. Dix, S. J. Marsland, S. O'Farrell, H. A. Rashid, P. Uotila, A. C. Hirst, E. Kowalczyk, M. Golebiewski, A. Sullivan, H. L. Yan, N. Hannah, C. Franklin, Z. A. Sun, P. Vohralik, I. Watterson, X. B. Zhou, R. Fiedler, M. Collier, Y. M. Ma, J. Noonan, L. Stevens, P. Uhe, H. Y. Zhu, S. M. Griffies, R. Hill, C. Harris, and K. Puri. 2013. The ACCESS coupled model: description, control climate and evaluation. Australian Meteorological and Oceanographic Journal 63:41-64.

Blomberg, S. P., and T. Garland. 2002. Tempo and mode in evolution: phylogenetic inertia, adaptation and comparative methods. Journal of Evolutionary Biology 15:899-910.

Blomberg, S. P., T. Garland, and A. R. Ives. 2003. Testing for phylogenetic signal in comparative data: Behavioral traits are more labile. Evolution 57:717-745.

Boisvert-Marsh, L., C. Perie, and S. de Blois. 2014. Shifting with climate? Evidence for recent changes in tree species distribution at high latitudes. Ecosphere 5:1-33.

Bouche, P. S., M. Larter, J.-C. Domec, R. Burlett, P. Gasson, S. Jansen, and S. Delzon. 2014. A broad survey of hydraulic and mechanical safety in the xylem of conifers. Journal of Experimental Botany 65:4419-4431.

Bouckaert, R., J. Heled, D. Kuehnert, T. Vaughan, C.-H. Wu, D. Xie, M. A. Suchard, A. Rambaut, and A. J. Drummond. 2014. BEAST 2: A software platform for Bayesian evolutionary analysis. PLOS Computational Biology 10:1-6.

Bowman, D., L. D. Prior, D. Y. P. Tng, Q. Hua, and T. J. Brodribb. 2011. Continental-scale climatic drivers of growth ring variability in an Australian conifer. Trees 25:925-934.

Broadhurst, L., M. Breed, A. Lowe, J. Bragg, R. Catullo, D. Coates, F. Encinas-Viso, N. Gellie, E. James, S. Krauss, B. Potts, M. Rossetto, M. Shepherd, and M. Byrne. 2017. Genetic diversity and structure of the Australian flora. Diversity and Distributions 23:41-52.

Brodribb, T., D. Bowman, S. Nichols, S. Delzon, and R. Burlett. 2010. Xylem function and growth rate interact to determine recovery rates after exposure to extreme water deficit. New Phytologist 188:533-542.

Brodribb, T., and R. S. Hill. 1999. The importance of xylem constraints in the distribution of conifer species. New Phytologist 143:365-372.

Brodribb, T. J., and H. Cochard. 2009. Hydraulic failure defines the recovery and point of death in water-stressed conifers. Plant Physiology 149:575-584.

Brodribb, T. J., and R. S. Hill. 1998. The photosynthetic drought physiology of a diverse group of southern hemisphere conifer species is correlated with minimum seasonal rainfall. Functional Ecology 12:467-471.

Broennimann, O., M. C. Fitzpatrick, P. B. Pearman, B. Petitpierre, L. Pellissier, N. G. Yoccoz, W. Thuiller, M.-J. Fortin, C. Randin, N. E. Zimmermann, C. H. Graham, and A. Guisan. 2012. Measuring ecological niche overlap from occurrence and spatial environmental data. Global Ecology and Biogeography 21:481-497.

Bromham, L., X. Hua, R. Lanfear, and P. F. Cowman. 2015. Exploring the relationships between mutation rates, life history, genome size, environment, and species richness in flowering plants. American Naturalist 185:507-524.

Burnham, K. P., and D. R. Anderson. 2002. Model Selection and Multimodel Inference: A Practical Information-Theoretic Approach. Springer-Verlag, New York.

Butler, M. A., and A. A. King. 2004. Phylogenetic comparative analysis: A modeling approach for adaptive evolution. American Naturalist 164:683-695.

Byrne, M., D. K. Yeates, L. Joseph, M. Kearney, J. Bowler, M. A. J. Williams, S. Cooper, S. C. Donnellan, J. S. Keogh, R. Leys, J. Melville, D. J. Murphy, N. Porch, and K. H. Wyrwoll. 2008. Birth of a biome: Insights into the assembly and maintenance of the Australian arid zone biota. Molecular Ecology 17:4398-4417.

Carpenter, R. J., M. P. Goodwin, R. S. Hill, and K. Kanold. 2011. Silcrete plant fossils from Lightning Ridge, New South Wales: new evidence for climate change and monsoon elements in the Australian Cenozoic1. Australian Journal of Botany 59:399-425.

Cavalli-Sforza, L. L., and A. W. F. Edwards. 1967. Phylogenetic analysis models and estimation procedures. American Journal of Human Genetics 19:233-257.

Cavender-Bares, J., D. D. Ackerly, S. E. Hobbie, and P. A. Townsend. 2016. Evolutionary Legacy Effects on Ecosystems: Biogeographic Origins, Plant Traits, and Implications for Management in the Era of Global Change. Pp. 433-462 *in* D. J. Futuyma, ed. Annual Review of Ecology, Evolution, and Systematics, Vol 47.

Choat, B. 2013. Predicting thresholds of drought-induced mortality in woody plant species. Tree Physiology 33:669-671.

Choat, B., E. Badel, R. Burlett, S. Delzon, H. Cochard, and S. Jansen. 2016. Noninvasive measurement of vulnerability to drought-induced embolism by x-ray microtomography. Plant Physiology 170:273-282.

Choat, B., A. R. Cobb, and S. Jansen. 2008. Structure and function of bordered pits: new discoveries and impacts on whole-plant hydraulic function. New Phytologist 177:608-626.

Choat, B., S. Jansen, T. J. Brodribb, H. Cochard, S. Delzon, R. Bhaskar, S. J. Bucci, T. S. Feild, S. M. Gleason, U. G. Hacke, A. L. Jacobsen, F. Lens, H. Maherali, J. Martinez-Vilalta, S. Mayr, M. Mencuccini, P. J. Mitchell, A. Nardini, J. Pittermann, R. B. Pratt, J. S. Sperry, M. Westoby, I. J. Wright, and A. E. Zanne. 2012. Global convergence in the vulnerability of forests to drought. Nature 491:752-755.

Christensen, B. A., W. Renema, J. Henderiks, D. De Vleeschouwer, J. Groeneveld, I. S. Castaneda, L. Reuning, K. Bogus, G. Auer, T. Ishiwa, C. M. McHugh, S. J. Gallagher, C. S. Fulthorpe, and I. E. Scientists. 2017. Indonesian throughflow drove australian climate from humid pliocene to arid pleistocene. Geophysical Research Letters 44:6914-6925.

Cochard, H., T. Holtta, S. Herbette, S. Delzon, and M. Mencuccini. 2009. New insights into the mechanisms of water-stress-induced cavitation in conifers. Plant Physiology 151:949-954.

Cook, L. G., N. B. Hardy, and M. D. Crisp. 2015. Three explanations for biodiversity hotspots: small range size, geographical overlap and time for species accumulation. An Australian case study. New Phytologist 207:390-400.

Cooper, N., G. H. Thomas, and R. G. FitzJohn. 2016a. Shedding light on the "dark side' of phylogenetic comparative methods. Methods in Ecology and Evolution 7:693-699.

Cooper, N., G. H. Thomas, C. Venditti, A. Meade, and R. P. Freckleton. 2016b. A cautionary note on the use of Ornstein Uhlenbeck models in macroevolutionary studies. Biological Journal of the Linnean Society - Linnean Society of London 118:64-77.

Cornwell, W. K., M. Westoby, D. S. Falster, R. G. FitzJohn, B. C. O'Meara, M. W. Pennell, D. J. McGlinn, J. M. Eastman, A. T. Moles, P. B. Reich, D. C. Tank, I. J. Wright, L. Aarssen, J. M. Beaulieu, R. M. Kooyman, M. R. Leishman, E. T. Miller, U. Niinemets, J. Oleksyn, A. Ordonez, D. L. Royer, S. A. Smith, P. F. Stevens, L. Warman, P. Wilf, and A. E. Zanne. 2014. Functional distinctiveness of major plant lineages. Journal of Ecology 102:345-356.

Costa-Saura, J. M., J. Martinez-Vilalta, A. Trabucco, D. Spano, and S. Mereu. 2016. Specific leaf area and hydraulic traits explain niche segregation along an aridity gradient in Mediterranean woody species. Perspectives in Plant Ecology Evolution and Systematics 21:23-30.

Crayn, D. M., M. Rossetto, and D. J. Maynard. 2006. Molecular phylogeny and dating reveals an Oligo-Miocene radiation of dry-adapted shrubs (former Tremandraceae) from rainforest tree progenitors (Elaeocarpaceae) in Australia. American Journal of Botany 93:1328-1342.

Crisp, M., and L. Cook. 2009. Explosive radiation or cryptic mass extinction? Interpreting signatures in molecular phylogenies. Evolution 63:2257-2265.

Crisp, M., and L. Cook. 2013. How was the Australian flora assembled over the last 65 million years? A molecular phylogenetic perspective. Annual Review of Ecology 44:303-324.

Crisp, M. D., and L. G. Cook. 2011. Cenozoic extinctions account for the low diversity of extant gymnosperms compared with angiosperms. New Phytologist 192:997-1009.

Crisp, M. D., and L. G. Cook. 2012. Phylogenetic niche conservatism: what are the underlying evolutionary and ecological causes? New Phytologist 196:681-694.

Cullen, L. E., and P. F. Grierson. 2007. A stable oxygen, but not carbon, isotope chronology of *Callitris columellaris* reflects recent climate change in north-western Australia. Climatic Change 85:213-229.

Cunningham, C. W., K. E. Omland, and T. H. Oakley. 1998. Reconstructing ancestral character states: a critical reappraisal. Trends in Ecology & Evolution 13:361-366.

Cupper, M. L., A. N. Drinnan, and I. Thomas. 2000. Holocene palaeoenvironments of salt lakes in the Darling Anabranch region, south-western New South Wales, Australia. Journal of Biogeography 27:1079-1094.

Cusimano, N., and S. S. Renner. 2014. Ultrametric trees or phylograms for ancestral state reconstruction: Does it matter? Taxon 63:721-726.

Darwin, C. 1859. On the Origin of the Species by Means of Natural Selection, or the Preservation of Favoured Races in the Struggle for Life. John Murray, London.

De La Torre, A. R., Z. Li, Y. Van de Peer, and P. K. Ingvarsson. 2017. Contrasting rates of molecular evolution and patterns of selection among gymnosperms and flowering plants. Molecular Biology and Evolution 34:1363-1377.

de Villemereuil, P., J. A. Wells, R. D. Edwards, and S. P. Blomberg. 2012. Bayesian models for comparative analysis integrating phylogenetic uncertainty. BMC Evolutionary Biology 12:1-16.

Delzon, S., C. Douthe, A. Sala, and H. Cochard. 2010. Mechanism of water-stress induced cavitation in conifers: Bordered pit structure and function support the hypothesis of seal capillary-seeding. Plant, Cell & Environment 33:2101-2111.

Di Cola, V., O. Broennimann, B. Petitpierre, F. T. Breiner, M. D'Amen, C. Randin, R. Engler, J. Pottier, D. Pio, A. Dubuis, L. Pellissier, R. G. Mateo, W. Hordijk, N. Salamin, and A. Guisan. 2017. ecospat: an R package to support spatial analyses and modeling of species niches and distributions. Ecography 40:774-787.

Diniz, J. A. F., C. E. R. De Sant'ana, and L. M. Bini. 1998. An eigenvector method for estimating phylogenetic inertia. Evolution 52:1247-1262.

Dodson, J. R. 1979. Late Pleistocene vegetation and environments near Lake Bullenmerri, Western Victoria. Australian Journal of Ecology 4:419-427.

Dolédec, S., D. Chessel, and C. Gimaret-Carpentier. 2000. Niche separation in community analysis: A new method. Ecology 81:2914-2927.

Domec, J.-C., B. Lachenbruch, and F. C. Meinzer. 2006. Bordered pit structure and function determine spatial patterns of air-seeding thresholds in xylem of Douglas-fir (*Pseudotsuga menziesii*; Pinaceae) trees. American Journal of Botany 93:1588-1600.

Domec, J. C., B. Lachenbruch, F. C. Meinzer, D. R. Woodruff, J. M. Warren, and K. A. McCulloh. 2008. Maximum height in a conifer is associated with conflicting requirements for xylem design. Proceedings of the National Academy of Sciences of the United States of America 105:12069-12074.

Donoghue, M. J., and E. J. Edwards. 2014. Biome shifts and niche evolution in plants. Annual Review of Ecology, Evolution, and Systematics 45:547-572.

Dray, S., and A.-B. Dufour. 2007. The ade4 package: Implementing the duality diagram for ecologists. Journal of Statistical Software 22:1-20.

Drummond, A., J. , M. Suchard, A. , D. Xie, and A. Rambaut. 2012. Bayesian phylogenetics with BEAUti and the BEAST 1.7. Molecular Biology and Evolution 29:1969-1973.

Duchene, S., and R. Lanfear. 2015. Phylogenetic uncertainty can bias the number of evolutionary transitions estimated from ancestral state reconstruction methods. Journal of Experimental Zoology Part B-Molecular and Developmental Evolution 324:517-524.

Earle, C. J. 2017. The Gymnosperm Database. http://www.conifers.org/.

Einstein, A. 1906. The theory of the Brownian Motion. Annalen Der Physik 19:371-381.

Elith, J., S. J. Phillips, T. Hastie, M. Dudik, Y. E. Chee, and C. J. Yates. 2011. A statistical explanation of MaxEnt for ecologists. Diversity and Distributions 17:43-57.

Etienne, R., S., and J. Rosindell. 2012. Prolonging the past counteracts the pull of the present: Protracted speciation can explain observed slowdowns in diversification. Systematic Biology 61:204-213.

Evans, M., X. Aubriot, D. Hearn, M. Lanciaux, S. Lavergne, C. Cruaud, P. P. Lowry, II, and T. Haevermans. 2014. Insights on the Evolution of Plant Succulence from a Remarkable Radiation in Madagascar (Euphorbia). Systematic Biology 63:698-711.

Evans, M. E. K., S. A. Smith, R. S. Flynn, and M. J. Donoghue. 2009. Climate, niche evolution, and diversification of the "Bird‐cage" evening primroses (Oenothera, Sections Anogra and Kleinia). The American Naturalist 173:225-240.

Farjon, A. 2005. A monograph of Cupressaceae and Sciadopitys. Royal Botanic Gardens, Kew, Richmond, Surrey, UK.

Feeley, K. J., M. R. Silman, M. B. Bush, W. Farfan, K. G. Cabrera, Y. Malhi, P. Meir, N. S. Revilla, M. N. R. Quisiyupanqui, and S. Saatchi. 2011. Upslope migration of Andean trees. Journal of Biogeography 38:783-791.

Fei, S. L., J. M. Desprez, K. M. Potter, I. Jo, J. A. Knott, and C. M. Oswalt. 2017. Divergence of species responses to climate change. Science Advances 3:1-9.

Felsenstein, J. 1973. Maximum-likelihood estimation of evolutionary trees from continuous characters. American Journal of Human Genetics 25:471-492.

Felsenstein, J. 1985. Phylogenies and the Comparative Method. American Naturalist 125:1-15.

Felsenstein, J. 2004. Inferring phylogenies. Sinauer Associates, Sunderland, Mass.

Fragnière, Y., S. Bétrisey, L. Cardinaux, M. Stoffel, and G. Kozlowski. 2015. Fighting their last stand? A global analysis of the distribution and conservation status of gymnosperms. Journal of Biogeography 42:809-820.

Freckleton, R., P. Harvey, and M. Pagel. 2002. Phylogenetic analysis and comparative data: a test and review of evidence. The American Naturalist 160:712-726.

Fujioka, T., J. Chappell, L. K. Fifield, and E. J. Rhodes. 2009. Australian desert dune fields initiated with Pliocene-Pleistocene global climatic shift. Geology 37:51-54.

Fujioka, T., J. Chappell, M. Honda, I. Yatsevich, K. Fifield, and D. Fabel. 2005. Global cooling initiated stony deserts in central Australia 2-4 Ma, dated by cosmogenic Ne-21-Be-10. Geology 33:993-996.

Gascuel, F., R. Ferriere, R. Aguilee, and A. Lambert. 2015. How ecology and landscape dynamics shape phylogenetic trees. Systematic Biology 64:590-607.

Gleason, S. M., D. W. Butler, K. Zieminska, P. Waryszak, and M. Westoby. 2012. Stem xylem conductivity is key to plant water balance across Australian angiosperm species. Functional Ecology 26:343-352.

Gleason, S. M., M. Westoby, S. Jansen, B. Choat, U. G. Hacke, R. B. Pratt, R. Bhaskar, T. J. Brodribb, S. J. Bucci, K.-F. Cao, H. Cochard, S. Delzon, J.-C. Domec, Z.-X. Fan, T. S. Feild, A. L. Jacobsen, D. M. Johnson, F. Lens, H. Maherali, J. Martinez-Vilalta, S. Mayr, K. A. McCulloh, M. Mencuccini, P. J. Mitchell, H. Morris, A. Nardini, J. Pittermann, L. Plavcova, S. G. Schreiber, J. S. Sperry, I. J. Wright, and A. E. Zanne. 2016. Weak tradeoff between xylem safety and xylem-specific hydraulic efficiency across the world's woody plant species. New Phytologist 209:123-136.

Gonzalez-Orozco, C. E., L. J. Pollock, A. H. Thornhill, B. D. Mishler, N. Knerr, S. Laffan, J. T. Miller, D. F. Rosauer, D. P. Faith, D. A. Nipperess, H. Kujala, S. Linke, N. Butt, C. Kulheim, M. D. Crisp, and B. Gruber. 2016. Phylogenetic approaches reveal biodiversity threats under climate change. Nature Climate Change 6:1110-1114.

Good-Avila, S. V., V. Souza, B. S. Gaut, and L. E. Eguiarte. 2006. Timing and rate of speciation in Agave (Agavaceae). Proceedings of the National Academy of Sciences of the United States of America 103:9124-9129.

Grafen, A. 1989. The phylogenetic regression. Philosophical Transactions of the Royal Society of London. Series B, Biological Sciences 326:119-157.

Greenwood, S., P. Ruiz-Benito, J. Martinez-Vilalta, F. Lloret, T. Kitzberger, C. D. Allen, R. Fensham, D. C. Laughlin, J. Kattge, G. Bonisch, N. J. B. Kraft, and A. S. Jump. 2017. Tree mortality across biomes is promoted by drought intensity, lower wood density and higher specific leaf area. Ecology Letters 20:539-553.

Gutiérrez-Ortega, J. S., Yamamoto, Takashi , A. P. Vovides, M. A. Pérez-Farrera, J. F. Martínez, F. Molina-Freaner, Y. Watano, and T. Kajita. 2017. Aridification as a driver of biodiversity: a case study for the cycad genus *Dioon* (Zamiaceae). Annals of Botany In press.

Hacke, U. G., J. S. Sperry, and J. Pittermann. 2004. Analysis of circular bordered pit function - II. Gymnosperm tracheids with torus-margo pit membranes. American Journal of Botany 91:386-400.

Hacke, U. G., J. S. Sperry, W. T. Pockman, S. D. Davis, and K. A. McCulloch. 2001. Trends in wood density and structure are linked to prevention of xylem implosion by negative pressure. Oecologia 126:457-461.

Haines, H. A., J. M. Olley, J. Kemp, and N. B. English. 2016. Progress in Australian dendroclimatology: Identifying growth limiting factors in four climate zones. Science of the Total Environment 572:412-421.

Hansen, T. F. 1997. Stabilizing selection and the comparative analysis of adaptation. Evolution 51:1341-1351.

Hansen, T. F., and E. P. Martins. 1996. Translating between microevolutionary process and macroevolutionary patterns: The correlation structure of interspecific data. Evolution 50:1404-1417.

Harmon, L. J., J. B. Losos, T. J. Davies, R. G. Gillespie, J. L. Gittleman, W. B. Jennings, K. H. Kozak, M. A. McPeek, F. Moreno-Roark, T. J. Near, A. Purvis, R. E. Ricklefs, D. Schluter, J. A. Schulte, O. Seehausen, B. L. Sidlauskas, O. Torres-Carvajal, J. T. Weir, and A. O. Mooers. 2010. Early bursts of body size and shape evolution are rare in comparative data. Evolution 64:2385-2396.

Harvey, P. H., R. M. May, and S. Nee. 1994. Phylogenies without fossils. Evolution 48:523-529.

Harvey, P. H., and M. D. Pagel. 1991. The comparative method in evolutionary biology. Oxford University Press, Oxford.

Heady, R. D. 1997. The wood anatomy of *Callitris* Vent. (Cupressaceae) : an SEM study. Department of Forestry. PhD thesis. Australian National University, Canberra, A.C.T.

Heady, R. D., and P. D. Evans. 2000. Callitroid (callitrisoid) thickening in *Callitris*. IAWA Journal 21:293-319.

Heibl, C., and C. Calenge. 2013. phyloclim: Integrating Phylogenetics and Climatic Niche Modeling. R package 0.9-4.

Hernandez-Hernandez, T., J. W. Brown, B. O. Schlumpberger, L. E. Eguiarte, and S. Magallon. 2014. Beyond aridification: multiple explanations for the elevated diversification of cacti in the New World Succulent Biome. New Phytologist 202:1382-1397.

Herold, N., M. Huber, D. R. Greenwood, R. D. Muller, and M. Seton. 2011. Early to Middle Miocene monsoon climate in Australia. Geology 39:3-6.

Heyduk, K., M. R. McKain, F. Lalani, and J. Leebens-Mack. 2016. Evolution of a CAM anatomy predates the origins of Crassulacean acid metabolism in the Agavoideae (Asparagaceae). Molecular Phylogenetics and Evolution 105:102-113.

Hijmans, R. J., S. E. Cameron, J. L. Parra, P. G. Jones, and A. Jarvis. 2005. Very high resolution interpolated climate surfaces for global land areas. International Journal of Climatology 25:1965-1978.

Hill, K. D. 1998. Pinophyta. Pp. 545-596 *in* P. M. McCarthy, ed. Flora of Australia, Vol 48. Ferns, gymnosperms, and allied groups. CSIRO Publishing, Melbourne.

Hill, R. S. 2004. Origins of the southeastern Australian vegetation. Philosophical Transactions of the Royal Society of London Series B-Biological Sciences 359:1537-1549.

Hill, R. S., and T. J. Brodribb. 1999. Turner review No. 2. Southern conifers in time and space. Australian Journal of Botany 47:639-696.

Hill, R. S., and D. C. Christophel. 2001. Two new species of *Dacrydium* (Podocarpaceae) based on vegetative fossils from Middle Eocene sediments at Nelly Creek, South Australia. Australian Systematic Botany 14:193-205.

Hill, R. S., T. Lewis, R. J. Carpenter, and S. S. Whang. 2008. *Agathis* (Araucariaceae) macrofossils from Cainozoic sediments in south-eastern Australia. Australian Systematic Botany 21:162-177.

Horn, J. W., Z. X. Xi, R. Riina, J. A. Peirson, Y. Yang, B. L. Dorsey, P. E. Berry, C. C. Davis, and K. J. Wurdack. 2014. Evolutionary bursts in Euphorbia (Euphorbiaceae) are linked with photosynthetic pathway. Evolution 68:3485-3504.

IPCC. 2014. Climate Change 2014: Synthesis Report. Contribution of Working Groups I, II and III to the Fifth Assessment Report of the Intergovernmental Panel on Climate Change *in* Core Writing Team, R. K. Pachauri, and A. Meyer, eds, Geneva, Switzerland.

IUCN. 2017. Red List of Threatened Species. http://www.iucnredlist.org.

Jimenez-Moreno, G., F. Burjachs, I. Exposita, O. Oms, A. Carrancho, J. J. Villalain, J. Agusti, G. Campeny, B. G. de Soler, and J. van der Made. 2013. Late Pliocene vegetation and orbital-scale climate changes from the western Mediterranean area. Global and Planetary Change 108:15-28.

Johnson, K. P., F. McKinney, and M. D. Sorenson. 1999. Phylogenetic constraint on male parental care in the dabbling ducks. Proceedings of the Royal Society B-Biological Sciences 266:759-763.

Jordan, G. J. 1995. Extinct conifers and conifer diversity in the Early Pleistocene of western Tasmania. Review of Palaeobotany and Palynology 84:375-387.

Kamilar, J. M., and N. Cooper. 2013. Phylogenetic signal in primate behaviour, ecology and life history. Philosophical Transactions of the Royal Society B-Biological Sciences 368:20120341.

Kelly, A. E., and M. L. Goulden. 2008. Rapid shifts in plant distribution with recent climate change. Proceedings of the National Academy of Sciences of the United States of America 105:11823-11826.

Kimura, M. 1968. Evolutionary rate at molecular level. Nature 217:624-626.

King, B., and M. S. Y. Lee. 2015. Ancestral state reconstruction, rate heterogeneity, and the evolution of reptile viviparity. Systematic Biology 64:532-544.

Klak, C., P. Hanacek, and P. V. Bruyns. 2017. Out of southern Africa: Origin, biogeography and age of the Aizooideae (Aizoaceae). Molecular Phylogenetics and Evolution 109:203-216.

Klak, C., G. Reeves, and T. Hedderson. 2004. Unmatched tempo of evolution in Southern African semi-desert ice plants. Nature 427:63-65.

Lanfear, R., S. Y. W. Ho, T. J. Davies, A. T. Moles, L. Aarssen, N. G. Swenson, L. Warman, A. E. Zanne, and A. P. Allen. 2013. Taller plants have lower rates of molecular evolution. Nature Communications 4:1-7.

Larter, M., T. J. Brodribb, S. Pfautsch, R. Burlett, H. Cochard, and S. Delzon. 2015. Extreme aridity pushes trees to their physical limits. Plant Physiology 168:804-807.

Larter, M., S. Pfautsch, J.-C. Domec, S. Trueba, N. Nagalingum, and S. Delzon. 2017. Aridity drove the evolution of extreme embolism resistance and the radiation of conifer genus *Callitris*. New Phytologist 215:97-112.

Lazzarin, M., A. Crivellaro, C. B. Williams, T. E. Dawson, G. Mozzi, and T. Anfodillo. 2016. Tracheid and pit anatomy vary in tandem in a tall *Sequoiadendron giganteum* tree. IAWA Journal 37:172-185.

Lenoir, J., J. C. Gegout, P. A. Marquet, P. de Ruffray, and H. Brisse. 2008. A significant upward shift in plant species optimum elevation during the 20th century. Science 320:1768-1771.

Leslie, A. B., J. M. Beaulieu, H. S. Rai, P. R. Crane, M. J. Donoghue, and S. Mathews. 2012. Hemisphere-scale differences in conifer evolutionary dynamics. Proceedings of the National Academy of Sciences 109:16217-16221.

Lewis, E. K., and A. N. Drinnan. 2013. The Miocene conifer flora of Balcombe Bay, Victoria, Australia. Australian Systematic Botany 26:145-155.

Lindsay, J. B. 2016. Whitebox GAT: A case study in geomorphometric analysis. Computers and Geosciences 95:75-84.

Litsios, G., and N. Salamin. 2012. Effects of phylogenetic signal on ancestral state reconstruction. Systematic Biology 61:533-538.

Losos, J. B. 2010. Adaptive radiation, ecological opportunity, and evolutionary determinism. American Society of Naturalists E. O. Wilson award address. American Naturalist 175:623-639.

Losos, J. B. 2011. Seeing the forest for the trees: The limitations of phylogenies in comparative biology. American Naturalist 177:709-727.

Lu, Y., J.-H. Ran, D.-M. Guo, Z.-Y. Yang, and X.-Q. Wang. 2014. Phylogeny and divergence times of gymnosperms inferred from single-copy nuclear genes. PLOS One 9:10.1371/journal.pone.0107679.

Macphail, M. K., E. A. Colhoun, and S. J. Fitzsimons. 1995. Key periods in the evolution of the cenozoic vegetation and flora in western Tasmania: The late pliocene. Australian Journal of Botany 43:505-526.

Maddison, D. R. 1994. Phylogenetic methods for inferring the evolutionary history and processes of change in discretely valued characters. Annual Review of Entomology 39:267-292.

Magallon, S., and M. J. Sanderson. 2001. Absolute diversification rates in angiosperm clades. Evolution 55:1762-1780.

Maherali, H., W. T. Pockman, and R. B. Jackson. 2004. Adaptive variation in the vulnerability of woody plants to xylem cavitation. Ecology 85:2184-2199.

Mao, K., R. I. Milne, L. Zhang, Y. Peng, J. Liu, P. Thomas, R. R. Mill, and S. S. Renner. 2012. Distribution of living cupressaceae reflects the breakup of pangea. Proceedings of the National Academy of Sciences of the United States of America 109:7793-7798.

Martins, E. P., and T. F. Hansen. 1997. Phylogenies and the comparative method: A general approach to incorporating phylogenetic information into the analysis of interspecific data. American Naturalist 149:646-667.

Martins, E. P., and T. F. Hansen. 1999. Phylogenies and the comparative method: a general approach to incorporating phylogenetic information into the analysis of interspecific data. American Naturalist 153:448-448.

Meseguer, A. S., J. M. Lobo, R. Ree, D. J. Beerling, and I. Sanmartin. 2015. Integrating fossils, phylogenies, and niche models into biogeography to reveal ancient

evolutionary history: The case of *Hypericum* (Hypericaceae). Systematic Biology 64:215-232.

Miller, C. R., N. P. James, and Y. Bone. 2012. Prolonged carbonate diagenesis under an evolving late cenozoic climate; Nullarbor Plain, southern Australia. Sedimentary Geology 261:33-49.

Mitchell, J. S. 2015. Extant-only comparative methods fail to recover the disparity preserved in the bird fossil record. Evolution 69:2414-2424.

Moen, D., and H. Morlon. 2014. Why does diversification slow down? Trends in Ecology & Evolution 29:190-197.

Moise, A., L. Wilson, M. Grose, P. Whetton, I. Watterson, J. Bhend, J. Bathols, L. Hanson, T. Erwin, T. Bedin, C. Heady, and T. Rafter. 2015. Evaluation of CMIP3 and CMIP5 models over the australian region to inform confidence in projections. Australian Meteorological and Oceanographic Journal 65:19-53.

Münkemüller, T., S. Lavergne, B. Bzeznik, S. Dray, T. Jombart, K. Schiffers, and W. Thuiller. 2012. How to measure and test phylogenetic signal. Methods in Ecology and Evolution 3:743-756.

Muscarella, R., P. J. Galante, M. Soley-Guardia, R. A. Boria, J. M. Kass, M. Uriarte, and R. P. Anderson. 2014. ENMeval: An R package for conducting spatially independent evaluations and estimating optimal model complexity for MAXENT ecological niche models. Methods in Ecology and Evolution 5:1198-1205.

Nee, S. 2006. Birth-death models in macroevolution. Annual Review of Ecology, Evolution and Systematics 37:1-17.

Nee, S., E. C. Holmes, R. M. May, and P. H. Harvey. 1994. Extinction rates can be estimated from molecular phylogenies. Philosophical Transactions of the Royal Society of London Series B-Biological Sciences 344:77-82.

Nie, Z. L., V. A. Funk, Y. Meng, T. Deng, H. Sun, and J. Wen. 2016. Recent assembly of the global herbaceous flora: evidence from the paper daisies (Asteraceae: Gnaphalieae). New Phytologist 209:1795-1806.

Nolf, M., R. Lopez, J. M. R. Peters, R. J. Flavel, L. S. Koloadin, I. M. Young, and B. Choat. 2017. Visualization of xylem embolism by X-ray microtomography: a direct test against hydraulic measurements. New Phytologist 214:890-898.

O'Donnell, A. J., L. E. Cullen, W. L. McCaw, M. M. Boer, and P. F. Grierson. 2010. Dendroecological potential of *Callitris preissii* for dating historical fires in semi-arid shrublands of southern Western Australia. Dendrochronologia 28:37-48.

Oakley, T., and C. Cunningham. 2000. Independent contrasts succeed where ancestor reconstruction fails in a known bacteriophage phylogeny. Evolution 54:397-405.

Ohta, T. 1992. The Nearly Neutral Theory of Molecular Evolution. Annual Review of Ecology and Systematics 23:263-286.

Ordonez, A., and J. W. Williams. 2013. Climatic and biotic velocities for woody taxa distributions over the last 16000 years in eastern North America. Ecology Letters 16:773-781.

Orme, D., Freckleton, R., Thomas, G., Petzoldt, T., Fritz, S., Isaac, N. & Pearse, W. 2013. caper: Comparative Analyses of Phylogenetics and Evolution in R.

Pagel, M. 1997. Inferring evolutionary processes from phylogenies. Zoologica Scripta 26:331-348

Pagel, M. 1999. Inferring the historical patterns of biological evolution. Nature 401:877-884.

Pagel, M. 2002. Modelling the evolution of continuously varying characters on phylogenetic trees. Pp. 269-286 *in* N. MacLeod, and P. L. Fortey, eds. Morphology, Shape and Phylogeny. CRC Press.

Paradis, E., J. Claude, and K. Strimmer. 2004. APE: Analyses of phylogenetics and evolution in R language. Bioinformatics 20:289-290.

Paull, R., and R. S. Hill. 2008. Oligocene *Austrocedrus* from Tasmania (Australia): Comparisons with *Austrocedrus chilensis*. International Journal of Plant Sciences 169:315-330.

Paull, R., and R. S. Hill. 2010. Early Oligocene *Callitris* and *Fitzroya* (Cupressaceae) from Tasmania. American Journal of Botany 97:809-820.

Pearson, R. G., C. J. Raxworthy, M. Nakamura, and A. T. Peterson. 2007. Predicting species distributions from small numbers of occurrence records: a test case using cryptic geckos in Madagascar. Journal of Biogeography 34:102-117.

Pebesma, E. J., and R. S. Bivand. 2005. Classes and methods for spatial data in R. R News 5.

Pennell, M. W., J. M. Eastman, G. J. Slater, J. W. Brown, J. C. Uyeda, R. G. FitzJohn, M. E. Alfaro, and L. J. Harmon. 2014. geiger v2.0: an expanded suite of methods for fitting macroevolutionary models to phylogenetic trees. Bioinformatics 30:2216-2218.

Phillips, S. J., R. P. Anderson, M. Dudík, R. E. Schapire, and M. E. Blair. 2017. Opening the black box: an open-source release of Maxent. Ecography 40:1–7.

Phillips, S. J., R. P. Anderson, and R. E. Schapire. 2006. Maximum entropy modeling of species geographic distributions. Ecological Modelling 190:231-259.

Piggin, J., and J. J. Bruhl. 2010. Phylogeny reconstruction of *Callitris* Vent. (Cupressaceae) and its allies leads to inclusion of *Actinostrobus* within *Callitris*. Australian Systematic Botany 23:69-93.

Pittermann, J., B. Choat, S. Jansen, S. A. Stuart, L. Lynn, and T. E. Dawson. 2010. The relationships between xylem safety and hydraulic efficiency in the Cupressaceae: the evolution of pit membrane form and function. Plant Physiology 153:1919-1931.

Pittermann, J., and J. Sperry. 2003. Tracheid diameter is the key trait determining the extent of freezing-induced embolism in conifers. Tree Physiology 23:907-914.

Pittermann, J., J. S. Sperry, U. G. Hacke, J. K. Wheeler, and E. H. Sikkema. 2006. Inter-tracheid pitting and the hydraulic efficiency of conifer wood: The role of tracheid allometry and cavitation protection. American Journal of Botany 93:1265-1273.

Pittermann, J., S. Stuart, T. Dawson, and A. Moreau. 2012. Cenozoic climate change shaped the evolutionary ecophysiology of the Cupressaceae conifers. Proceedings of the National Academy of Sciences of the United States of America 109:9647-9652.

Pittermann, S. J., J. Sperry, S. , U. Hacke, G. , J. Wheeler, K. , and H. Elzard. 2005. Torus-margo pits help conifers compete with angiosperms. Science 310:1924.

Pokorny, L., R. Riina, M. Mairal, A. S. Meseguer, V. Culshaw, J. Cendoya, M. Serrano, R. Carbajal, S. Ortiz, M. Heuertz, and I. Sanmartin. 2015. Living on the edge: timing of Rand Flora disjunctions congruent with ongoing aridification in Africa. Frontiers in Genetics 6:1-16.

Potter, P. E., and P. Szatmari. 2009. Global Miocene tectonics and the modern world. Earth-Science Reviews 96:279-295.

Pound, M. J., A. M. Haywood, U. Salzmann, and J. B. Riding. 2012. Global vegetation dynamics and latitudinal temperature gradients during the Mid to Late Miocene (15.97-5.33 Ma). Earth-Science Reviews 112:1-22.

Price, T. D., D. M. Hooper, C. D. Buchanan, U. S. Johansson, D. T. Tietze, P. Alstrom, U. Olsson, M. Ghosh-Harihar, F. Ishtiaq, S. K. Gupta, J. Martens, B. Harr, P. Singh, and D. Mohan. 2014. Niche filling slows the diversification of Himalayan songbirds. Nature 509:222-232.

Prinzing, A., W. Durka, S. Klotz, and R. Brandl. 2001. The niche of higher plants: evidence for phylogenetic conservatism. Proceedings of the Royal Society B-Biological Sciences 268:2383-2389.

Prior, L. D., P. F. Grierson, W. L. McCaw, D. Y. P. Tng, S. C. Nichols, and D. M. J. S. Bowman. 2012. Variation in stem radial growth of the Australian conifer, *Callitris columellaris*, across the world' 's driest and least fertile vegetated continent. Trees 26:1169-1179.

Purvis, A., S. A. Fritz, J. Rodriguez, P. H. Harvey, and R. Grenyer. 2011. The shape of mammalian phylogeny: patterns, processes and scales. Philosophical Transactions of the Royal Society B-Biological Sciences 366:2462-2477.

Puttick, M. N., and G. H. Thomas. 2015. Fossils and living taxa agree on patterns of body mass evolution: a case study with Afrotheria. Proceedings of the Royal Society B-Biological Sciences 282:1-9.

Pybus, O. G., and P. H. Harvey. 2000. Testing macro-evolutionary models using incomplete molecular phylogenies. Proceedings of the Royal Society B-Biological Sciences 267:2267-2272.

Pye, M. G., P. A. Gadek, and K. J. Edwards. 2003. Divergence, diversity and species of the Australasian *Callitris* (Cupressaceae) and allied genera: evidence from ITS sequence data. Australian Systematic Botany 16:505-514.

QGIS, D. T. 2016. QGIS Geographic Information System. https://qgis.org/en/site/. Open Source Geospatial Foundation Project.

Quigley, M. C., T. Horton, J. C. Hellstrom, M. L. Cupper, and M. Sandiford. 2010. Holocene climate change in arid Australia from speleothem and alluvial records. Holocene 20:1093-1104.

R-Core-Team. 2017. R: A Language and Environment for Statistical Computing. R Foundation for Statistical Computing, Vienna, Austria. http://www.R-project.org/, Vienna, Austria.

Rabosky, D. L. 2009. Heritability of extinction rates links diversification patterns in molecular phylogenies and fossils. Systematic Biology 58:629-640.

Rabosky, D. L. 2013. Diversity-dependence, ecological speciation, and the role of competition in macroevolution. Annual Review of Ecology, Evolution, and Systematics 44:481-502.

Rambaut , A., and A. J. Drummond. 2013. Tracer v 1.6. http://tree.bio.ed.ac.uk/software/tracer/.

Revell, L., D. Mahler, P. Peres-Neto, and B. Redelings. 2012. A new phylogenetic method for identifying exceptional phenotypic diversification. Evolution; international journal of organic evolution 66:135-146.

Revell, L. J. 2010. Phylogenetic signal and linear regression on species data. Methods in Ecology and Evolution 1:319-329.

Revell, L. J. 2012. phytools: an R package for phylogenetic comparative biology (and other things). Methods in Ecology and Evolution 3:217-223.

Revell, L. J., L. J. Harmon, and D. C. Collar. 2008. Phylogenetic signal, evolutionary process, and rate. Systematic Biology 57:591-601.

Ridley, M. 1983. The Explanation of Organic Diversity. Oxford University Press, Oxford.

Robinson, D. F., and L. R. Foulds. 1981. Comparison of phylogenetic trees. Mathematical Biosciences 53:131-147.

Sakaguchi, S., D. Bowman, L. Prior, M. Crisp, C. Linde, Y. Tsumura, and Y. Isagi. 2013. Climate, not Aboriginal landscape burning, controlled the historical demography and distribution of fire-sensitive conifer populations across Australia. Proceedings of the royal society b-biological sciences 280:1-9.

Sakaguchi, S., T. Sugino, Y. Tsumura, M. Ito, M. D. Crisp, D. Bowman, A. J. Nagano, M. N. Honjo, M. Yasugi, H. Kudoh, Y. Matsuki, Y. Suyama, and Y. Isagi. 2015. High-throughput linkage mapping of Australian white cypress pine (Callitris glaucophylla) and map transferability to related species. Tree Genetics & Genomes 11.

Sakaguchi, S., Y. Tsumura, M. D. Crisp, D. Bowman, and Y. Isagi. 2014. Genetic evidence for paternal inheritance of the chloroplast in four Australian Callitris species (Cupressaceae). Journal of Forest Research 19:244-248.

Saladin, B., A. B. Leslie, R. O. Wuest, G. Litsios, E. Conti, N. Salamin, and N. E. Zimmermann. 2017. Fossils matter: Improved estimates of divergence times in *Pinus* reveal older diversification. BMC Evolutionary Biology 17:1-15.

Sanmartin, I., and A. S. Meseguer. 2016. Extinction in Phylogenetics and Biogeography: From Timetrees to Patterns of Biotic Assemblage. Frontiers in Genetics 7:1-17.

Schnitzler, J., C. H. Graham, C. F. Dormann, K. Schiffers, and H. Peter Linder. 2012. Climatic niche evolution and species diversification in the Cape flora, South Africa. Journal of Biogeography 39:2201-2211.

Schnitzler, J., C. Theis, P. D. Polly, and J. T. Eronen. 2017. Fossils matter – understanding modes and rates of trait evolution in Musteloidea (Carnivora). Evolutionary Ecology Research 18:187-200.

Schoener, T. W. 1970. Nonsynchronous spatial overlap of lizards In patchy habitats. Ecology 51:408-418.

Schulte, P. J., U. G. Hacke, and A. L. Schoonmaker. 2015. Pit membrane structure is highly variable and accounts for a major resistance to water flow through tracheid pits in stems and roots of two boreal conifer species. New Phytologist 208:102-113.

Sherratt, E., M. del Rosario Castañeda, R. J. Garwood, D. L. Mahler, T. J. Sanger, A. Herrel, K. de Queiroz, and J. B. Losos. 2015. Amber fossils demonstrate deep-time stability of Caribbean lizard communities. Proceedings of the National Academy of Sciences 112:9961–9966.

Sipos, B., T. Massingham, G. E. Jordan, and N. Goldman. 2011. PhyloSim - Monte Carlo simulation of sequence evolution in the R statistical computing environment. BMC Bioinformatics 12:1-6.

Slater, G. J., L. J. Harmon, and M. E. Alfaro. 2012. Integrating fossils with molecular phylogenies improves inference of trait evolution. Evolution 66:3931-3944.

Sniderman, J. M. K. 2011. Early Pleistocene vegetation change in upland south-eastern Australia. Journal of Biogeography 38:1456-1470.

Sniderman, J. M. K., J. D. Woodhead, J. Hellstrom, G. J. Jordan, R. N. Drysdale, J. J. Tyler, and N. Porch. 2016. Pliocene reversal of late Neogene aridification. Proceedings of the National Academy of Sciences of the United States of America 113:1999-2004.

Spencer, A. R. T., G. Mapes, R. M. Bateman, J. Hilton, and G. W. Rothwell. 2015. Middle Jurassic evidence for the origin of Cupressaceae: A paleobotanical context for the roles of regulatory genetics and development in the evolution of conifer seed cones. American Journal of Botany 102:942-961.

Sperry, J. S., U. G. Hacke, and J. Pittermann. 2006. Size and function in conifer tracheids and angiosperm vessels. American Journal of Botany 93:1490-1500.

Stadler, T. 2017. Treesim: Simulating phylogenetic trees. R package version 2.3. https://CRAN.R-project.org/package=TreeSim.

Stayton, C. T. 2015. The definition, recognition, and interpretation of convergent evolution, and two new measures for quantifying and assessing the significance of convergence. Evolution 69:2140-2153.

Stebbins, G. L. 1952. Aridity as a stimulus to plant evolution. American Naturalist 86:33-44.

Stein, A., K. Gerstner, and H. Kreft. 2014. Environmental heterogeneity as a universal driver of species richness across taxa, biomes and spatial scales. Ecology Letters 17:866-880.

Steven, J. P., and D. Miroslav. 2008. Modeling of species distributions with Maxent: new extensions and a comprehensive evaluation. Ecography 31:161-175.

Symonds, M. R. E., and S. P. Blomberg. 2014. A Primer on Phylogenetic Generalised Least Squares. Pp. 105-130 *in* L. Z. Garamszegi, ed. Modern Phylogenetic Methods and Their Application in Evolutionary Biology. Springer-Verlag, Berlin.

Tavare, S. 1986. Some probabilistic and statistical problems in the analysis of DNA sequences. Pp. 58-86 *in* R. Miura, ed. Some Mathematical Questions in Biology-DNA Sequence Analysis. American Mathematical Society, Providence, Rhode Island.

Taylor, K. E., R. J. Stouffer, and G. A. Meehl. 2012. An overview of CMIP5 and the experiment design. Bulletin of the American Meteorological Society 93:485-498.

Thuiller, W., G. F. Midgley, M. Rouget, and R. M. Cowling. 2006. Predicting patterns of plant species richness in megadiverse South Africa. Ecography 29:733-744.

Toon, A., M. D. Crisp, H. Gamage, J. Mant, D. C. Morris, S. Schmidt, and L. G. Cook. 2015. Key innovation or adaptive change? A test of leaf traits using Triodiinae in Australia. Scientific Reports 5:1-12.

Trueba, S., R. Pouteau, F. Lens, T. S. Feild, S. Isnard, M. E. Olson, and S. Delzon. 2017. Vulnerability to xylem embolism as a major correlate of the environmental distribution of rain forest species on a tropical island. Plant Cell and Environment 40:277-289.

Tyree, M. T., S. D. Davis, and H. Cochard. 1994. Biophysical perspectives of xylem evolution - is there a tradeoff of hydraulic efficiency for vulnerability to dysfunction. IAWA Journal 15:335-360.

Tyree, M. T., and F. W. Ewers. 1991. The hydraulic architecture of trees and other woody-plants. New Phytologist 119:345-360.

Tyree, M. T., and M. H. Zimmermann. 2002. Xylem Structure and the Ascent of Sap. Springer-Verlag, Berlin.

UNEP. 1997. World atlas of desertification. UNEP (United Nations Environment Programme), London.

Valli, A., A. Koponen, T. Vesala, and J. Timonen. 2002. Simulations of water flow through bordered pits of conifer xylem. Journal of Statistical Physics 107:121-142.

VanDerWal, J., H. T. Murphy, A. S. Kutt, G. C. Perkins, B. L. Bateman, J. J. Perry, and A. E. Reside. 2013. Focus on poleward shifts in species' distribution underestimates the fingerprint of climate change. Nature Climate Change 3:239-243.

Vaziri, M., A. Du Plessis, D. Sandberg, and S. Berg. 2015. Nano X-ray tomography analysis of the cell-wall density of welded beech joints. Wood Material Science and Engineering 10:368-372.

Vicente-Serrano, S. M., C. Gouveia, J. J. Camarero, S. Begueria, R. Trigo, J. I. Lopez-Moreno, C. Azorin-Molina, E. Pasho, J. Lorenzo-Lacruz, J. Revuelto, E. Moran-Tejeda, and A. Sanchez-Lorenzo. 2013. Response of vegetation to drought time-scales across global land biomes. Proceedings of the National Academy of Sciences of the United States of America 110:52-57.

Warren, D. L., R. E. Glor, and M. Turelli. 2008. Environmental niche equivalency versus conservatism: Quantitative approaches to niche evolution. Evolution 62:2868-2883.

Webb, C. O., D. D. Ackerly, M. A. McPeek, and M. J. Donoghue. 2002. Phylogenies and community ecology. Annual Review of Ecology and Systematics 33:475-505.

Webster, A., and A. Purvis. 2002. Testing the accuracy of methods for reconstructing ancestral states of continuous characters. Proceedings Of The Royal Society B-Biological Sciences 269:143-149.

Whang, S. S., and R. S. Hill. 1999. Late Palaeocene Cupressaceae macrofossils at Lake Bungarby, New South Wales. Australian Systematic Botany 12:241-254.

White, J. D. M., S. L. Jack, M. T. Hoffman, J. Puttick, D. Bonora, V. Visser, and E. C. February. 2016. Collapse of an iconic conifer: long-term changes in the demography of *Widdringtonia cedarbergensis* using repeat photography. BMC Ecology 16:1-11.

Wiens, J. J. 2004. Speciation and ecology revisited: Phylogenetic niche conservatism and the origin of species. Evolution 58:193-197.

Wilf, P., and K. R. Johnson. 2004. Land plant extinction at the end of the Cretaceous: a quantitative analysis of the North Dakota megafloral record. Paleobiology 30:347-368.

Wilson, J. P. 2016. Hydraulics of Psilophyton and evolutionary trends in plant water transport after terrestrialization. Review of Palaeobotany and Palynology 227:65-76.

Wolf, A., N. B. Zimmerman, W. R. L. Anderegg, P. E. Busby, and J. Christensen. 2016. Altitudinal shifts of the native and introduced flora of California in the context of 20th-century warming. Global Ecology and Biogeography 25:418-429.

Yang, Z.-Y., J.-H. Ran, and X.-Q. Wang. 2012. Three genome-based phylogeny of Cupressaceae s.l.: Further evidence for the evolution of gymnosperms and Southern Hemisphere biogeography. Molecular Phylogenetics and Evolution 64:452-470.

Yedid, G., J. Stredwick, C. A. Ofria, and P. M. Agapow. 2012. A comparison of the effects of random and selective mass extinctions on erosion of evolutionary history in communities of digital organisms. PLOS One 7:1-13.

Zevenbergen, L. W., and C. R. Thorne. 1987. Quantitative analysis of land surface topography. Earth Surface Processes and Landforms 12:47-56.

Zwieniecki, M. A., and F. Secchi. 2015. Threats to xylem hydraulic function of trees under "new climate normal" conditions. Plant Cell and Environment 38:1713-1724.

Appendix:

Field Guide

Photographic Guide to Native Plants of the Australian Capital Territory

This field guide is a 360 page, image-rich book covering 327 native plant species. Each species is presented by one page (*Eucalyptus* two pages per species). Each species page has at least four photographs featuring the whole plant, flowers, fruit and key identification features. Distribution maps, altitude graphs, full-scale size bars of leaf, flower and fruit. For each genus, the number of species for the ACT, Australia and worldwide are presented. Scale bar measurements were taken from herbarium specimens. Location data for distribution maps was sourced from Australia's Virtual Herbarium and the Atlas of Living Australia. This is the first plant field guide to use data from those sources.

The strength of citizen science rests on having accurate field identifications. This guide is therefore an important contribution to engage the public in science and give them the material to make correct identifications.

A small set of example pages are presented here to highlight the innovative approach taken in this field guide. Because I am unable to present the whole book here, two book reviews are included.

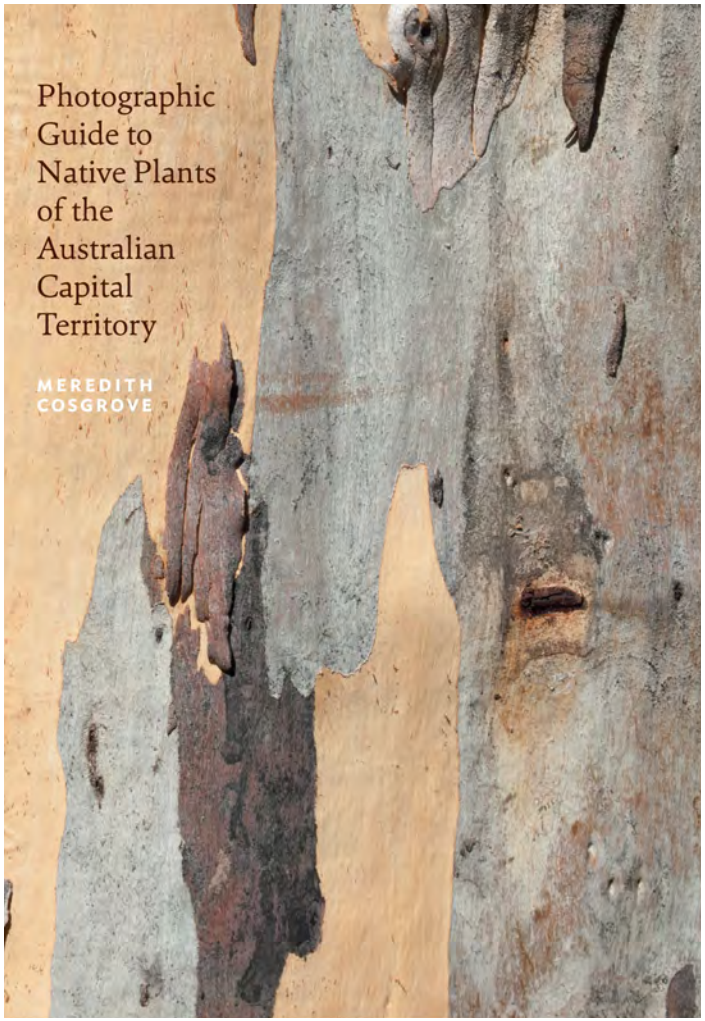

How to use this book

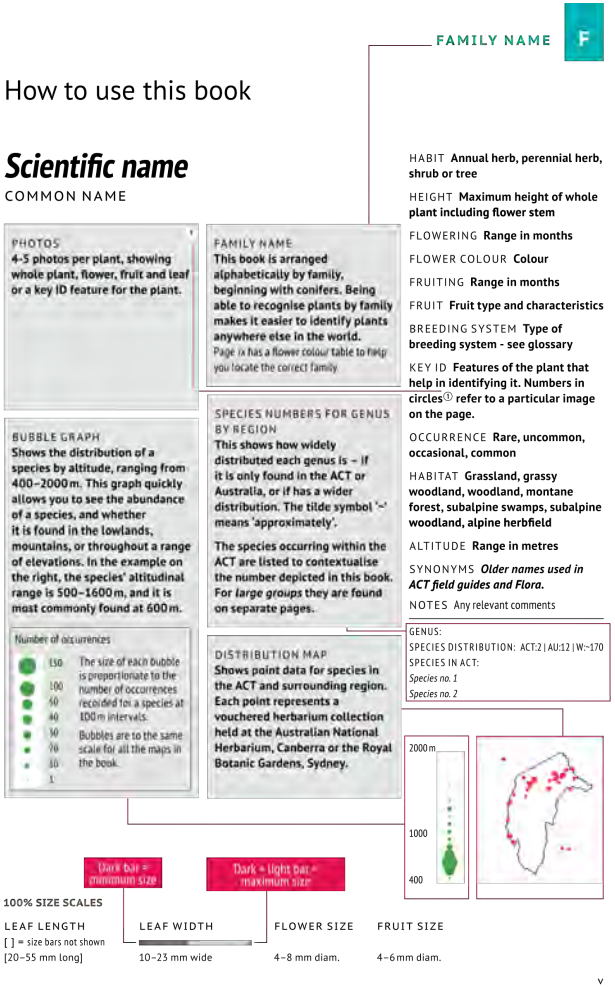

Lomandra longifolia

SPINY-HEADED MATRUSH

HABIT **Perennial herb**

HEIGHT **To 1 m**

FLOWERING **October–January**

FLOWER COLOUR **Pale yellow**

FRUITING **December–March**

FRUIT **Capsule, ovoid, tip pointed, splitting into 3, maturing to glossy brown.**①

BREEDING SYSTEM **Dioecious, male flowers,**② **female flowers.**③

KEY ID **Plants form large, dense tussocks. Leaves strap-like, tips coloured orange, brown or grey, with 2 or 3 jagged points.**④

OCCURRENCE **Common**

HABITAT **Grassland, woodland, forest**

ALTITUDE **480–1640 m**

NOTES Often forms extensive colonies in areas that get infrequent flooding or run-off. The male inflorescences are more branched than female inflorescences, with more male flowers in each cluster.

GENUS: Lomandra
SPECIES DISTRIBUTION: ACT:4 | AU:53 | W:53
SPECIES IN ACT:
L. bracteata
L. filiformis
L. longifolia
L. multiflora

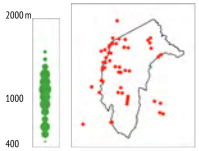

100% SIZE SCALES

LEAF LENGTH	LEAF WIDTH	FLOWER SIZE	FRUIT SIZE
[300–700 mm long]	4–8 mm wide	2–3 mm diam.	5–7 mm diam.

Dillwynia phylicoides

SMALL-LEAVED PARROT-PEA

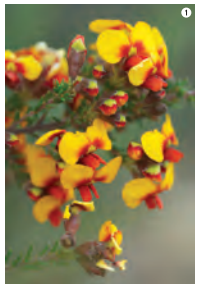

HABIT **Shrub**

HEIGHT **To 1.5 m**

FLOWERING **October–December**

FLOWER COLOUR **Standard yellow with red markings, keel bright red.**①

FRUITING **November–January**

FRUIT **Legume, ovoid, covered in long, soft hairs, sheathed by calyx. 2 seeds per pod.**②

BREEDING SYSTEM **Hermaphroditic**

KEY ID **Leaves linear, channelled, spirally twisted.**③

OCCURRENCE **Common**

HABITAT **Grassy woodland, woodland**

ALTITUDE **550–830 m**

SYNONYMS
Dillwynia retorta* var. *phylicoides

NOTES Often forms an open understorey in woodland.

SUBFAMILY: **Faboideae**
GENUS: Dillwynia
SPECIES DISTRIBUTION: ACT:5 | AU: 37 | W:37
SPECIES IN ACT:
D. phylicoides
D. prostrata
D. sericea
D. sieberi
D. sp. Yetholme (P. C. Jobson 5080)

100% SIZE SCALES

LEAF LENGTH	LEAF WIDTH	FLOWER SIZE	FRUIT SIZE
3–4 mm long	0.5–1 mm wide	5–8 mm long	4–7 mm long

Eucalyptus dalrympleana

MOUNTAIN GUM

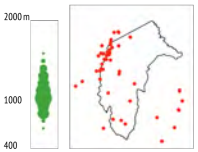

100% SIZE SCALES

ADULT LEAF LENGTH
[100–200 mm long]

ADULT LEAF WIDTH
12–30 mm wide

BUD SIZE
6–7 mm long

FRUIT SIZE
6–8 mm diam.

HABIT **Tree**

HEIGHT **To 40 m**

FLOWERING **March–May**

FLOWER COLOUR **White**

FRUITING **January–December**

BARK **Smooth, with blotches of white, cream and grey. Coloured in pink, cream and green when shedding in autumn.**①

JUVENILE LEAVES **Opposite, without stems, round to oval, pale green to bluish-green.**② **Juvenile plant.**③

ADULT LEAVES **Lance-shaped, glossy green, with wavy margins, same colour on both sides.**④

BUDS **3 buds per inflorescence, buds ovoid, caps conical.**⑤

FRUIT **Capsule, cup-shaped, on a very short stem or no stem, valves projecting slightly.**⑥

BREEDING SYSTEM
Hermaphroditic

OCCURRENCE **Common**

HABITAT **Woodland, montane forest**

ALTITUDE **620–1120 m**

NOTES Tall forest trees with straight trunks, usually growing with *E. pauciflora* in wet forest at higher altitudes.

GENUS: Eucalyptus
SUBGENUS: Symphyomyrtus
SPECIES DISTRIBUTION:
ACT:25 | AU:824 | W:825
SPECIES IN ACT: *See page 240*

KEY ID **Tall forest tree. Bark smooth, white, cream and grey.**
Juvenile leaves opposite, sessile, round to oval, pale green to bluish-green.
Adult leaves lance-shaped, glossy green, with wavy margins, the same colour on both sides.
3 buds per inflorescence, buds with operculum scar.

This beautifully presented little book uses 1388 colour photographs to provide visual assistance in the identification of 325 flowering plants and two conifers native to the Australian Capital Territory. The nomenclature is right up to date, with modern phylogenetically based families and recently named species – *Coronidium montanum* was named just last year. Assignment of genera to families follows the Australian Plant Name Index and Australian Plant Census, which largely follow the Angiosperm Phylogeny Group arrangement. Some users, conditioned to classically based families, may not recognise Phrymaceae or wonder why *Veronica* is not in Scrophulariaceae. Perhaps a reference to the Angiosperm Phylogeny Group website may have pointed the way to those interested, as well as to name change sceptics, to learn how 'total evidence' is used in modern systematics and taxonomy.

Genera are arranged alphabetically within families, as are species within genera. Most taxa (species and subspecies) occupy one page with images of habit, leaves, flowers and fruit, as well as a brief description and notes on breeding systems, flowering and fruiting times, abundance, preferred habitat, distribution and altitudinal range. Each *Eucalyptus* taxon, because of the inclusion of images of bark and juvenile leaves, spreads over two pages. Bark is also shown for some tree species of *Acacia*. Thumbnail distribution maps (extending outside the ACT boundary to Lake George, part of the Southern Alps and the Tinderry Mountains) use point data from verified herbarium records and the distribution of a taxon over its altitudinal range is presented in a bubble graph. 'Key ID', distinguishing feature(s) by which the plant may be identified, are also included.

There are introductory glossaries of botanical terms, with floral arrangements, leaf morphology and *Eucalyptus* characters illustrated in a pictorial glossary, as well as a key to families based on flower colour and floral morphology. Images of major habitats, together with an indication of their altitudinal occurrence, are presented.

At 210 × 150 mm, the guide fits into parka pocket or backpack. Of course a book of this size cannot include the total vascular flora of the region, and there may be some frustration when your species from a distant mountain top does not appear. This is diminished by the listing of all species per genus native to the region not given the full treatment, enabling the user to search elsewhere. Under each genus, inclusion appears to be generally based on abundance. For example, of the 28 species of *Eucalyptus* native to the ACT, 19 are treated; those not included are usually known from few remote populations, such as *E. cinerea* subsp. *triplex* and *E. perriniana*. But I noticed *Pterostylis umbrina* that is known from a single verified occurrence was included. But then orchids are always the spoilt darlings.

All photographs are by the author, remarkably taken within seven years. A wonderful achievement to have these beautifully detailed images of the plants, the genera placed in phylogenetically circumscribed families and the names of taxa 'hot off the press'. Altogether an exemplary field guide.

Ian Telford, N.C.W. Beadle Herbarium, University of New England, Armidale.

Some Recent Natural History Publications #21
August 2015

****

Photographic Guide to Native Plants of the Australian Capital Territory
Meredith Cosgrove
Meadow Argus. 360 pages. RRP $45

Here in the ACT we are remarkably, perhaps unreasonably, blessed with quality field guides to what is, after all, a small geographical entity. Hitherto however we have not had a reasonably comprehensive text-and-illustrations guide to plants. There is an out-of-print flora, some localised guides (including, I should acknowledge, a couple of contributions from me, now long unavailable) and a textless photo-only one. But Cosgrove, a PhD student in botany at the ANU, has I think now filled the gap admirably. I've long voiced my reservations about photo field guides, but she has got around most of the problems by using multiple photos – mostly four but up to five – per species, each species being allocated a page. The text is succinct but apparently adequate (I've not been motivated to field test it in the frigid months since I acquired it, but that will change very soon) – habit, height, flowering, fruiting, breeding system (an unusual addition, whose usefulness I've not yet determined), occurrence (ie how common it is), habitat, altitude, key ID features and brief notes on interesting feature or similar species. Maps are precise, based on herbarium specimens, and usefully extend beyond the ACT borders – as plants generally do! There is also a curious – and again useful – little vertical graph of altitude frequency. The inclusion of life-size scale bars for leaf, flower and fruit size is an excellent innovation. Taxonomy is of course up to date, and based on the Australian Plant Census. For a look at some pages, go to the Meadow Argus website http://meadow-argus.com/. I think all us who step outside in the ACT need this book – and spring's coming!